POLITECNICO DI TORINO

MASTER OF SCIENCE IN CIVIL ENGINEERING

MASTER THESIS

Refined modelling and analysis of masonry building aggregates.

Supervisors

Prof. Fabio Di Trapani

Prof. Guido Camata

Co-supervisor

Ing. Marilisa Di Benedetto

Candidate

Sofía Villar

Academic year 2022/2023

Content

List of Figures

List of Tables

1. Introduction

Building aggregates are conditioned to urban historical construction process and interact with each other under seismic action, giving the aggregate different characteristics from individual building units. The building aggregate's response to seismic action is associated with distinct factors such as confinement, quality of connections between adjacent units, damage accumulation, and inherent mechanical properties of each structure such as span between walls, connection between floors and walls, roofing system, and both in-height and in-plan irregularities (1). The transformation process of historical centers over time has led to a need for specific analysis of these structures. However, the lack of specific regulations opens up a range of possibilities in assessing their seismic risk, which is still an ongoing issue for research and engineering practice.

The knowledge of how individual units behave is insufficient to provide information on the overall behavior of the aggregate due to a lack of consideration for the interaction between units, known as the "Aggregate Effect". This is further complicated by the activation of in-plane and out-of-plane mechanisms that depend on the presence of flexible or rigid slabs (2), (3),

This study aims to develop a refined finite element model for aggregate buildings able to assess the potentially beneficial impact of the aggregate effect in units, as well as test the validity of pushover analysis in capturing the dynamic behavior of these structures. To do this, the work is divided into two parts: a calibration stage using a full-scale masonry building and a numerical analysis stage on a reference aggregate building.

The selected case for calibration is a two-story rectangular masonry building tested at the University of Pavia (4). The model was reproduced in order to find the material parameters that best matched the experimental results, taking into account the values suggested in multiple studies (5), (6), (7).

The reference aggregate building was studied hypothesizing two floor typologies: "Rigid floor" and "Flexible floor". Both cases were analyzed under two different assumptions. First, assuming a rigid wall-to-wall connection, which will be referred to as "Fully

Connected". Secondly, assuming that external units are non-rigidly connected to the central one but capable of rising frictional and contact stresses, which will be referred to as "Semi-connected Units". Additionally, all units were analyzed as individual isolated structures in both floor configurations. The analyses included a modal analysis to assess the fundamental mode of the structure; a non-linear static analysis using a lateral force distribution proportional to the fundamental mode; and a non-linear dynamic analysis using a component of the L'Aquila earthquake.

The software chosen for the study was STKO (Scientific ToolKit for OpenSees) (8), which provided a framework to take advantage of OpenSees (9),as well as innovating material constitutive models to increase the reliability of the results.

2. Seismic response of building aggregates

2.1 Open issues

Several seismic events have exposed the considerable seismic risk associated with unreinforced masonry structures in building aggregates, particularly those located in historical centers of small municipalities (Fig. 1). These small historical centers are the result of an extensive building expansion process that has created interconnected structures with different materials, construction methods, heights, conditions, and, occasionally, repairs.

Figure 1. Building Aggregate, Visso, Italy. (8)

It is important to understand the growth mechanism of aggregates to correctly assess the degree of connection between units. Different assessments showed that it was common to leave protruding stones in recently constructed buildings to allow the subsequent expansion. This process led to “open” units that share one or more walls with adjacent structures as portrayed in Fig. 2. This can only be identified by understanding the expansion process from historical cadastral plans (9).

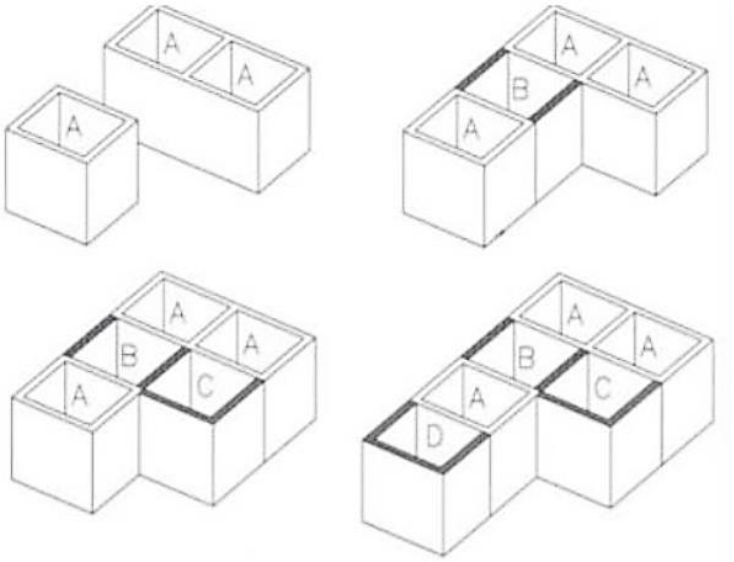

Figure 2. Growth mechanism of aggregates. B, C and D are the "open units" (11)

When analyzing a building aggregate, it is necessary to identify, initially, the Structural Units (US) that compose the aggregate, highlighting the actions that can derive from each contiguous Structural Unit.

According to the NTC18, the portion of the aggregate that constitutes the US includes cells linked in elevation and plan by a common construction process, and considers all elements affected by the transmission of vertical loads to the ground. The US must ensure the continuous transfer of loads to the foundation and is generally delimited by open spaces, structural joints, or adjacent buildings constructed, for example, with different construction and structural types, or with different materials, or in different periods. Among the structural interactions with adjacent buildings, it is necessary to consider: the actions (both vertical and horizontal) coming from the floors or walls of adjacent USs; the thrusts of arches and vaults belonging to contiguous USs; the thrusts coming from contrast arches or tie rods anchored to other buildings; and the pounding effect between adjacent USs.

These various factors make it challenging to assess the seismic risk of masonry buildings in aggregate, which remains an ongoing issue for both research and engineering practice. The absence of specific regulations regarding the seismic assessment of unreinforced masonry aggregates, resulted in multiple study typologies among which we can find:

- Empirical methods: consists in a large-scale approach that defines vulnerability classes based on post-earthquake data. This enables the calibration of a vulnerability model for each recognized class through statistical analyses, which can be performed quickly with minimal data, making it suitable for analyzing numerous structures or an entire large city.
- Holistic methods: usually based on assessing the expected damage considering components such as vulnerability, hazard, and exposure. Useful for a multi-scale analysis that also consider the interconnection between these relevant factors to have an integrated understanding of the situation.
- Analytical/mechanical methods: use numerical models and building simulations to determine the structural capacity of buildings. A thorough comprehension of the building's characteristics and extensive structural calculations are required, making them unsuitable for large-scale analysis.

Analytical methods (10) consider the most detailed aspects of buildings such as the geometry, layout of openings, structural details, mechanical properties, diaphragm typologies, and restraints. If applied to a set of representative case studies, which vary in their building features, it is possible to obtain more results that can account for the variability of the Italian buildings present in historical centers.

However, it is often the case that the outcomes of previous studies cannot be considered as fully conclusive due to the potential oversimplification of the modelling procedures employed, for example, by considering only in-plane behavior and neglecting out-of-plane mechanisms. Most studies tend to use frame models that follow the aforementioned premise yet are able to successfully capture the “Aggregate Effect”, which considers the impact of the interaction between structural units on overall behavior. The study on the vulnerability feature of masonry buildings in aggregate (11) emphasizes the challenges in accurately representing the seismic behavior using pushover analyses, as well as the inherent complexity in integrating both in-plane and out-of-plane behaviors without relying on advanced numerical models.

2.2 Structural behavior

2.2.1 The “Aggregate Effect”

For an isolated building, if it is relatively regular in plan, there are typically no significant differences in behavior between the two main directions. However, aggregate buildings are characterized by a predominant direction, shaped by the walls of the multiple adjacent units. This leads to an accentuated difference of behavior in longitudinal and transverse direction (9)

Mutual support among units was believed to be a crucial factor in construction, as each unit depends on the stabilizing influence of adjacent ones during earthquakes. Each unit absorbs the forces transmitted by the previous structure, while the following building produces a buttress effect on it. At present, it is not univocally decided whether the aggregate effect is beneficial or not since it depends on multiple factors, one of them being the unit-to-unit connection. In best case scenarios, aggregates are modeled using a 3D approach using either 3D elements or 2D shell elements. In these cases, the perfectly rigid connection often assumed during the modelling stage can be a simplification that drastically changes the response during analysis. Therefore, many studies are currently introducing interface elements with materials, based on Coulomb friction theory and Herz impact theory to reproduce friction and pounding effects between units. A study carried out using STKO (12), for example, focuses on the influence in the wall-to-floor connections and unit-to-unit connection considering the aforementioned variables. On the other hand, the most widespread method is frame modeling approach, in which piers and spandrels are simulated as beams and columns. This approach has proven to be useful in capturing the aggregate effect but risks losing accuracy since interaction between walls and tangential stress transference is neglected. In the next chapter different modelling approaches will be further discussed.

2.2.2 Floor typologies

Another factor that highly contributes to the response is the connection between structural elements, especially the floor-to-wall connection and rigidity of said floor. The presence of concrete slabs, timber or steel floors varies the slab rigidity and, therefore, changes the distribution of inertial forces developed during earthquake. The presence of a slab is

responsible for the degree of stiffness of the floor. In general, two extreme cases can be considered: a rigid floor and a flexible floor.

The concrete slab is the typical example of a rigid floor. Its deformability is very low; therefore, the in-plane infinite stiffness hypothesis can be assumed. This means that the slab has 3 degrees of freedom: displacement in two perpendicular in-plane directions and in-plane rotation. Consequently, inertial forces on walls will be distributed proportionally to their stiffness. The following scheme (Figs. 3, 4) can be adopted to estimate the forces.

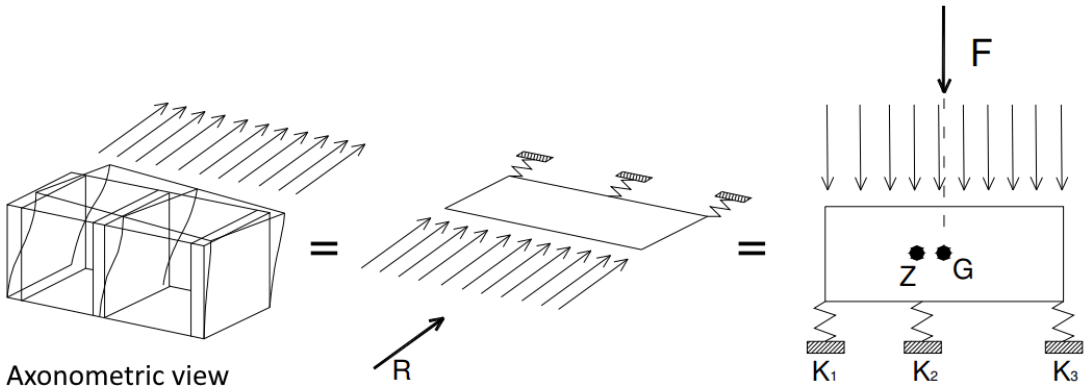

Figure 3 Rigid Floor scheme

In the picture (Fig.3),

- Z: barycenter of stiffness
- G: barycenter of masses
- F: resultant of the seismic force developed

The walls are modelled as springs and the slab as an infinitely rigid beam supported by them. The beam behaves as a rigid body, rotating and translating without experiencing deformation. Then, the reaction of each spring is:

$$R_i = F\frac{k_i}{\sum_{j=1}^{n} k_j} + F.K_i\frac{(x_i - x_z)(x_G - x_z)}{\sum k_i(x_i - x_z)^2}$$

Where the position of the barycenter x_z is:

$$x_z = \frac{\sum_{j=1}^{n} k_j x_j}{\sum_{j=1}^{n} k_j}$$

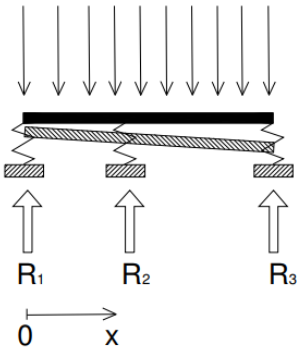

Figure 4 Reactions on walls, rigid floor.

The more rigid, the higher the capacity of absorbing forces, and the seismic response improves. However, this assumption can easily be violated due to damages, poor slab-to-wall connection, or the presence of alternative construction solutions.

The flexible floor is characterized by a flexible slab or a series of flexural beams. They provide finite to almost null stiffness. As we can see below, the lack of rigidity causes the walls that are perpendicular to the direction of the force to go out of plane. In this case, inertial forces on walls are distributed based on the mass that weights over them. The following scheme (Figs. 5, 6) is used instead:

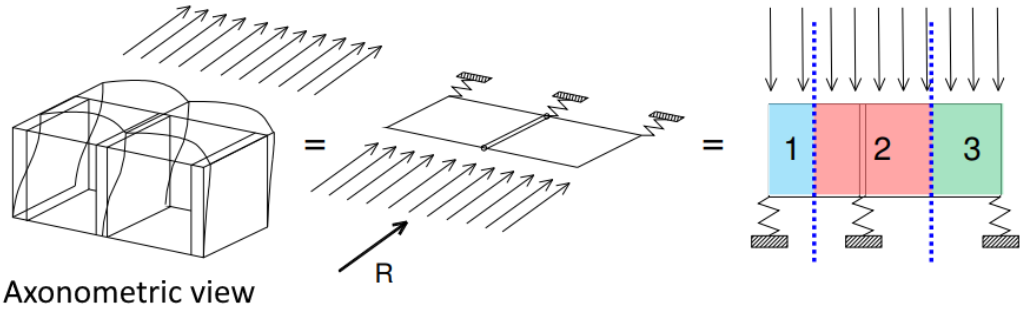

Figure 5 Flexible Floor scheme.

In this case, the beam is articulated at each wall, therefore, free to deform. The influence area method can be used to calculate the mass that corresponds to each wall. Then, the reaction force on each wall is:

$$R_1 = \frac{R}{L_1 + L_2}\frac{L_1}{2}$$

$$R_2 = \frac{R}{L_1 + L_2}\frac{L_1 + L_2}{2}$$

$$R_3 = \frac{R}{L_1 + L_2}\frac{L_2}{2}$$

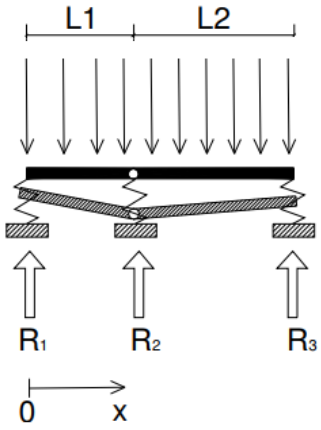

Figure 6 Reactions on walls, flexible floor.

2.2.3 Local effects

The seismic response of masonry buildings (both isolated and in aggregate) depends as well on local failure mechanisms. This means that portions of the building can lose the equilibrium and adopt a rigid body behavior, rotating or sliding. The local analysis involves identifying all these possible mechanisms that may result from the seismic actions in the portion under examination (13). The quality of the masonry texture should also be considered because poor quality masonry can undergo disintegration before the activation of the local kinematic mechanisms. Local mechanisms are in general amplified when there is absence of a rigid diaphragm behavior of the slab.

Among the most common local failures we can find:

- Overturning mechanism of the facades, which involves the rotation around a hinge of the entire wall perpendicular to the earthquake direction. This is caused by the lack of proper connection wall-to-wall as well as the lack of well-anchored floors that provides a connection rigid enough to prevent rotation. When the wall-to-wall connection is strong, we often observe the tilt of only a portion, as shown in (Fig.

7). In this case, the weakening is produced by the presence of openings, from which the crack extends until reaching the top of the wall. (14)

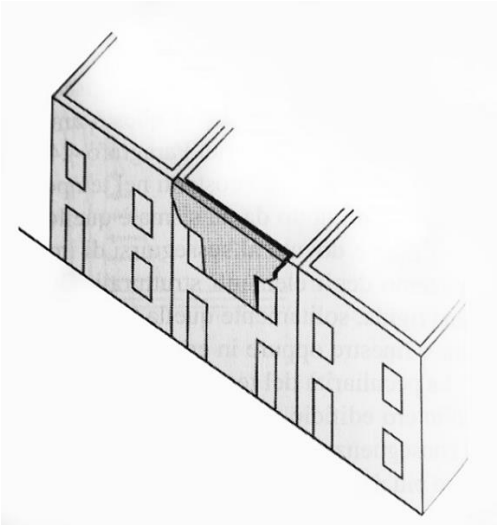

Figure 7 Tilt of facades. (14)

- Vertical flexural mechanism, in which the central part of the wall perpendicular to the earthquake bulges due to hinges formed at the superior and inferior borders, as shown in (Fig. 8). This is caused by the thrust of the floor towards the wall due to a poor connection at the floor level (14).

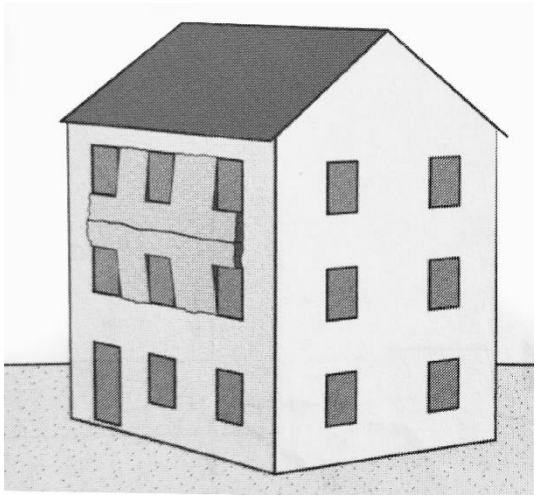

Figure 8 Vertical flexural mechanism. (14)

- Horizontal flexural mechanism, where the top part of the wall rotates around oblique plastic hinges. In this case, the walls are strongly interconnected yet the

wall-roof connection remains weak, allowing the roof to move forward, as shown in (Fig. 9) (14).

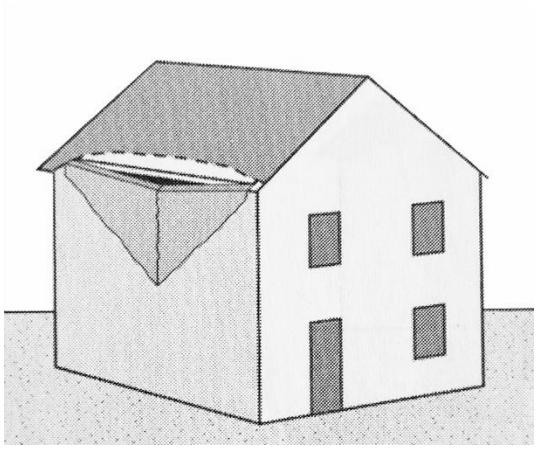

Figure 9 Horizontal flexural mechanism. (14)

These various collapse types can also present themselves together, generating compound mechanisms. This occurs when corner present proper connections between orthogonal walls that converge in a node, involving parts of these in the collapse mechanism. One of the most observed forms is the wedge (Fig. 10.b), but this may vary according to the floor typology (14).

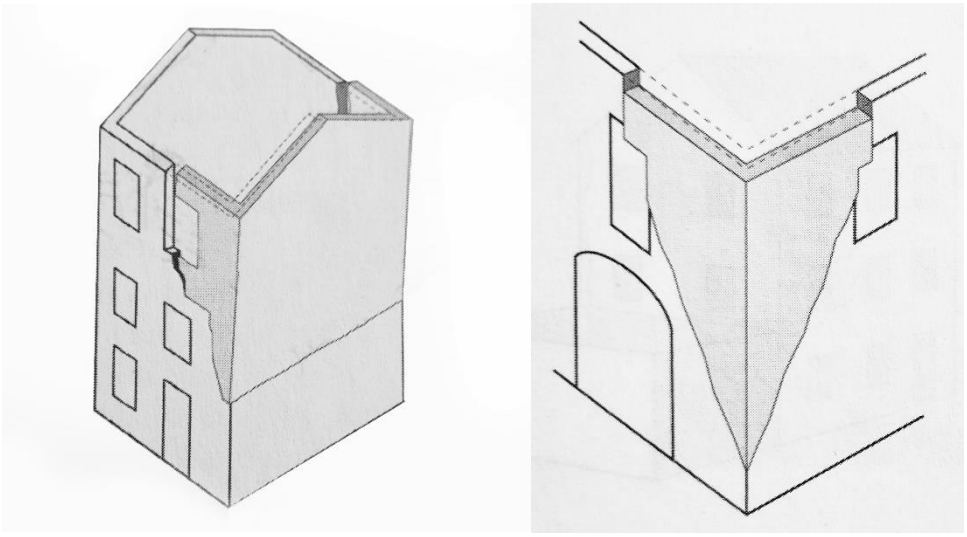

Figure 10 Compound mechanisms. (14).

2.2.4 Crack patterns

In-plane collapse mechanism can be identified by the crack pattern formed in the masonry (Fig. 11). Among these, we can find:

- Sliding: the tensile horizontal cracks in bedjoints create sliding planes. This failure mechanism is possible for low levels of vertical load and/or low friction coefficient.
- Rocking: the increase of horizontal loads or displacements causes the bedjoints to crack in tension and transfer the load to the compressed masonry. This produces crushing on the corner an overturning of the pier. Tensile cracks can appear on the opposite corner.
- Shear cracking: diagonal cracks form across bricks or following the mortar path depending on the mortar strength, brick strength and brick-mortar interface.

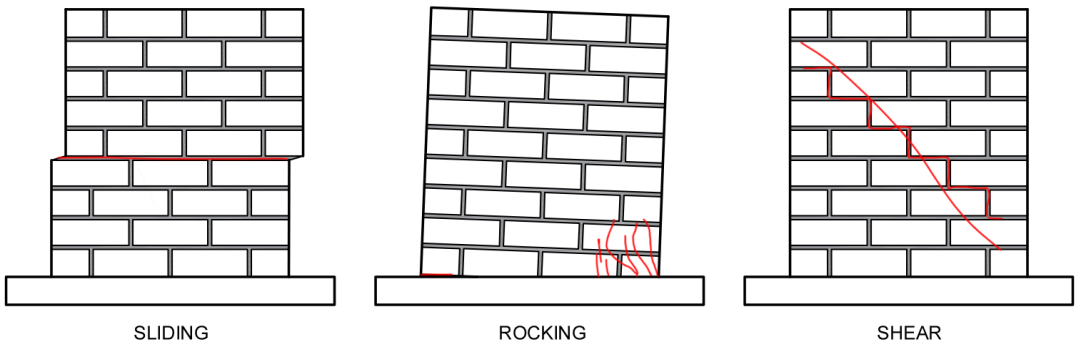

Figure 11 Crack patterns

3. Numerical modelling of masonry structures

The primary reason for the non-linear behavior of masonry is its limited or insignificant ability to withstand tension. When a force is applied to a masonry structure, the parts in tension are likely to crack or break while the parts of the structure that can resist the force are the ones that are being compressed. As the force increases, the resisting cross-sections will become cracked or damaged, reducing the effective resisting area of the structure. This reduction in resistance causes the mechanical response to become non-linear, even when subjected to low-stress levels. Accurately capturing this behavior depends fundamentally in the choice of the constitutive model and the modelling strategy.

In response to the increased interest in seismic performance of masonry buildings, non-linear Finite Element models have been used to analyze masonry structures, yielding diverse solutions across different modeling scales. Among these, we can identify three main approaches that range from more to less detailed: micro-modeling, the homogenized masonry approach, and the Equivalent Frame Method (15)

3.1 Micro-modelling

The micro-model is the approach that is closest to reality. This requires individual models of bricks, mortar, and their interaction. Therefore, detailed material parameters are needed for both. In this category, we can find detailed micro-modelling (Fig. 12.a) and simplified micro-modelling (Fig. 12.b). The simplification made for the last one is that the mortar/brick interaction is not considered as the interface is not modelled. This approach can be done both in 2D and 3D, with considerable differences in the computational effort, to capture both in and out-of-plane behavior. For the case of walls made of one layer of bricks with a regular pattern, a plane stress assumption can simplify the model at the expense of neglecting the triaxial compression in bedjoints. Additionally, this approach is able to describe the process of crack propagation and the effects of size can be

accounted for by using scaling laws for strength and brittleness, analyzing dimensions, and applying fractal geometry (16), (17)

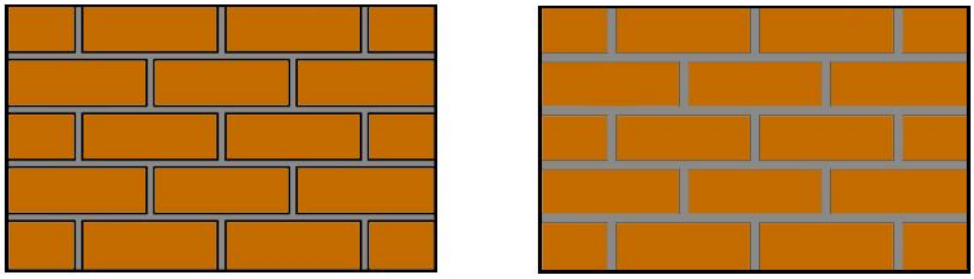

Figure 12 a) micro-modelling; b) simplified micro-modelling.

Although micro modelling is a very precise tool for the reasons already mentioned, requires a very high computational effort. This is because of the refined mesh needed, derived from the small dimension of bricks and the thickness of mortar. In addition, poor convergence can be an issue due to damage growth, strength degradation, and strain localization. The use of parallel computing and robust integration algorithms for constitutive models can considerably mitigate these drawbacks (17)

Among the examples in the literature, the study conducted by Petracca et al (17), used the micro-modelling approach to model a masonry building under static cyclic conditions. The study shows that by incorporating the microstructure into the numerical mesh, micro-modeling can precisely capture the complex geometrical interactions and failure mechanisms that occur at the micro-level as it can be seen in Figure 13.

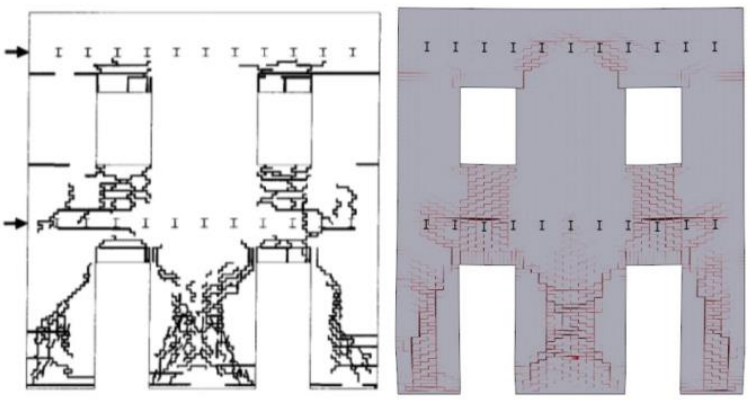

Figure 13. Damage comparison with experimental results (17).

Moreover, the study focused on the improvements in velocity of computation achieved with the use of a new constitutive model based on continuum damage in combination with the implicit/explicit algorithm. With this algorithm, if the only source of nonlinearity was the constitutive model (neglecting other source of non-linearities), the nonlinear problem would become linear within the step, securing convergence (17).

As reported in the study, the entire mesh was composed of about 177000 elements and 60000 nodes. The mesh was partitioned into 24 sub-domains and analyzed with OpenSeesMP in almost 3 hours considering a subdivision of 3200 steps. Although the study showed a remarkable calculation speed, it still presented a very high computation cost and the need of a computer with high performance capabilities to extend the micro-modelling approach to a larger scale (17).

3.2 Homogenized masonry

Homogenized masonry or meso-modelling considers the masonry as a continuum. Brick and mortar material parameters are not distinguished as it uses as input a unique material (Fig 14). To execute this methodology, the material parameters are defined with respect to the compressive strength acquired from the diagonal compression test conducted on a segment of the masonry wall. The defined parameters are allowed to vary within a certain range, hence, to affirm the model authenticity. A precise calibration of these parameters should be performed using experimental tests on wall specimens. These values can also be obtained from numerical homogenization (18) although this is not common in practice due to its complexity.

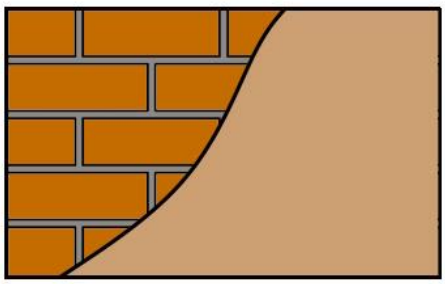

Figure 14. Homogenized masonry.

Among the advantages, the computational effort is less than the required for micro modelling due to two main reasons. Firstly, the number of elements no longer depends on the size of the physical elements (for example, the thickness of the mortar), so a coarser mesh can be used. Secondly, since the interaction between the two different material elements is not modelled, the number of calculations needed for each element and each step is significantly reduced.

The main issue of this approach relies on the constitutive model's difficulty to accurately capture characteristics like strength anisotropy and the impact of the micro-structural components' arrangement and size that may lead to neglecting local phenomena such as the sliding mechanism.

In addition, conventional constitutive models based on plasticity, damage, or a mixture of the two are inadequate when it comes to representing the "size effect". The "size effect" occurs when a material property shows variation for two structures that are geometrically similar but have different sizes. In quasi-brittle materials, both structural brittleness and material strength have been observed to depend on scale (17). The consideration of the "size effect" is of relevance when calibrating material models, as the selection of experimental tests to be employed in the calibration process must be carefully chosen. Typically, material parameters determined for a small-scale model may not be appropriate for larger models.

Within the references in the literature, it can be mentioned the work done by Nicola Tarque et al. in (19). The study focuses on the calibration of adobe material used for construction and the subsequent numerical modeling using both micro-modeling and homogenized masonry approaches. Regarding the continuum approach, the total-strain model and the concrete damage plasticity model were tested. The results were confronted with the experimental results of a quasi-static cyclic in-plane test on an adobe wall representative of the typical Peruvian constructions. All three models were able to accurately reproduce the results obtained during the experimental test, as it can be observed in Figure 15.

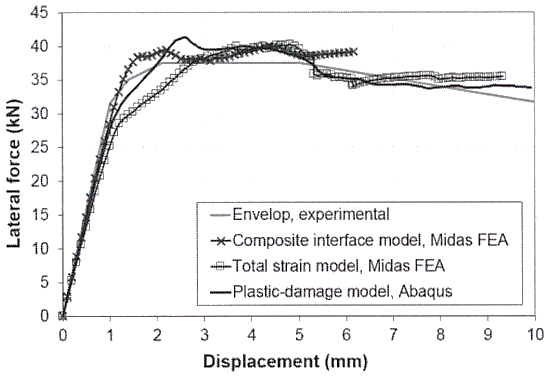

Figure 15. Comparison between the different modeling approaches and the experimental envelope (19)

Moreover, a sensitivity study was then performed using the concrete damage plasticity model (continuum approach) to assess the influence of both tensile and compressive strength on the global behavior. As it can be seen in Figure 16, the variation of the compressive strength showed very limited influence. The duplication of the parameter did not have a significative impact in the resistance of the wall. However, the variation of the tensile strength had a major impact on the response (19).

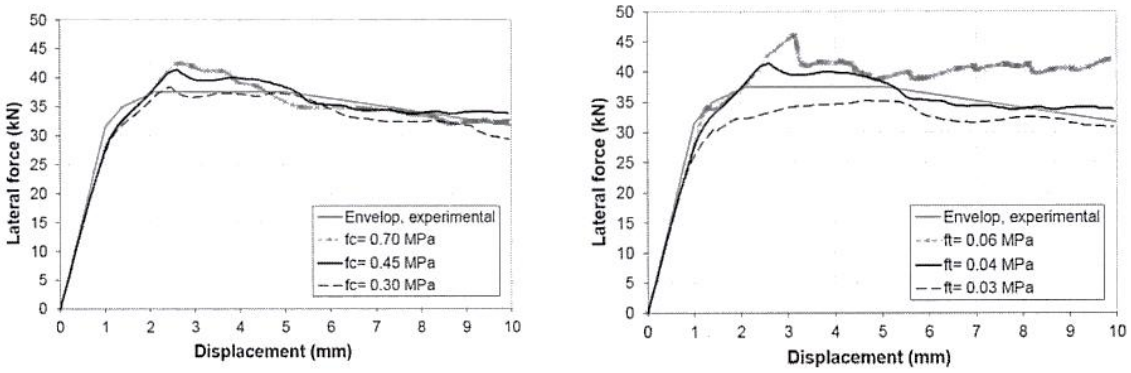

Figure 16. Sensitivity study. a) variation of the compressive strength; b) variation of the tensile strength. (19)

A similar conclusion was reached when performing a sensitivity analysis on the fracture energies. Figure 17 shows that the change in the compressive fracture energy implied no change in the curve, whereas the variation of the tensile fracture energy showed very different curves including an early collapse due to its low value (19).

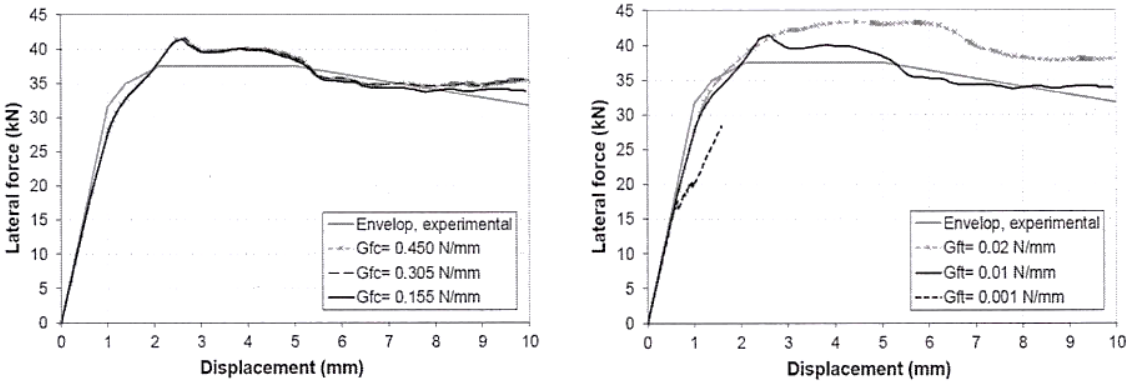

Figure 17. Sensitivity study. a). variation of the compressive fracture energy; b) variation of the tensile fracture energy (19)

Having established the difference between micro modeling and homogenized masonry, it could be stated that the former is the most accurate strategy to capture the complexities of the seismic response of masonry. However, due to the difficulty and size of the building aggregate, a method that would reduce both modeling and analysis time while including both in-plane and out-of-plane behavior is needed. The homogenized masonry turns out to be a good compromise between micro-modelling and the Equivalent Frame Method (explained below), provided that a calibration of the material properties is carried out.

3.3 Equivalent frame modelling

The equivalent frame model simplifies the masonry horizontal and vertical elements, called spandrels and piers respectively, in a one-dimension element connected to each other by rigid nodes. The 1D elements can be modelled as beams while nodes can be modelled as rigid links. The flexible length of the elements (H_{eff}), and therefore the length of the rigid link, can be defined by the formulation proposed by Dolce that considers the inter-story height, the dimension of the pier's base, and the height and position of the openings (Fig. 18) (20).

$$H_{eff} = h' + \frac{1}{3}\frac{D(H-h')}{h'}$$

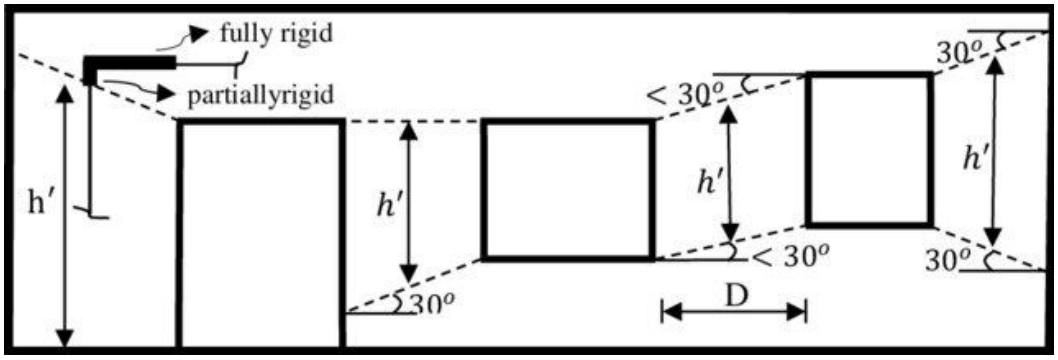

Figure 18. Effective height of piers and spandrels (20)

Validation studies and numerical tests have demonstrated that the EFM (Equivalent Frame Method) can be effectively used for analyzing the structural integrity of newly constructed unreinforced masonry buildings. However, there are still uncertainties that prevent its use for modeling existing ones. This is because the simplified interpretation of the structural behavior may be constrained by the presence of irregular geometries. For instance, when there are pier-to-spandrel geometrical relationships that do not conform to a typical frame configuration (15).

There may be additional uncertainties when determining structural details, the history of loads placed on the structure, any damage that may have occurred, and any restoration efforts made. The accurate incorporation of these details into the equivalent frame approach remains problematic for existing constructions because of the morphological changes that usually occur over their lifespan (21).

This method is widely spread due to its simplicity and velocity of computation. However, out-of-plane behavior cannot be reproduced, neglecting one of the principal collapse mechanisms of aggregate buildings. This limits the analysis to regular buildings, in which the decoupling of the in-plane and out-of-plane behavior can be considered valid. Another critical issue is brought in by modelling piers and spandrels connected by nodes, which are unable to transfer tangential stresses. This changes a predominantly tangential behavior to a flexural one, losing the most important source of resistance in masonry. An accurate calibration of the properties of the masonry wall as a unique material is necessary, considering the masonry as a homogeneous material.

The study conducted by M. Angiolini et al. (11), used this approach to assess the impact of the "aggregate-effect" and the combination of in-plane and out-of-plane mechanisms

on the fragility curves of two selected case studies. To achieve this, the research involves comparing the results of structural units analyzed separately and as part of the aggregate using both nonlinear static analysis (pushover) and nonlinear dynamic analysis. The study simulated the in-plane response of unreinforced masonry buildings using a 3D Equivalent Frame model (Fig. 19). On the other hand, the evaluation of out-of-plane mechanisms was conducted separately but based on floor accelerations obtained from post-processing data from the global 3D model (11).

The two case studies were two structural units in unreinforced masonry buildings located in Catania and Visso (Italy). The assumption made was that the two structural units were constructed after the reference building and were added to it without doubling the boundary walls.

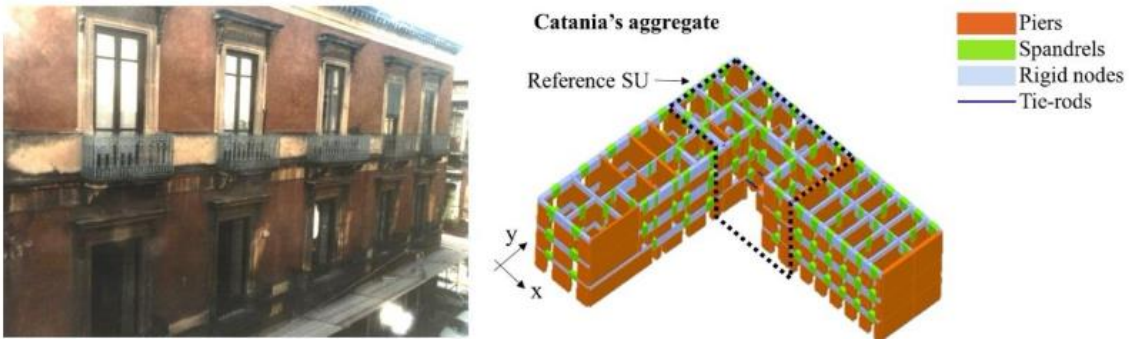

Figure 19. Equivalent Frame Model of the Catania case study (11).

The results emphasize the challenges of accurately representing the seismic behavior of structural units that interact with each other using pushover analyses. The study also indicates that it is impossible to combine in-plane and out-of-plane mechanisms without resorting to advanced numerical models (11).

The present study is analogous to the one carried out by M Angiolini et al. (9) but, instead, takes the advantages of an advanced constitutive damage model and the homogenized masonry approach to take into account the combination between in-plane and out-of-plane mechanisms in the overall behavior of the aggregate.

4. Mechanical modelling of homogenized masonry with Opensees STKO

4.1 Introduction to OpenSees

The models required for the analysis are carried out using the software framework “Open System for Earthquake Engineering Simulation” (OpenSees). It was developed by the “Pacific Earthquake Engineering Research Center” (PEER) with the objective of creating a computational platform for research in the field of seismic engineering (22)

OpenSees is an open-source software based on the compilation of codes written in the Tcl programming language (Tool Command Language). Using appropriate commands available in this programming language, it is possible to define the geometry of the model to be analyzed, assign the materials to each element, assign the mechanical characteristics of each material, assign the loads, and perform both static and dynamic analyses. However, a graphical interface is not available, making it difficult to use for complex models.

For this reason, we chose to develop our models using STKO (Scientific Tool Kit for OpenSees) (23). It provided a user-friendly graphical interface to take advantage of OpenSees, as well as innovating material constitutive models to increase the reliability of the results. The software enables the modelling in a CAD environment and the insertion of properties, conditions and loads using dropdown menus facilitating the process.

The basic modelling workflow is based on the definition of:

1. Geometry
2. Physical properties
3. Element properties
4. Conditions (loads and constraints)
5. Analysis steps

4.2 Definition of the geometry

In terms of geometry, there are two possible methods to define a 3D model of masonry: using 3D-solid elements or using 2D shells. The primary difference in terms of strategy is based on the computational effort required and the ability to capture out-of-plane mechanisms. Due to the implementation of layered shells, which enable the definition of multiple integration points in the direction of the shell thickness, the 2D-shell approach was the most suitable option. Thus, the masonry was modeled utilizing faces, while the beams were represented as lines, to which physical (geometry and constitutive models) and element properties were allocated.

4.3 Description of the elements

Two kinds of elements were used in the models. Beams were modelled using the fiber section approach with *ForceBeamColumn* elements, whereas masonry walls were modelled using a layered shell element.

4.3.1 Layered Shell

The layered Shell is based on the principles of composite mechanics. It discretizes the three-dimensional nonlinear behavior into several layers in the thickness direction. This allows the simplification of the model by using shell elements instead of solid elements but still benefits from the 3D response. Each layer is defined by its thickness and the material assigned to it. The number of layers is selected considering the different materials and the need of additional integration points to better capture the out-of-plane behavior (Fig. 21) (25).

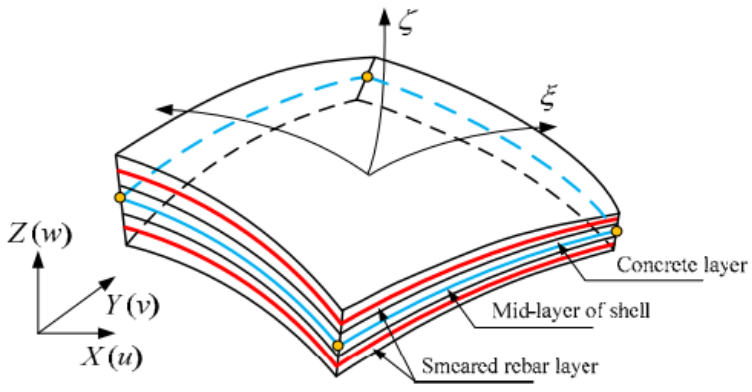

Figure 20 Layered Shell, example of application (25)

The multi-layer shell element first calculates the axial strains and curvature of the central layer. Based on the plane-section assumption, the strains of each layer are then determined. Next, the stresses of each integration point on each layer are calculated according to the constitutive model for that layer. Finally, the standard numerical integration method is used to compute the internal forces (25).

The type of element used in it is the *ASDShellQ4* included in STKO, which is a 4-node thick shell with an enhanced membrane behavior. Due to its Enhanced Assumed Strain method, it can show a linear variation of strain (even if the displacement is linear and not quadratic). In this way, only one-half of the element will localize. This feature makes the element less affected by geometry distortion. However, it can directly impact in the definition of the fracture energy of the material. For this reason, calibration of the model using experimental test is of outmost importance. Since the *ASDShellQ4* element is a thick-shell element, it accounts for out-of-plane transverse shear deformability as well. It supports three-dimensional constitutive models, which allows the coupling of out-of-plane shear, membrane and bending behavior (26)

4.3.3 Zero Length Contact element

The contact element implemented to simulate the friction and contact forces between Semi-connected units was the *zeroLengthContactASDimplex.* It is a 2-node zero-length contact element that follows the Mohr-Coulomb criterion with no cohesion such as:

$$T_M = -\sigma_m \mu$$

It is penalty based, therefore two penalty stiffness should be defined for tangential and normal stresses (K_t and K_n)

It can be used in both 2D and 3D problems and supports both 2 and 3 DOFs in 2D problems, and both 3,4 and 6 DOFs in 3D problems. The two nodes can have different DOFs, so this element can be easily used to connect different element types such as (Solids (3 DOFs) to Beams/Shells (6 DOFs) or UP-Solids (4 DOFs).

It can be arbitrarily oriented in space, using a user-defined contact vector. Moreover, the orientation “from element” is available so that it can be applied to curved surfaces. If not specified, the global X axis is considered as contact vector (Fig. 22).

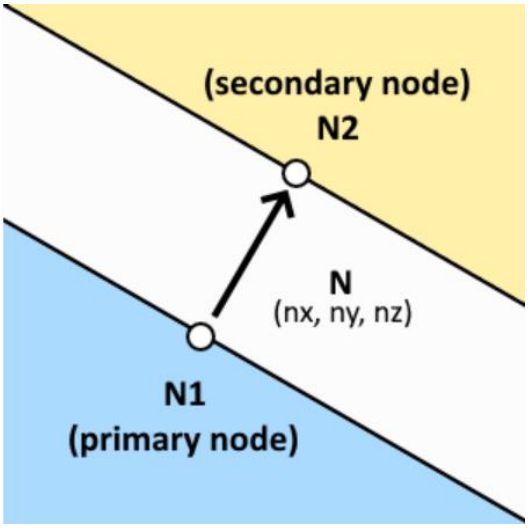

Figure 21. Nodes and contact direction. (27)

This element present in STKO enables the distributed option, useful when a spread contact along an edge or surface is needed instead of a node-to-node spring. STKO performs a nodal lumping of Kn and Kt using the tributary area of every node (27).

4.3.1 Fiber Section.

In the modeling of 1D elements, the selection of an appropriate methodology for plasticity analysis hinges upon the choice between concentrated and distributed plasticity approaches. The former involves the localization of plastic deformation capacity at precise points within the element, which can be achieved through the pre-definition of control sections or by incorporating non-linear springs. In contrast, distributed plasticity allows for the automatic identification of points where plastic deformation is likely to occur. This is possible with fiber elements, as each fiber has an associated constitutive law that enables the identification of sections where fiber stresses reach the plastic limit (Fig. 20).

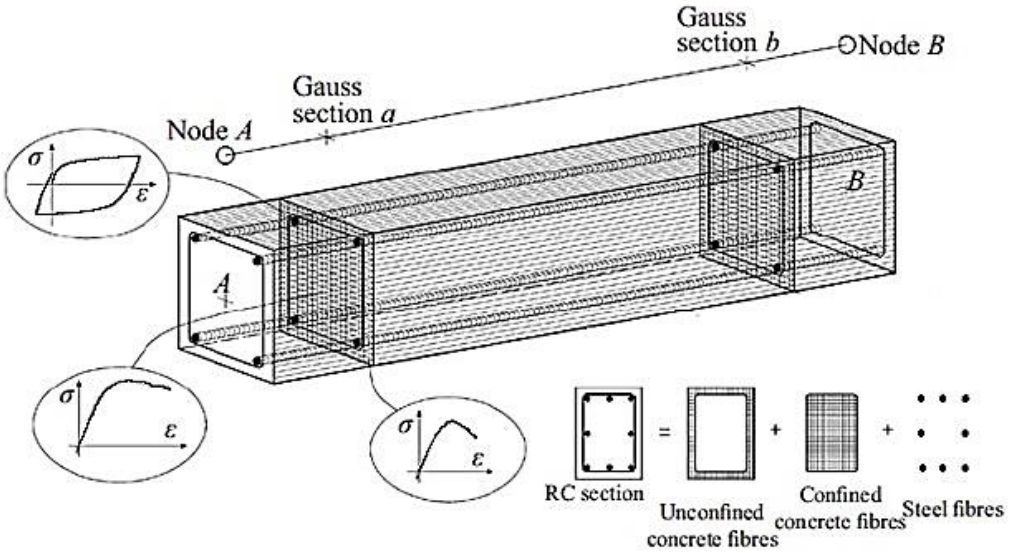

Figure 22 Fiber beam-column element, discretization of the typical concrete cross-section (24)

To introduce this aspect, two primary types of structural elements are available for modeling: displacement-based (DB) and force-based (FB). While DB elements are only used for distributed plasticity analysis and are formulated with displacement fields, FB elements are formulated using force and moment fields, enabling the governing equations to achieve equilibrium through stiffness. The force-based approach was implemented by means of the *ForceBeamColumn* property available in Opensees.

4.4 Description of the constitutive model

To construct the model, the initial phase involves selecting suitable materials. OpenSees offers a variety of materials that can be employed to define the cross-sectional area of the elements. Each material is represented in the software by its constitutive model: the stress-strain relationship that characterizes its behavior under typical conditions.

4.4.1 ASDConcrete3D

The material implemented in the masonry is ASDConcrete3D, which is based on its predecessor, DamageTC3D. Using the latter, the damage on an element in one direction would manifest in all directions. This meant that a failure in tension would result in a loss in the resistance to compression. With the new proposed material, structures can withstand multiple failure mechanisms. The material presents 3 options according to the

number of parameters to be inserted by the user: 1P, 4P, 6P. 9P and User-Defined, depending on the degree of specificity needed. The User-Defined mode enables the user to modify the curve trend by directly inserting the vectors that shape it. This feature was used in the work to create the behavior law for the mortar outline between the lintels and the masonry.

The constitutive model is based on the continuum damage mechanics. It employs the d+/d- tension-compression damage framework. To account for different behaviors under tension and compression, this model incorporates two scalar damage indexes and two failure criteria for tensile and compressive stress states. A brief description of the theory follows (28).

Variables referred to the current time-step have no subscripts. From the previous time step (subscript n), we extract the effective stress $\bar{\sigma}_n$ and we define the stress tensor and the step increment corresponding to the actual time step. These can be considered trial magnitudes.

$$C_0 : (\epsilon - \epsilon_n)$$
$$\tilde{\sigma} = \bar{\sigma}_n + C_0 : (\epsilon - \epsilon_n)$$

Using the positive principal stresses (σ_i) and their principal directions (p_i), we split the stress tensor into its positive and negative parts.

$$\tilde{\sigma}^+ = \sum_{i=1}^{3} \langle \tilde{\sigma}_i \rangle p_i \otimes p_i$$
$$\tilde{\sigma}^- = \tilde{\sigma} - \tilde{\sigma}^+$$

From the trial effective stress tensor, two scalars are computed for both tensile τ^+ and compressive τ^- behavior using the damage surfaces:

$$\tilde{\tau}^+ = f(\tilde{\sigma}) = H(\tilde{\sigma}_{max}) \left[\frac{1}{1-\alpha} \left(\alpha \tilde{I}_1 + \sqrt{3\tilde{J}_2} + \beta \langle \tilde{\sigma}_{max} \rangle \right) \frac{1}{\phi} \right]$$

$$\tilde{\tau}^- = f(\tilde{\sigma}^-) = \left[\frac{1}{1-\alpha} \left(\alpha \tilde{I}_1 + \sqrt{3\tilde{J}_2} + \gamma \langle -\tilde{\sigma}_{max} \rangle \right) \right]$$

In these expressions,

- $\tilde{I}_1$ is the first invariant of $\tilde{\sigma}$
- $\tilde{J}_2$ is the second invariant of the deviator of $\tilde{\sigma}$
- σ_{max} is the maximum principal stress.
- $\alpha = \frac{4}{33}, \beta = \frac{23}{3}, \gamma = 3\,, \phi = 10$

These measures are converted into their trial total-strain counterparts x^+, x^- considering the equivalent plastic strain from the previous step:

$$\tilde{x}^{\pm} = \frac{\tilde{\tau}^{\pm}}{E} + \; x_{pl,n}$$

To impose the irreversibility of plasticity and damage, the strain is updated:

$$\tilde{x}^{\pm} = \begin{cases} \dfrac{\eta}{\eta + \Delta t} x_n^{\pm} + \dfrac{\Delta t}{(\eta + \Delta t)} \tilde{x}^{\pm} & , if\ \tilde{x}^{\pm} > x_n^{\pm} \\ x_n^{\pm} & , otherwise \end{cases}$$

Finally, the plastic and cracking damage variables are obtained from the stress tensor expressions:

$$\bar{\sigma}^+ = \left(1 - d_{pl}^+\right)\tilde{\sigma}^+$$

$$\bar{\sigma}^- = \left(1 - d_{pl}^-\right)\tilde{\sigma}^-$$

$$\bar{\sigma} = \bar{\sigma}^+ + \bar{\sigma}^-$$

$$\sigma = (1 - d_{cr}^+)\bar{\sigma}^+ + (1 - d_{cr}^-)\bar{\sigma}^-$$

Figure 23 presents a schematic representation of the elastic predictor followed by the plastic and damage correctors in a representative uniaxial case.

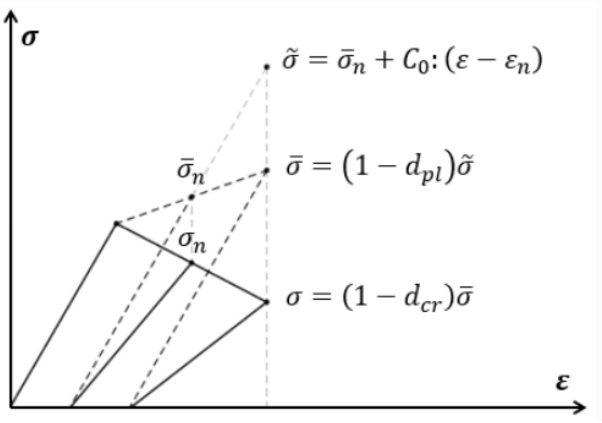

Figure 23: schematic representation of the elastic predictor followed by the plastic and damage correctors in a representative uniaxial case (16)

The ASDConcrete3D, as well as its predecessor, allows the user to implement implicit/explicit integration scheme (IMPL-EX algorithm) as well as the autoregularization. Both are explained below.

IMPL-EX algorithm

To improve the robustness of the analysis, the IMPL-EX algorithm was introduced as an available option within the *ASDConcrete3D* material in STKO. (29)

This algorithm aids in overcoming the strong nonlinearities introduced by the DamageTC3D model. The primary concept is to divide the computation of the constitutive model into two stages: an explicit extrapolation and an implicit correction. During the global implicit iterative procedure, the strain tensor is computed in each element and sent to the constitutive model. In the standard integration, the damage variables r+ and r- are nonlinear functions of the trial effective stress tensor and, consequently, this makes the global problem nonlinear. In the presence of softening, this may introduce negative eigenvalues. With the IMPL-EX algorithm, these variables are extrapolated from previous values at time tn-1 and tn. In this way, the variables will depend linearly on the strain. This improves the convergence and reduces the analysis time (29).

The problem of strain localization

Structures inherently possess imperfections, such as the imperceptible variation in the element's area or the changes in material characteristics due to heterogeneity. These imperfections tend to accumulate additional stresses, causing the first damaged regions.

However, when numerical models are used, these imperfections are absent, which creates problems for constitutive models that consider softening behavior. Let's consider a two-element structure (e_1, e_2). If both elements are subjected to the same stress, due to imperfections, one element should locally damage. However, the software cannot decide which is the damaged element and localization never occurs. On the other hand, if e_1 goes into softening behavior, e_2 will unload to maintain equilibrium reaching the same stress value as e_1 (Fig. 24).

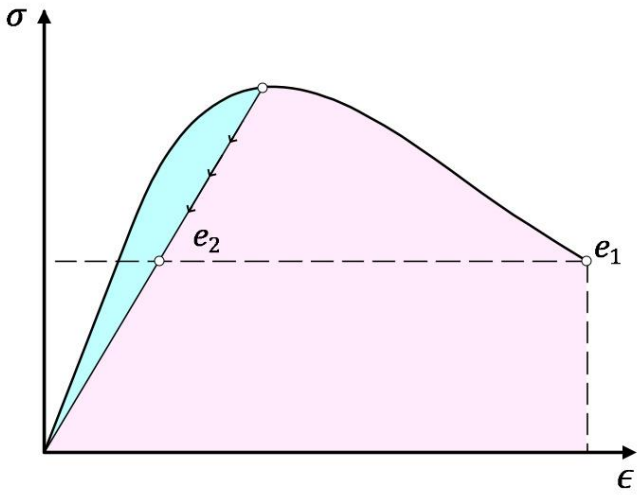

Figure 24. Energy dissipated by e_2 and e_1

In plain sight, we can observe that the energy dissipated by e_1 is much higher than the energy dissipated by e_2. The bigger the size of the elements, the more energy they will dissipate even if the fracture energies (Gt and Gc, explained below) are the same. In this case, a change in the mesh will directly impact on the result. For this reason, by introducing the autoregularization, the input fracture energies will be divided by the element's characteristic length, to obtain a mesh-size independent response (18)

The tensile fracture energy is the energy required to propagate a crack in a material due to tension. It is represented by the area under the softening curve. The value of fracture energy varies depending on the type and characteristics of the material, as well as the dimensions and geometry of the element. This parameter is most relevant when employing brittle materials with low tensile resistance such as concrete or masonry since provides insight on their behavior under tension during the cracked phase. In absence of

experimental data, both fracture energies can be calculated using the following formulation as a function of the compressive strength.

According to the Model Code (30) the tensile fracture energy can be calculated as:

$$G_t = 0.073 f_{cm}^{0.18} \quad [N/mm]$$

Where f_{cm} is the compressive tensile strength of the masonry in MPa.

The calculation of the compressive fracture energy is instead carried out following the formulation of "Guidelines for Nonlinear Finite Element Analysis of concrete structures", which can be also used for masonry (31).

$$G_c = 250 G_t \quad [N/mm]$$

It's important to mention that the values recommended by the formulations serve as a reliable starting point for defining constitutive models. Nonetheless, slight modifications may be necessary during the calibration process to achieve a suitable match with experimental data, as long as the values remain within an acceptable range.

5. Analysis Methods

During this study, various analyses were conducted to estimate the seismic response of the different aggregate building cases. Initially, a modal analysis was performed to evaluate the dynamic characteristics of the building and determine its fundamental mode of vibration. The results of this analysis were used as input for the subsequent Pushover analysis, which was conducted to assess the reaction at the base in relation to the displacements of a significant point. Finally, the Pushover analysis was compared with a non-linear analysis based on a time history of an existing earthquake to determine whether the former type of analysis accurately represented the seismic response and to evaluate the aggregate effect on the single units. This chapter aims to provide a deeper understanding of the theory behind these analysis methods employed in the following chapters.

5.1 Modal Analysis

The modal analysis has the main purpose to dynamically characterize the structure by means of its fundamental period T (or natural frequency ω or f), modes of vibration, and amount of mobilized mass for each mode, obtained from an eigenvalue analysis. These results provide a first insight of both global and local mechanisms that may develop during an earthquake.

The natural frequencies of a structure are the frequencies at which the structure will oscillate when subjected to a small vibration. These frequencies depend on the mass, stiffness, and damping of the structure and are calculated using mathematical methods (32).

Mode shapes, on the other hand, describe the patterns of motion that occur at each natural frequency. Each mode shape is a unique vibration pattern that shows how different parts of the structure move in response to a particular frequency of excitation. The shape of the mode is determined by the geometry of the structure and can be used to identify areas of high stress or potential failure (32).

The process of modal analysis enables the splitting of a system with N degrees of freedom into N individual one-degree of freedom systems (or modes). The total response will be the superposition of the single modes (not the sum). Mathematically this can be expressed according to the following expressions:

The motion equation for a damped system, in absence of the external force is:

$$[M]\{X\} + [C]\{X\} + K\{X\} = \{F\}$$

If we assume a decomposed system, each mode will follow the equation of the simple oscillator given:

$$\ddot{p}_i + 2\zeta_i\omega_i\dot{p}_i + \omega_i^2 pi = u_g(t).g_i$$

The set of N coupled differential equations in nodal displacements (x) has been transformed to the set of N uncoupled equations in modal coordinates (p). In this equation ζ_i is the damping ratio for the i-th mode and g_i is the variable that relates the multiple-degree of freedom system to the single-degree of freedom system. However, as g_i is dependent on the normalization constant, p_i is not unique. For this reason, p_i is multiplied by the eigenvector component in so that the displacement on all components of $\{X\}$ are unique (32). The displacement vector $\{X\}$ can therefore be expressed as:

$$\{X\} = [\Psi]\{p\}$$

Where $[\Psi]$ is the matrix of eigenvectors and $\{p\}$ is the vector of the principal coordinates. The size of the system will depend on the number of modes to be considered.

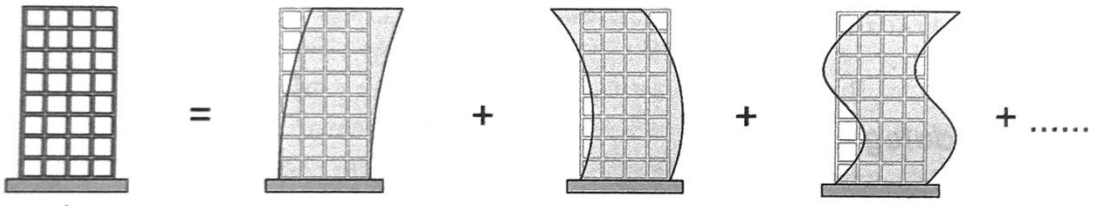

Figure 25. Modal decomposition representation (33)

The resolution of the motion equation by finding the displacement components for each mode allows as well as the determination of the maximum seismic forces when introducing the elastic response spectrum. The elastic response spectrum is a graphical representation of the maximum response of a structure to seismic ground motion at

different periods of vibration. It is constructed based on earthquake magnitude, distance to the earthquake fault, fault mechanism, wave-travel-path geology, and local soil conditions (32). In this study, modal analysis was performed to obtain the necessary parameters for defining loads and damping in subsequent analyses, rather than to assess the forces themselves. Therefore, the elastic response spectrum is not described in detail. More information can be found in the literature.

5.2 Non-Linear Static Analysis

The non-linear static analysis, also known as the "Pushover" analysis, is an iterative incremental procedure used to calculate the response of a structure when applying horizontal loads or displacements. The response is measured as a curve that associates the reaction forces at the base of the structure with the displacement of a significative point. This approach involves gradually incrementing the horizontal load applied to the structure, and at each increment or "step," reaching equilibrium by iterating. The load increment, denoted as P_i, is a multiple of the nominal load, P_0, such that $P_i = \lambda_i P_0$, where λ_i represents the load factor of the i-th increment (33).

In non-linear systems, the proportional relationship between the load and displacement, represented by the stiffness matrix, is no longer valid. To determine the non-linear response, an initial load value must be assumed ($\lambda_{i-1} P_0$), which corresponds to a displacement U_{i-1}. As the load is incremented by increasing the load factor, the displacement that corresponds to the next step is unknown due to the non-linearity of the system (33).

To achieve a solution, an approximation is carried out by assuming linear behavior between two steps, provided they are infinitesimally small. At this stage, the effective (inelastic) resistance mobilized by the structure due to the displacement U_f can be verified for the considered step, and the value of the residual load R can be evaluated (Fig 26). This process is repeated until the prefixed tolerance criteria are met, which can be based on displacements, forces, or the product of both (energy) (33).

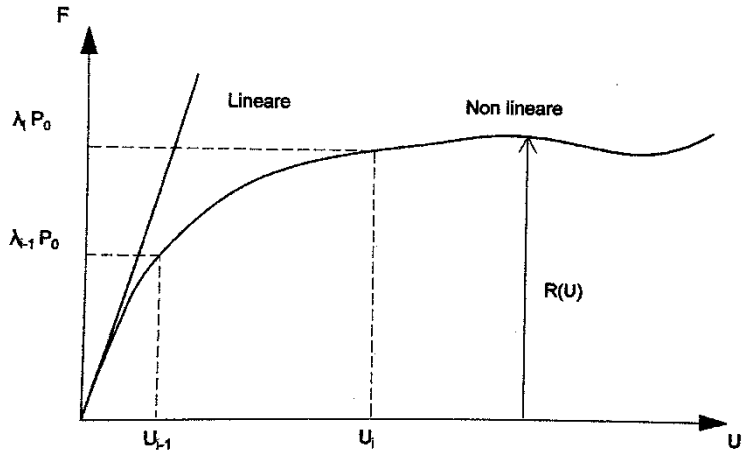

Figure 26. Non-linear static analysis (33)

5.2.1 Newton Raphson

Regarding the solution procedures for non-linear problems, the most utilized approaches are the Newton-Raphson or modified Newton-Raphson methods (33).

The Newton-Raphson method is referred to as indirect because it gives an approximate solution obtained through an iterative process, which starts from the result obtained in the previous step *k*, such as:

$$\Delta U^{k+1} = [K(t)^k]^{-1} R(t) - F^{int}(t)^k$$

Where:

$$U(t)^{k+1} = U(t)^k + \Delta U^{k+1}$$

The iterative process will stop when the difference between two successive roots is small enough. In the Newton method, the error is proportional to the square of the error in the previous step, which is called quadratic convergence. But the computational cost of this method is high because the solver calculates the stiffness matrix *K* at each step. A modified Newton-Raphson method can be used to reduce computational costs by only calculating the stiffness matrix once and then keeping it constant for the remaining steps.

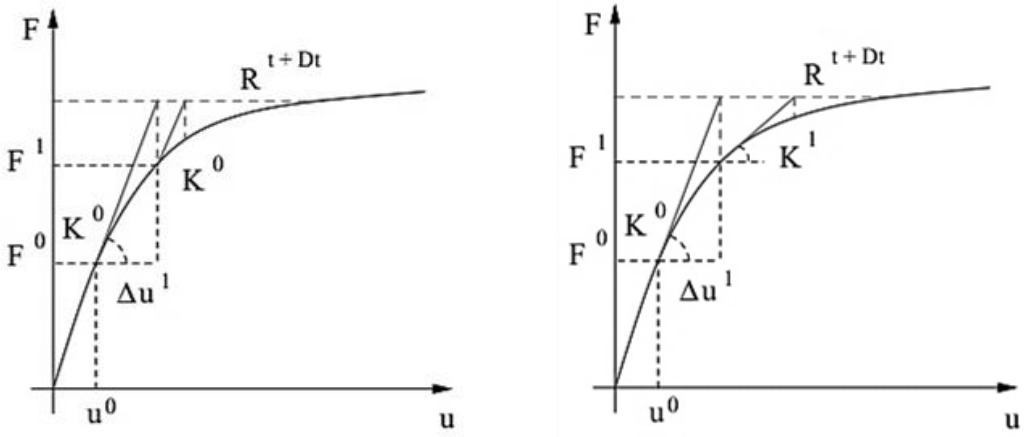

Figure 27. Representation of the method, a) Newton Raphson; b) Modified Newton Raphson (34)

5.2.2 Lateral force distributions

To ensure the accuracy of pushover analysis with regards to the building's response, it is crucial to select an appropriate load profile. The challenge lies in the fact that the structure's reaction to seismic activity is primarily determined by the inertial forces that are generated in its elements because of displacements (and acceleration) caused by the ground motion. Pushover analysis, on the other hand, is an inverse procedure where forces are applied to capture the structure's displacement. Therefore, it is essential to select a load profile that closely resembles the seismic response. There are various load distributions available, the most used are explained below:

5.2.2.1 Distribution proportional to the static forces

This distribution relies on the assumption that the first mode of vibration is representative. This means that the participation mass of the first frequency should be superior to 75%. In this case, the displacement components can be represented as a function of the quote of the masses. The force to be applied at each floor is calculated using the following formula,

$$F_i = \frac{z_i W_i}{\sum z_j W_j} V_b$$

Where:

- W_i, W_j are the seismic weight of the i-th and j-th mass.
- z_i, z_j are the quotes at which the i-th and j-th mass are located.
- V_b is the base shear of the structure.

This distribution is commonly regarded as inverse triangular due to the shape that results when the masses are similar at each floor. It intends to simulate the trend of the inertial forces generated during an earthquake in a regular building (33)

5.2.2.2 Distribution proportional to the fundamental mode of vibration

This distribution considers the fundamental mode in the calculation of the forces to be applied at each floor. For each direction, the eigenvectors are calculated and multiplied by the vector of the masses, whose components are the values of the mass at each floor, to obtain the force vector. Each component will be:

$$F_i = \phi_{1i} m_i$$

The purpose of this distribution is to accurately represent the deformation profile of the first mode shape, making it an optimal choice as it considers both masses and displacements from a previous analysis. However, this method is only applicable to structures with a participation mass of more than 75% in the first mode (33)

5.2.2.3 Distribution proportional to the masses.

This distribution is usually known as “uniform” because generally the masses at each floor are equal, therefore, the profile derived from this is constant along the height of the structure. At each floor, the force to be applied is

$$F_i = m_i$$

Where m_i is the mass belonging to the i-th floor.

This distribution intends to magnify the displacement and resistance demand on the lower floors of the structure. In fact, the resultant force is usually lower than the resultant from triangular distributions incrementing the floor shear force with respect to the overturning moment (33).

5.2 Non-Linear Dynamic Analysis

The non-linear dynamic analysis is the most advanced and accurate in simulating the real effects of the seismic action on a structure as it includes all three components (two horizontal perpendicular and one vertical). The analysis requires a 3D non-linear model and a considerable computation effort to perform the numerical integration of the motion equation defined as (33):

$$M\ddot{U} + C\dot{U} + F(U) = -MR\ddot{x_g}$$

Where:

- M is the mass matrix.
- C is the damping matrix.
- F is the internal forces vector.
- $U, \dot{U}$ and $\ddot{U}$ re the displacements, velocity, and acceleration respectively
- R is the vector related to the influence of the earthquake, proportional to the masses and to the ground acceleration.

To perform the analysis, once defined the geometric model, the following steps are needed:

- Definition of the seismic mass. In most softwares, mass and loads are treated separately, therefore it is important to double check the specific requirement according to the program used. Masses can be defined as lumped in the nodes or distributed along an edge or surface.
- Definition of the non-linear constitutive model, to ensure the dissipation of energy and possibly capture the damage.
- Definition of the damping, using models proposed in the literature that consider a viscous damping proportional to the masses and/or stiffness such as the Rayleigh damping model.
- Selection of the time history (accelerograms) to be assigned at the base of the structure. These can be either natural, artificial, or synthetic (33).

5.2.1 Definition of the viscous damping, Rayleigh method.

The seismic energy absorbed by a structure during a seismic event can be dissipated in many ways. A first typology of damping is the hysteretic damping, which is implicitly considered in the non-linear constitutive model that characterizes the inelastic response of the material. However, there is a quantity of dissipated energy that cannot be modelled as it comes from the frictional forces between structural and non-structural elements, friction forces in the cracks of the masonry, among others. A way to consider this additional dissipation of energy is applying the Rayleigh model, which is proportional to the mass and stiffness of the structure. A further explanation is given as it was the selected method to introduce damping in the dynamic analysis of the aggregate (32).

Two independent systems are considered, one will have a mass-proportional damping and the second, a stiffness-proportional damping such as:

$$c = a_0 m \quad \text{and} \quad c = a_1 k$$

The constants a0 and a1 have units of s−1 and s, respectively. For both damping matrices the, matrix C is diagonal. Stiffness proportional damping can be considered as the energy dissipation arising from story deformations. For the first system, the generalized damping and damping ratio of each mode can be computed as

$$C_i = a_0 M_i \quad \text{and} \quad \zeta_i = \frac{a_0}{2}\frac{1}{\omega_i}$$

Consequently, a_0 can be derived.

$$a_0 = 2\zeta_i \omega_i$$

Similarly, for the second system, the generalized damping for each mode and damping ratio are. In this case, any other mode should be considered, for example the j-th.

$$C_i = a_1 \omega_j^2 M_j \quad \text{and} \quad \zeta_j = \frac{a_1}{2}\,\omega_j$$

Therefore,

$$a_1 = \frac{2\zeta_j}{\omega_j}$$

Since Rayleigh damping considers both damping typologies, we can express:

$$c = a_0 m + a_1 k$$

$$\zeta_n = \frac{a_0}{2}\frac{1}{\omega_n} + \frac{a_1}{2}\,\omega_n$$

The coefficients a_0 and a_1 can be determined from specific damping ratios that belong to two different modes. Expressing the damping ratio equation in matrix form, we have

$$\frac{1}{2}\begin{bmatrix} 1/\omega_i & \omega_i \\ 1/\omega_j & \omega_j \end{bmatrix}\begin{Bmatrix} a_0 \\ a_1 \end{Bmatrix} = \begin{Bmatrix} \zeta_i \\ \zeta_j \end{Bmatrix}$$

If we consider that the damping ratio is the same for each mode, from the system of equations, a_0 and a_1 can be calculated as:

$$a_0 = \zeta\frac{2\omega_i\omega_j}{\omega_i+\omega_j} \quad \text{and} \quad a_1 = \zeta\frac{2}{\omega_i+\omega_j}$$

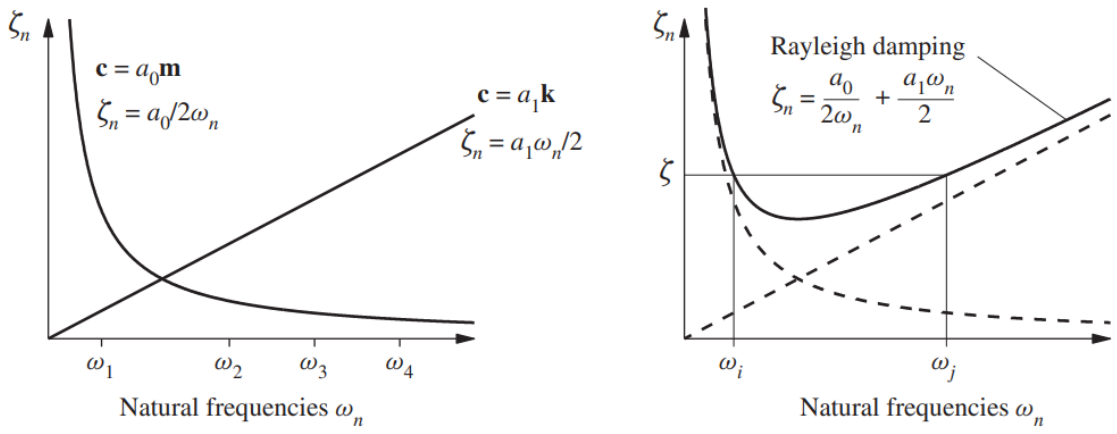

Figure 28. a)variations of modal damping with frequencies; b)Rayleigh damping (32).

6. Validation of the homogenized masonry modelling approach

To validate the model, a calibration of the material properties used for the constitutive model is carried out. When using the homogenized masonry approach, this is especially important due to the difference in the crack evolution with respect to the micro-modelling approach. As previously explained in chapter 3, masonry is prone to softening behavior with low stress. This behavior causes great instability in the numerical models and increases the dependence on fundamental parameters such as the tensile strength.

The selection of the case study was based on the requirement of having a model that remains valid when scaled up to a larger size, as explained in chapter 3 regarding the "size effect." For this reason, a masonry building was chosen rather than calibrating the model using a single wall.

6.1 Description of the case study

The case consists of a two-story rectangular masonry building tested at the University of Pavia and described in detail in (4). The four walls that make up the structure have a total thickness of 250 mm. The dimensions of the building were 6 m by 4.4 m in plan and 6.4m height. The wall “D”, named “Door Wall”, which was parallel to the loading, was Semi-connected from the transverse walls. These two were connected to the adjacent “Window Wall” by the corner with an interlocking brick pattern. More detail regarding the dimensions of the building can be found in Fig. 29.

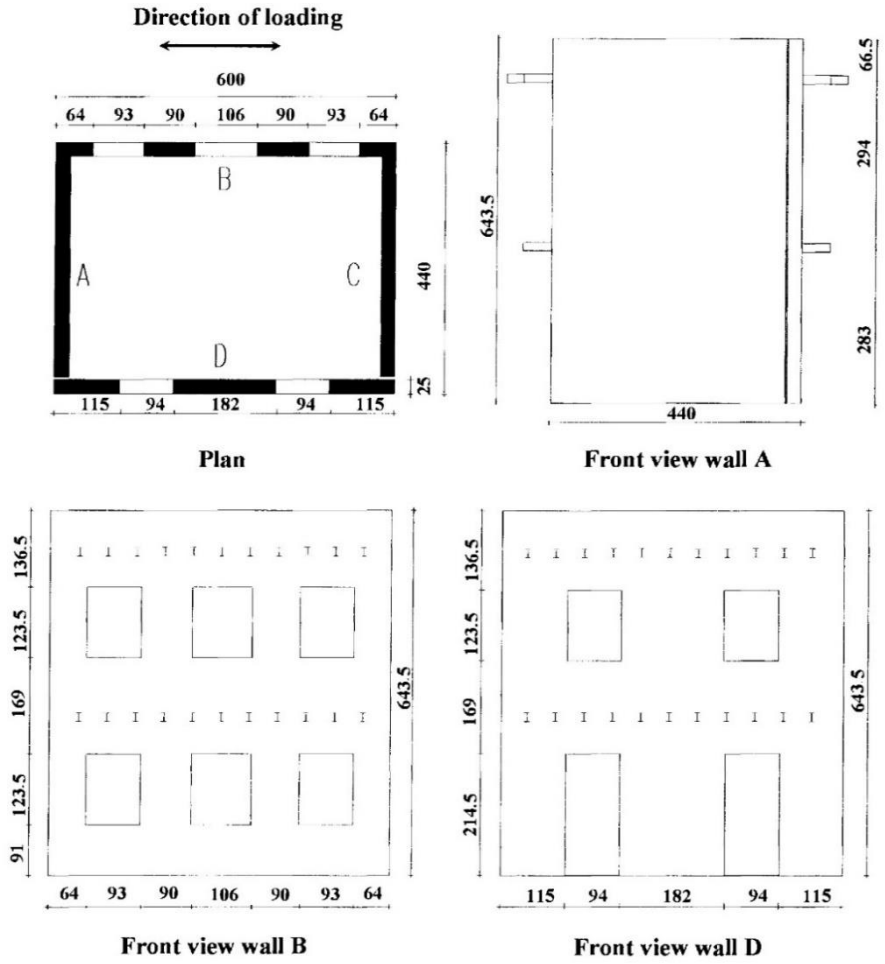

Figure 29. Dimension of the building (4).

The connection between the Door Wall and the rest of the structure was done by the floor beams: A series of equally spaced steel "I" profiles with 140mm of height designed to simulate the flexible diaphragm (4).

Vertical loads are applied though beams using concrete blocks. A total of 248.4 kN was applied to the first floor and 236.8 kN to the second floor, reaching approximately 10 kN/m^2 per floor (4).

A dynamic test in a shaking table was performed to measure the loads in both floors. They were nearly equal because the mass and peak accelerations of both levels were the same. Similarly, due to the pinned connection between beams and walls, the force in the Door Wall and Window Wall were equal. Therefore, the displacements were governed by the stiffness of each wall. From these results the authors concluded that four equal

concentrated forces should be applied though the intersection between beams and walls at the floor level, as shown in Fig. 30 (4).

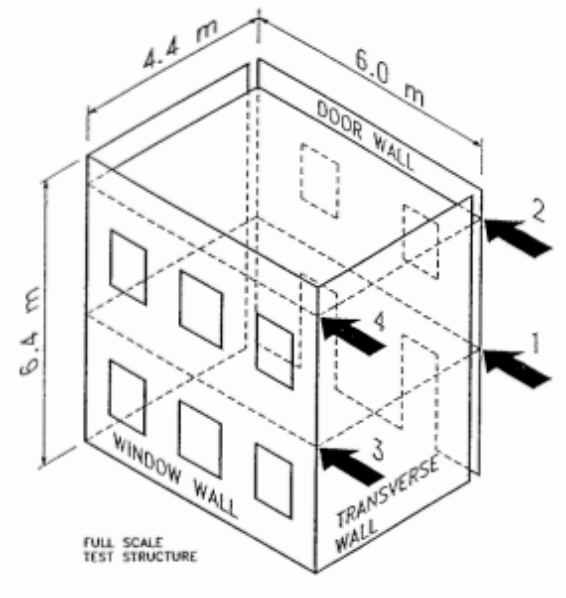

Figure 30. Forces applied during experimental cyclic tests (4)

A sequence of test runs was then performed in which the maximum top displacement in each wall was gradually increased until the maximum desired drift for the run is achieved. Each test involved multiple cycles, including a preliminary loading cycle, two cycles at the desired maximum displacement, and a degradation cycle. From the tests, the results obtained for each wall are represented in Fig. 31.

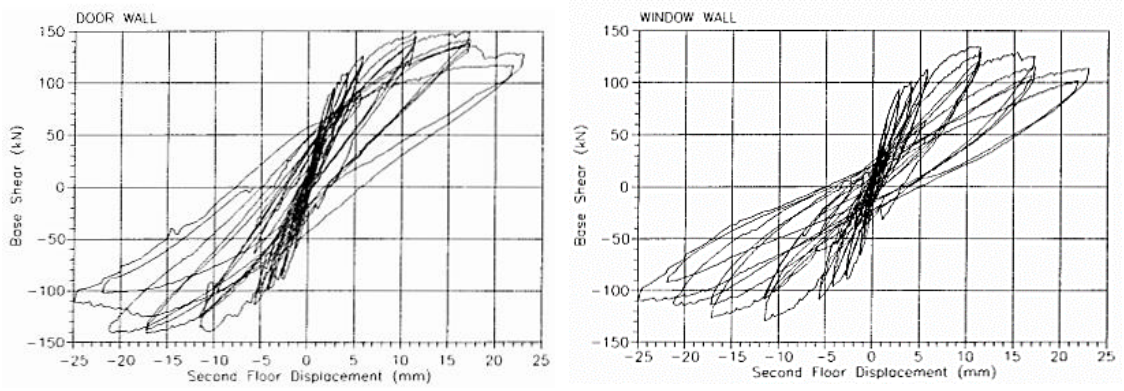

Figure 31. Results from experimental test. a) Door Wall; b) Window Wall (4)

6.2 Numerical model

As indicated by the authors, due to the flexible floor and the disconnection between the Door Wall and the Window Wall, this experiment could be analyzed in 2D. However, it was decided to proceed with the full 3D model to consider the influence of the lateral walls in the overall results.

By means of STKO, we reproduced the experimental test using the homogenized masonry approach. According to the source, the "Door Wall" was not properly connected to the rest of the masonry structure at the corners. Instead, it was connected to the rest of the structure through the use of beams. The other three walls were modelled using the merge command, that allowed the full Boolean intersection between the nodes, as shown in Fig. 32.

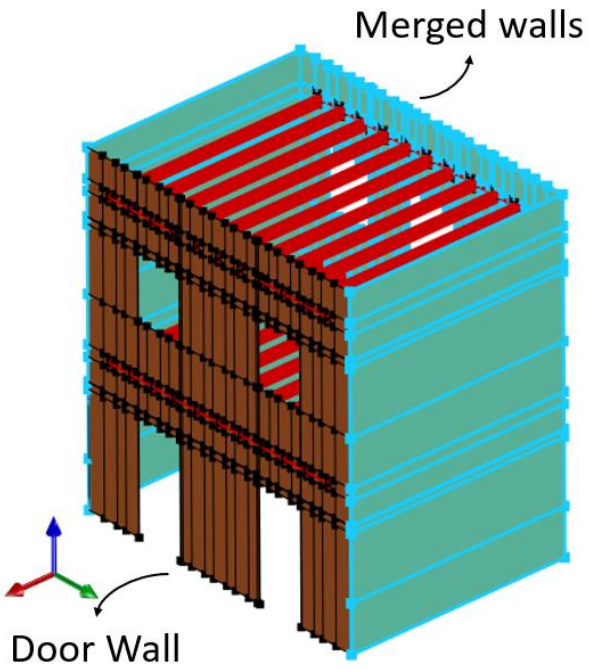

Figure 32. 3D model

To take advantage of the velocity of a 4-node element and the *ASDShellQ4*, all walls were designed as a composition of smaller faces that followed the design of openings to make sure each element had 4 nodes (Fig. 33)

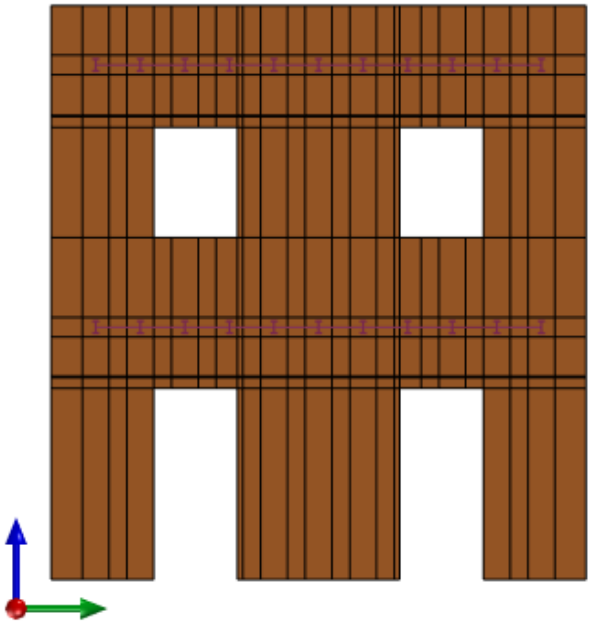

Figure 33. Optimized geometry

The four horizontal forces applied in the experimental test were introduced in our model as punctual forces on the beam ends. All push forces are equal for each beam with a resultant equal to 1N. Because of the nodal forces, a simple embedded connection was not enough. The nodal forces would immediately pull out the beams from the wall causing localized damage and preventing the transfer of forces to the rest of the wall. For this reason, beams were connected to walls using a node-to-node intersection with a Rigid Link type beam applied to it. In this case, the nodes connected have both the translational and rotational degrees of freedom constrained. To avoid the concentrated damage on the wall, a rigid region was created around each beam. All beam ends were selected as master nodes while the regions were chosen as slaves. For this command to work properly it was important to leave some space between on region and the next, as shown in Fig. 34.

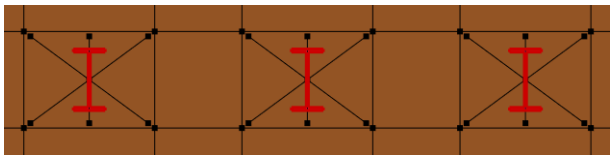

Figure 34. Beam-to-wall connection, rigid regions around the beams.

According to the source images of the experiment, the beams seem to be connected to each other by the ends by an external beam. Since we do not have information about the

dimensions, we calibrated a circular steel bar until finding the diameter that best matched the experimental curve. This was achieved with a diameter of 5 mm.

6.3 Material parameters

The walls were modelled using the *ASDConcrete3D* constitutive model using the IMPL-EX algorithm that provides a faster and easy to achieve convergence, as explained in chapter 4.

The material parameters used where taken from the suggestion provided in (35) where a numerical analysis was performed on the same experimental tests.

Regarding the constituent materials, terracotta bricks with an average compressive strength of 16 MPa on cubic samples were chosen, along with a mortar composed of hydrated lime and sand in a volume ratio of 1:3 and a compressive strength between 2 MPa and 3 MPa.

Characterization tests carried out on masonry prisms resulted in a compressive strength of about 6.2 MPa, while the tensile strength was found to be 0.18 MPa. The elastic modulus was determined to be 1490 MPa. These values were optimal, with the exception of the tensile strength, which was reduced to 0.15 MPa to better match the experimental results.

Additionally, tensile plasticity was assumed to be 0. Parameters are reported on table 1.

Table 1. Masonry physical properties

f_t $[MPa]$	f_{cp} $[MPa]$	G_t $[J/m^2]$	G_c $[J/m^2]$	E $[MPa]$	ν [-]
0.15	6.2	80	14000	1490	0.2

The resultant surface is reported in Fig. 35

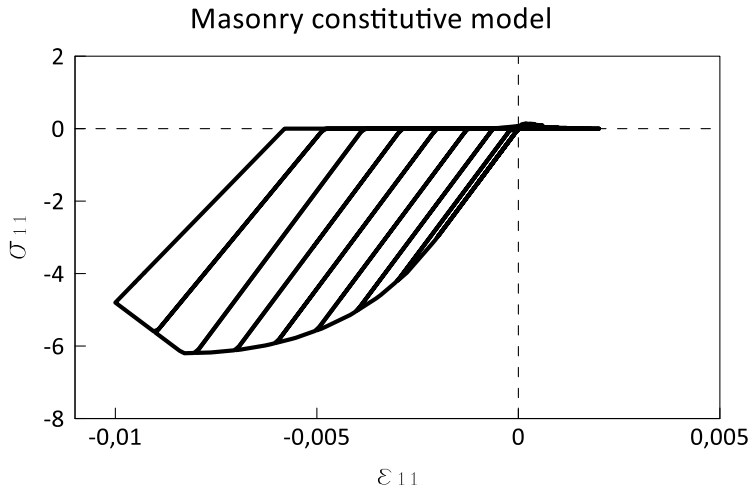

Figure 35. Masonry constitutive model.

6.4 Non-linear static analysis

For the case study, two pushover analyses have been carried out: one only pushing the door wall and measuring the displacement of the top floor and respective reaction force at its base; and a second one pushing only the "Window Wall" measuring its top floor displacement and reaction force at base. The lateral forces followed a uniform mass-proportional profile (explained in section 5.2.2) since both stories had similar masses. The value of the nodal force on each beam were identical, such as the total load applied to the structure was equal to 1N.

The analyses were done using a displacement control with a target displacement equal to the maximum displacement measured on the experimental tests. The mesh was set to 10cm as it proved a good compromise between the results and the capacity of computation using only 4 cores for a total of 12330 nodes and 17799 elements (Fig. 36). The number of steps was set to 300, resulting on an analysis duration of 1 hour and 6 minutes.

Color	ID	Nodes	Elements
	0	2886	4930
	1	3128	4005
	2	2923	5021
	3	2965	3843

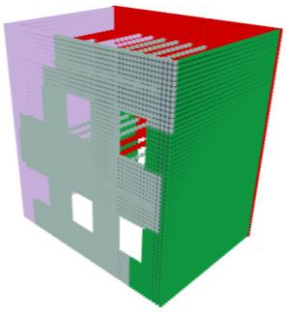

Figure 36. Model Partitioning

6.5 Results

Door wall

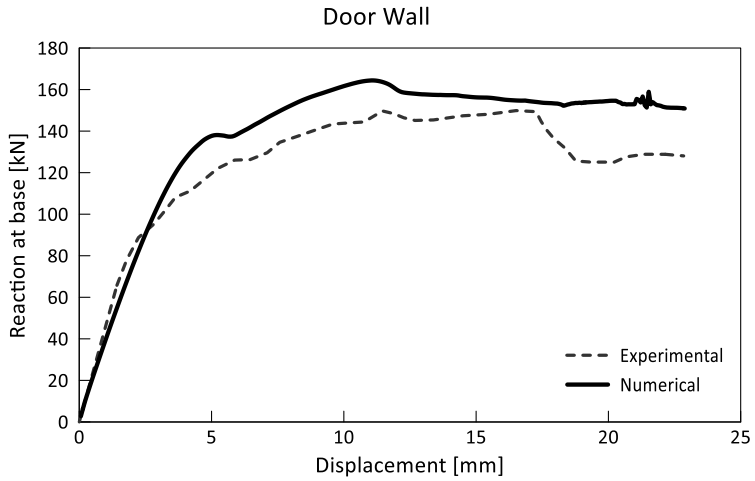

Figure 37. Comparison between experimental and numerical curves, Door Wall.

The numerical curve from Fig. 37 shows the first peak at 5 mm, in correspondence with the experimental one, but with a 15 kN difference that is maintained over almost all steps. This first fall happens when the crack that develops from the right bottom of the right window reaches the flexural damage at the beam level. The second peak is achieved at a resistance of 165 kN, at 11mm, when the shear cracks along both spandrels is fully developed. The successive softening branch involves the evolution of the shear cracks in the central and right pier as shown in Fig 38.a.

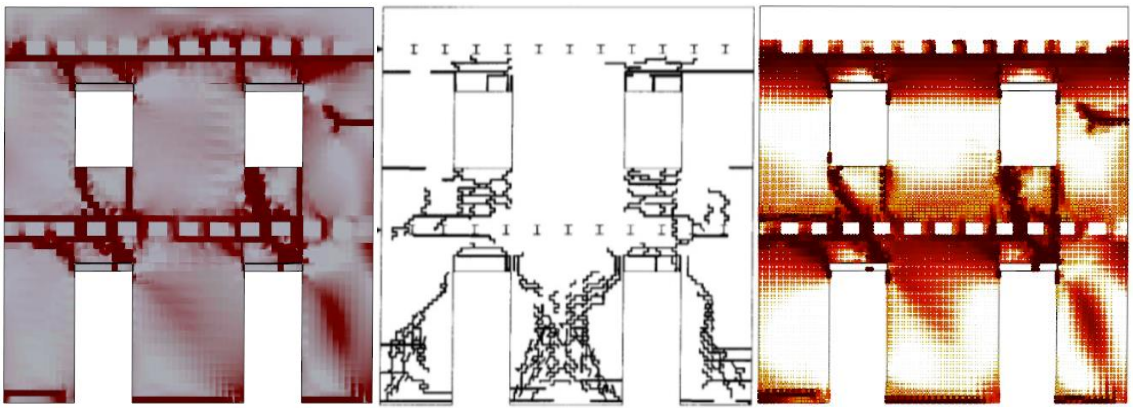

Figure 38. Door Wall results comparison. a) numerical model maximum force principal; b)experimental model; c) numerical model damage

Window Wall

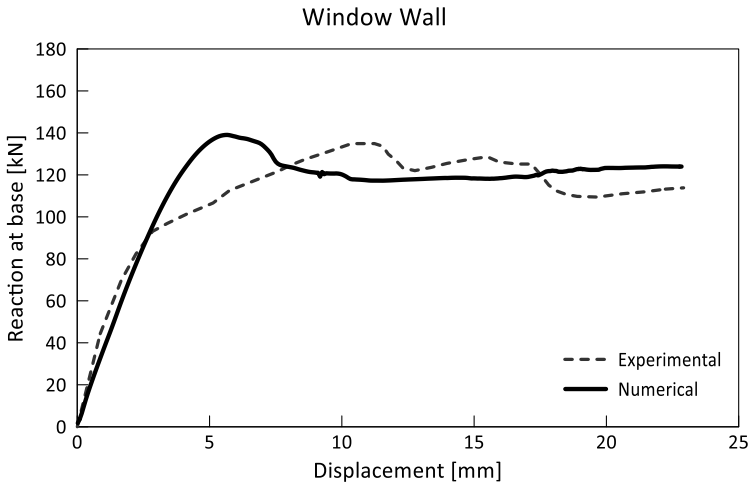

Figure 39. Comparison between experimental and numerical curves, Window Wall.

At 5 mm, the curve for the numerical model (Fig. 39) reaches its peak, whereas the experimental curve reaches its peak at 12 mm. This difference is acceptable given the dissimilarities between crack propagation in a homogenized model and a physical masonry sample, particularly in low-tensile-strength samples. In the latter, cracks tend to follow mortar joints, resulting in a gradual decrease in resistance. In homogenized masonry, however, cracks follow the shortest path across the masonry. As a result, the numerical model accumulates more resistance before abruptly losing it in fewer steps, as can be seen in the curve. The damage comparison is shown in Fig. 40.

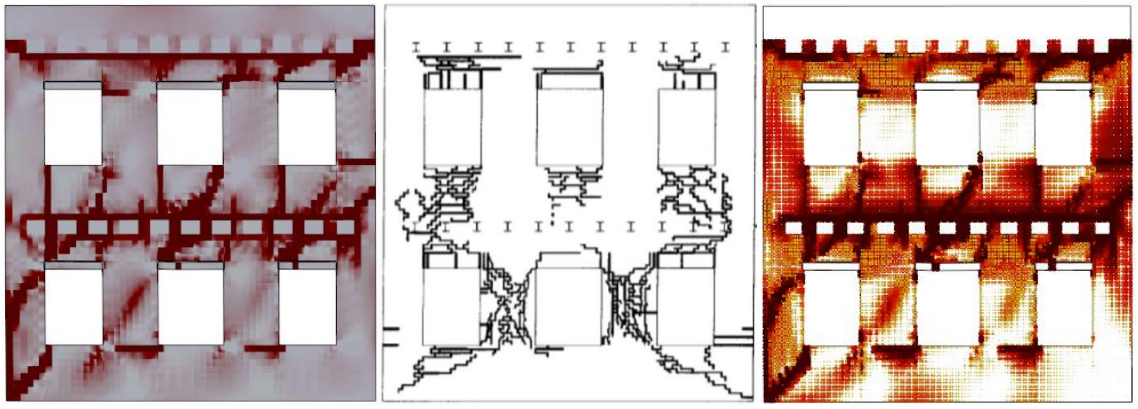

Figure 40. Window Wall results comparison. a) numerical model maximum force principal; b)experimental model; c) numerical model damage

Both results show a good match between the envelope taken from the experimental test and the numerical analysis. The model exhibited a high degree of susceptibility to

variations in material parameters, due to the extensive flexural damage observed in the structure following the application of vertical loads. When horizontal forces are applied, shear cracks begin to form. If these cracks spread to the damaged area early in the pushover analysis, the building's resistance decreases drastically. To control the evolution of these cracks, precise calibration of tensile strength and fracture energy was needed.

7. Case study tests of masonry building aggregate

7.1 Description of the reference case study

This study focuses on capturing the possible beneficial effect of aggregate construction. For this reason, the model under consideration was created as a group of similar single units. This allowed us to compare the results obtained from the external units when pushed in both positive and negative directions, without the influence of geometrical differences in the response.

The aggregate is composed by 3 units of three stories each. The central unit (Unit 2) shares the same divisor wall with Unit 1 and Unit 3. The aggregate is 24x12.6 m in the longitudinal and transverse direction respectively, being 11.2m tall. In the Fig. 41 the 3D model is shown. Detailed dimensions are reported in the appendix.

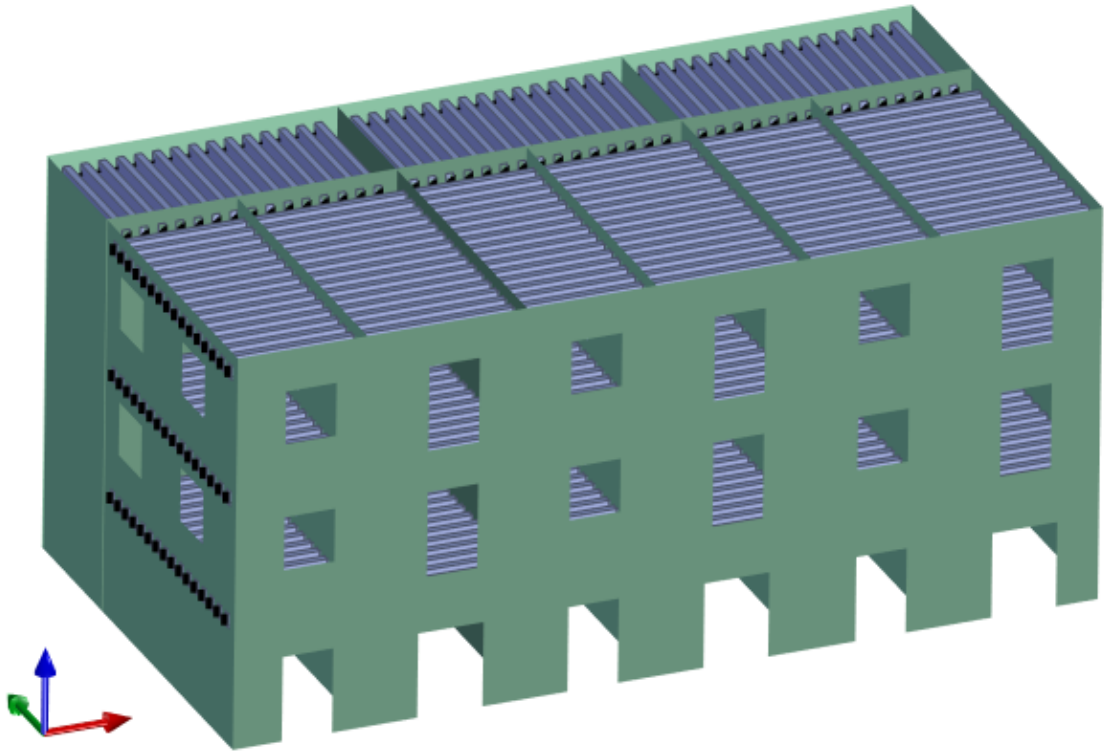

Figure 41. a) 3D Model

In the longitudinal direction, the aggregate has 3 walls that will be denominated “Front Wall”, “Middle Wall” and “Back Wall”. These walls have openings disposed asymmetrically, except for the back wall, which has 1 centered opening per story. The opening’s disposition for each wall can be observed in Fig. 42, 43 and 44 respectively.

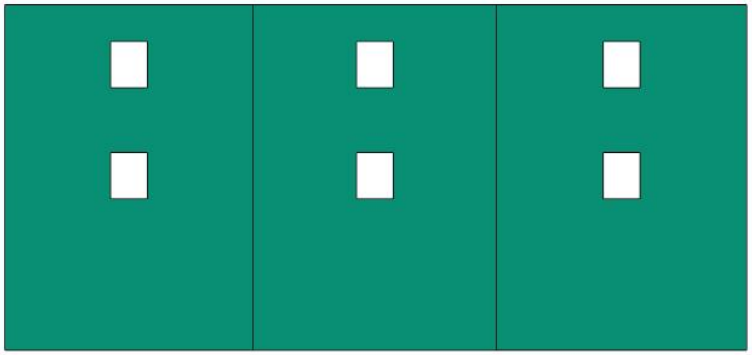

Figure 42. Back Wall

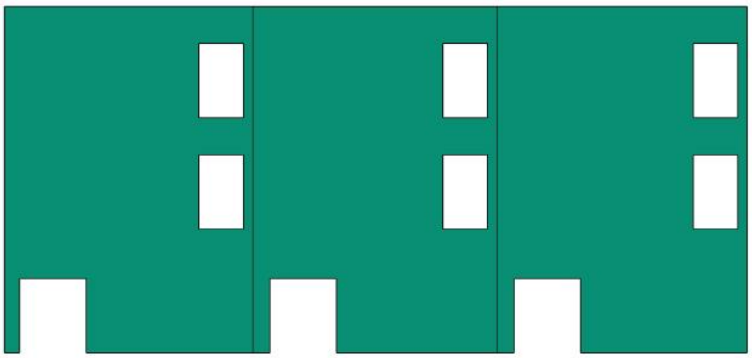

Figure 43. Middle Wall

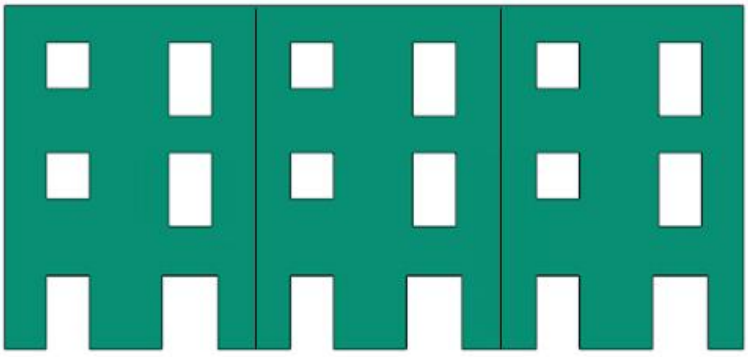

Figure 44. Front Wall

In the transverse direction (Y), the internal walls of each unit and the two external walls of the aggregate contain openings, as shown in Fig 45.

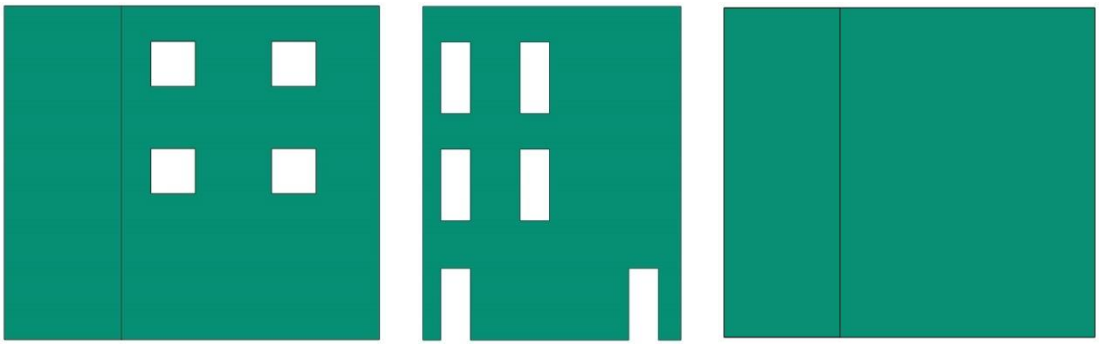

Figure 45. a) External walls; b) internal walls; c) U1-U2 and U2-U3 shared walls

All external walls present a thickness of 50cm, while internal and shared walls have a thickness of 50cm in the first story and then a thickness of 30cm in the second and third story.

The aggregate was studied hypothesizing two floor typologies: “Rigid Diaphragm” and “Flexible Floor” (explained in Chapter 2). For both typologies, the aggregate was analyzed as “Fully Connected” and “Semi-connected”. The “Fully Connected” scheme, implies that the connection of the longitudinal walls from Unit 1 and Unit 3 to the transverse divisor walls of Unit 2 is infinitely rigid. The “Semi-Connected” scheme considers these walls detached, but capable of arise contact and frictional stresses in the contact point marked with blue circles in Fig. 46.a. Additionally, the individual models of the units were analyzed as well, denominated as “Isolated.”

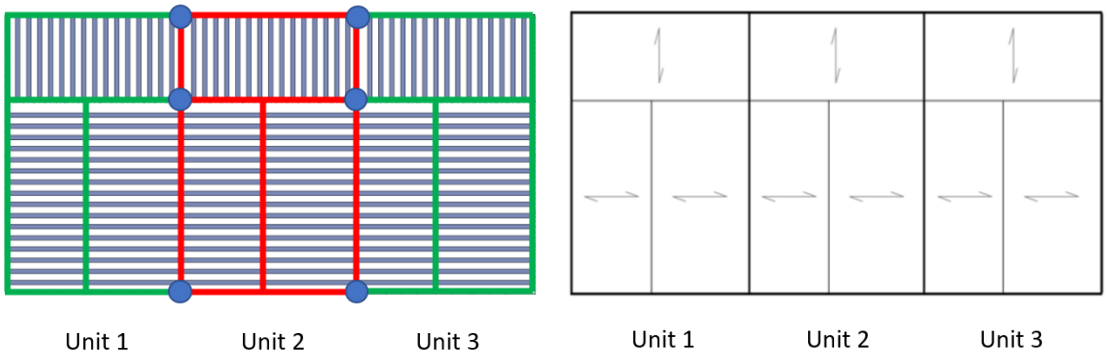

Figure 46. a) Contact points between units, Semi-connected case; b) orientation of slabs.

We conducted three types of analyses on the models. The first was a modal analysis, which helped us to identify the fundamental mode. We used the eigenvectors and frequencies of interest as input for the subsequent analyses. Next, we performed pushover analyses in both positive and negative X directions. We used a modal distribution of forces and compared the results with those obtained from a non-linear dynamic analysis.

For this analysis, we used a component of the L'Aquila earthquake as the acceleration input in the longitudinal direction of the aggregate.

7.1.1 Geometrical model

The geometry followed the premises established for the calibration model (chapter 6), where masonry was modelled using sewed faces to satisfy the 4-node element condition for the use of the *ASDShellQ4.* Faces we assigned a Layered Shell type of element with 5 integration points for the 50cm walls and 3 integration points for 30cm walls.

For the "Fully Connected" case, all walls were rigidly connected using the *merge* command. For the "Semi-connected" case, to introduce the contact forces, it was necessary to perform a node-to-element interaction between the faces (masters) and edges (slaves) involved. A zero-length contact element *zeroLengthContactASDimplex* was assigned to the interaction to introduce the Mohr-Coulomb friction law. The parameters introduced in STKO were the following:

Table 2. Contact element settings.

Dimension	3D
K_n	1e+08
K_t	1e+08
μ	0,7
Impl-ex	Yes
Distributed	Yes
Orientation type	From Element
Rigid Gap	No

Wood beams were introduced using the fiber section approach with a *forceBeamColumn* element with dimensions of 40x20 cm. In this case, beams were attached to the masonry walls using an embedded node-to-element interaction, with masonry faces as masters and beam ends as slaves.

To improve the dynamic response, it was necessary to include lintels. The presence of horizontal elements resistant to bending over the openings is a key element to prevent

bricks from falling due to their own weight. Additionally, they can increase the in-plane resistance of the spandrels. If lintels are properly anchored to the wall, the spandrel over the opening can be considered not only as a shear resistant element but as a bending resistant one. However, lintels cannot be attached directly to the masonry wall in the numerical modelling since the lintel is the first to detach during a seismic event. Merging it to the wall would overestimate masonry's capacity. To correctly simulate the sliding of lintels over the openings, an outline of mortar was introduced as shown in Fig. 47.

Figure 47. Lintel geometry

The two floor typologies in analysis were characterized with the difference in stiffness of the slab. In both cases wood beams were present as they also served for the vertical loading of the structure. In the flexible floor model, a wood plate of 3cm was added to provide a finite stiffness and some degree of containment to transverse walls when out-of-plane mechanisms are activated. Geometrically, the plate was merged to the beams to secure a rigid connection yet remained Semi-connected from the walls.

For the Rigid Diaphragm case, 1 master node for each floor was added and fixing it so the displacement in the x and y direction, and the rotation around z were allowed. Subsequently, a node-to-node interaction with a *rigidDiaphragm* condition was created between the master nodes and the borders of the walls, for the three stories.

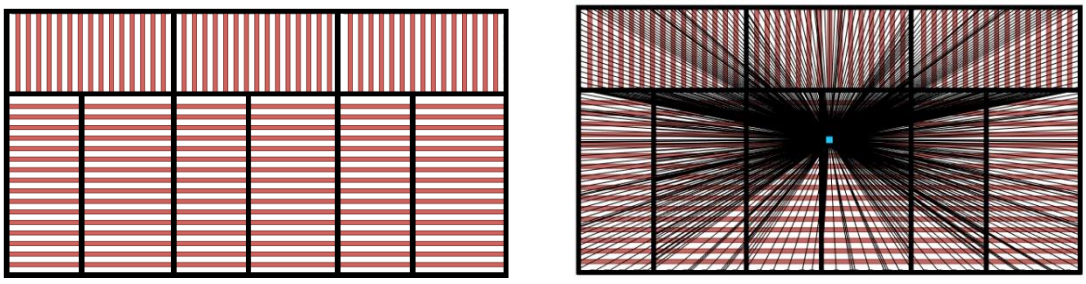

Figure 48. a) Flexible Floor; b) Rigid Diaphragm

7.1.2 Material parameters

Two types of material were used in the creation of the model: masonry and wood. Wood was used for both beams and the plates present in the flexible floor case. Wood physical properties and embedded settings are reported in table 3.

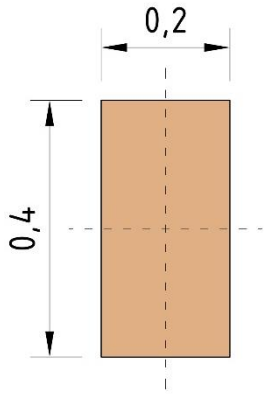

Table 3. Embedded settings

Penalty	5e+07
Constrain rotations	Yes

Table 4. Wood physical properties

$E\ [MPa]$	10000
$G\ [MPa]$	300

Figure 49. Wood beams physical properties and embedded settings

All materials that compose the masonry walls are modeled using the *ASDConcrete3D* constitutive model explained in chapter . Masonry material parameters used were taken from the previous calibration step detailed in chapter 6, table 1. Lintel material properties were chosen assuming a unique solid brick, as observed in multiple historical constructions. Material properties are reported in table 5.

Table 5. Lintel physical properties

f_t $[MPa]$	f_{cp} $[MPa]$	G_t $[J/m^2]$	G_c $[J/m^2]$	E $[MPa]$	ν [-]
1.6	16	120	30000	9600	0.2

Regarding the mortar surrounding the lintels, a user-defined setting was used. This choice was based on the need of a particular behavior that could not be designed using the pre-established 6P or 9P settings. The mortar is characterized by a purely elastic compression and a plateau behavior in tension. To define it, STKO gives the possibility to insert the three vectors that define the behavior curves for both compression and tension independently. The settings are reported in table 6.

Table 6. User-defined mortar parameters

Elasticity	E	1490
	ν	0.2
Tension	T_e	$[0\ ;\ 6.71141 \cdot 10^{-7};\ 1]$
	T_s	$[0\ ;0{,}001\ ;\ 0{,}001]$
	T_d	$[1\ ;1\ ;1]$
Compression	C_e	$[0\ ;1]$
	C_s	$[0\ ;1490]$
	C_d	$[1\ ;1]$

The resultant curve can be observed in Fig. 50.

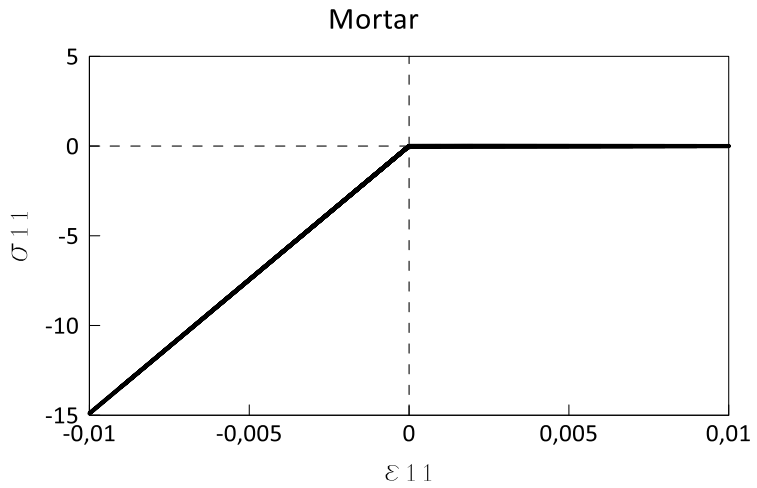

Figure 50. Mortar constitutive model

7.1.3 Loads, conditions, and analysis settings

A complete fixity of the walls at their base was considered for all cases.

Vertical loads were applied as edge forces to beams with a 2.5kN/m distributed load, following the typical magnitude of slab loads for these buildings. Masonry self-weight was instead applied as face forces distributed on the shells with a value equal to the specific weight of the masonry multiplied by the thickness of the shell. Both types of vertical loads were converted to masses and included in the model for the modal and non-linear dynamic analysis.

Pushover Analysis

Pushover forces were applied differently according to the floor typology. On the simplest case, the Rigid Diaphragm case, forces could be applied as nodal forces to the master node since the rigid connection was able to transmit the force to the masonry with any major numerical instability. On the other hand, several attempts were made to create the flexible floor. Initially, the wood slab was not taken into consideration, so forces were applied directly to the wall. This caused several convergence issues because damaged pieces of the wall would detach from the structure. Since a force was still applied, the piece of wall would experience infinitely large displacements causing convergence failure. This problem was solved by introducing the wood slab and applying a distributed face force.

A uniform profile was initially considered but later discarded due to the high stress caused at the base of the front wall. The presence of multiple openings caused the base piers to fail prematurely thus not allowing the complete development of the resistance in the rest of the building. The modal distribution (further explained in chapter 5) proved to be the most suitable as it considered both the response from the modal analysis and the masses of each floor.

The analysis settings were defined using a Penalty Method. Due to the presence of several multi-point constrain handlers that imply the reduction of the matrix may introduce errors. Therefore, Penalty Method was best suited. The penalty is chosen according to this general rule: computing the typical stiffness order of magnitude (OOM) of the model and increase it by 8. The penalty values alphaS and alphaM will be the 10^{OOM+8}. This increment is because a floating-point number will have 16 significative digits, so by adding 8 we are between the accuracy of the constrain and the numerical conditioning of the stiffness matrix.

Both the numberer and the system command were chosen to support the use of multiple processors during the analysis. These are the Parallel Reverse Cuthill-McKee Numberer and Mumps, respectively. In all pushover analysis a displacement control was used with a target displacement of 30 mm, using an Adaptive Time Step to secure convergence.

The algorithm selected was Krylov-Newton as it updates the stiffness matrix at a given interval to reduce the analysis time. The number of iterations before the stiffness matrix is reformed (*maxDim*) was set to 30.

The Norm-Increment Displacement convergence test was used with an iteration number between 15 to 30 (according to each model needs) and a tolerance of 0.0001. This test was chosen because of its compatibility with the constrain handler.

Non-linear dynamic analysis

Regarding the dynamic input, a component of L'Aquila earthquake was selected. The ground motion used in the present study was recorded in the station L'Aquila – v Aterno – Colle Grilli, in the North-South direction. It was introduced by adding a definition type *path* that allows the introduction of a non-constant time series defined by vectors. The ground motion record and correspondent elastic spectrum is reported in Fig. 41

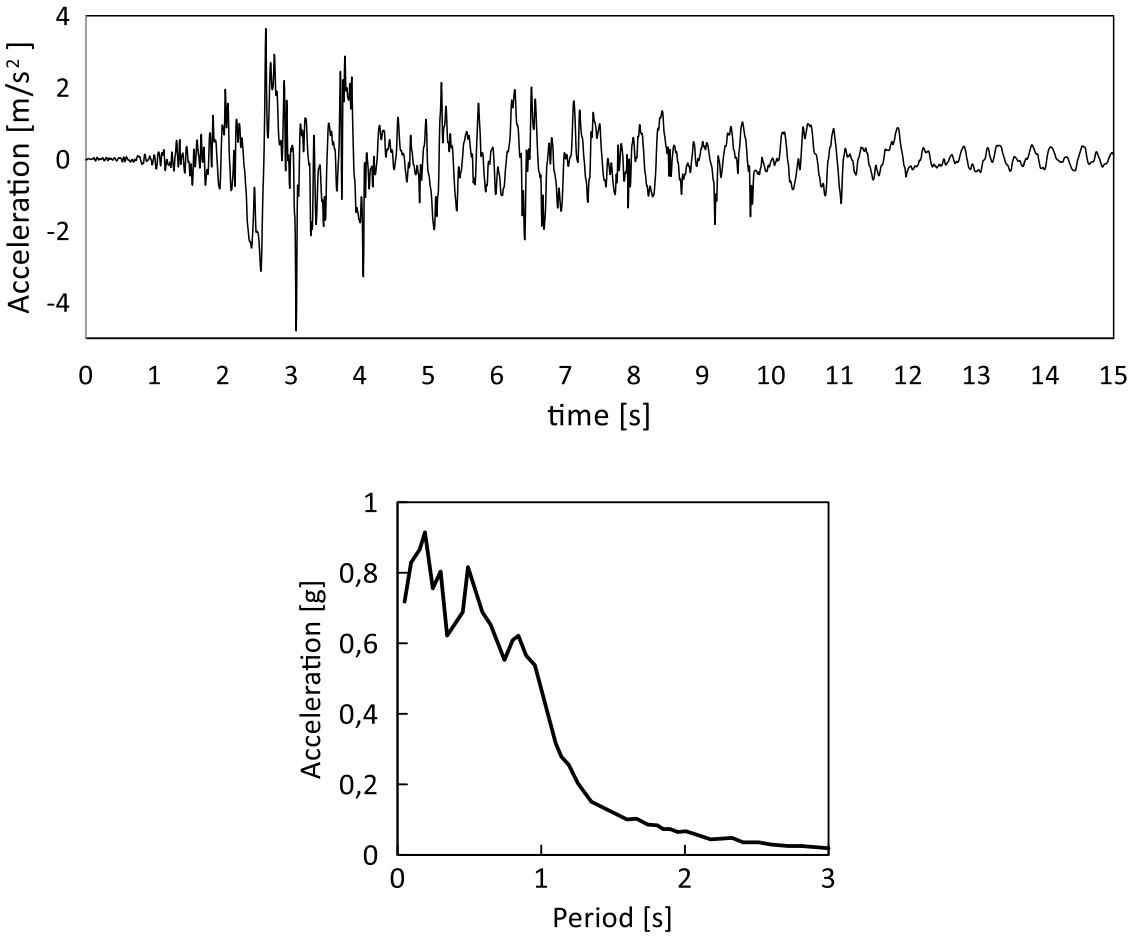

Figure 51. L'Aquila ground motion record and elastic spectrum.

The damping was introduced using the Rayleigh model using the first and second frequencies obtained from the modal analysis of each case. The damping ratio was set to 3%, which is the typically adopted value for masonry structures.

For the dynamic analysis, a transient analysis using TRBDF2 as integrator was selected. TRBDF2 (or Trapezoidal Rule-Backward Differentiation Formula 2) is a numerical integration method used to solve ordinary differential equations using a combination of the trapezoidal rule and backward differentiation formula. Firstly, TRBDF2 uses the trapezoidal rule to compute an initial estimate of the solution by approximating the area under the curve of the function between two points using a trapezoid. Secondly, it uses the backward differentiation formula to improve the accuracy of the solution by estimating the derivatives at the current time step using information from the previous time steps. The analyses were carried out using an adaptive time step with 3000 increments. System command, numberer, constrain handler and algorithm remained the same as established for the pushover.

7.1.4 Mesh architecture

The size of the mesh chosen was 300mm. Although it was a coarse mesh, the *ASDConcrete3D* has proven to be highly stable and able to produce accurate results almost mesh independent. Due to the large number of elements, all models were partitioned to run in multiple processors. The aggregate model used 12 processors with an average of 2400 elements per partition. The isolated model used 6 processors with an average of 2500 elements each (Fig. 52).

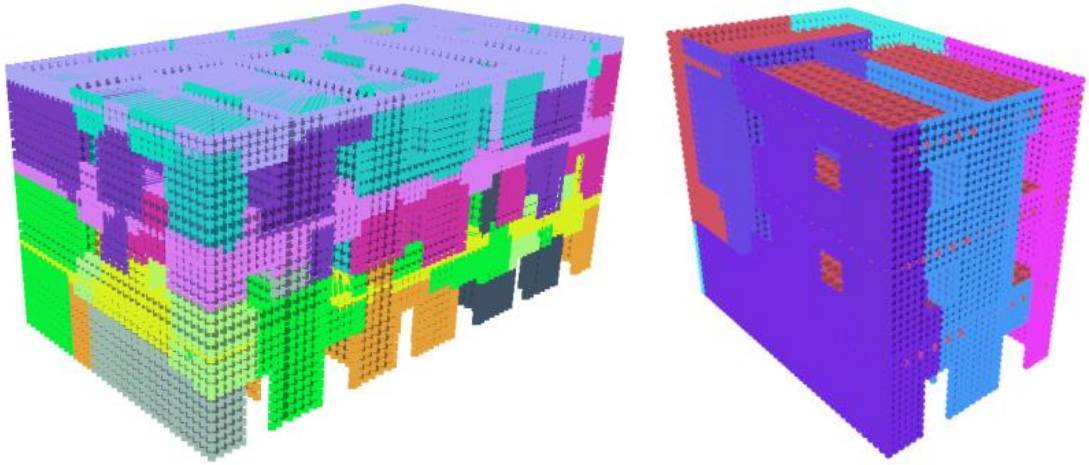

Figure 52. Partitioned model. a) Aggregate building; b) isolated unit

7.2 Rigid Diaphragm case

The Rigid Diaphragm case was the simplest, however, it became more unstable when analyzing the Semi-connected Units model because of the presence of multiple constrains in it.

For this case 6 different analysis were performed.

1. Aggregate fully connected Pushover.
2. Isolated Units pushover
3. Aggregate fully connected non-linear dynamic analysis.
4. Isolated Units non-linear dynamic analysis
5. Semi-connected aggregate Pushover.
6. Semi-connected aggregate non-linear dynamic analysis.

Additionally, a modal analysis of the aggregate and isolated units was carried out to establish the lateral distribution of forces for the pushover analysis and the frequencies used in the Rayleigh damping model.

The modal analysis was performed using the *eigen* command available in Opensees. The main issue with this command is that it does not support the Penalty Method as constrain handler, for this reason, after the vertical loading it was necessary to erase the previously used analysis settings. This can be done using the *wipe analysis* command. During the eigenvalue analysis, Opensees automatically chooses the appropriate constrain handler.

7.2.1 Aggregate fully connected Pushover.

The results from the modal analysis showed that the fundamental modal shape (Fig. 53) was mainly a displacement along the longitudinal (x) axis with a slight rotation around z.

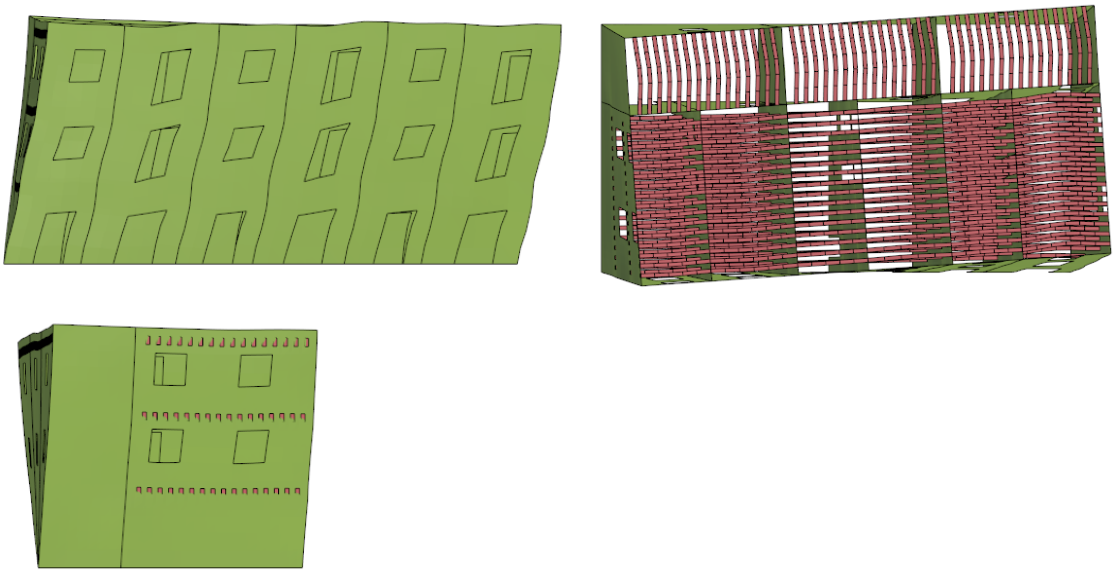

Figure 53. RD Aggregate Fundamental modal shape.

The dynamic properties of the structure are reported in table 7 and 8.

Table 7. Eigenvalue analysis results

MODE	OMEGA $[rad/s]$	FREQUENCY $[1/s]$	PERIOD $[s]$
1	39.75	6.32	0.158
2	42.19	6.71	0.148
3	54.34	8.64	0.115
4	97.08	15.45	0.064
5	101.51	16.15	0.061

Table 8. Modal participation mass ratios [%]

MODE	M_X	M_Y	M_Z	RM_X	RM_Y	RM_Z
1	67.0557	0.3254	0.0002	0.0805	5.4193	9.6206
2	0.4017	69.6957	0.0181	18.7799	0.0340	0.0057
3	8.5994	0.0287	7.90E-05	0.0091	1.7264	65.5089
4	0.2295	8.0823	0.1906	15.1859	0.4352	0.4453
5	3.9572	1.0192	3.7349	3.4921	15.7628	1.6520

We can observe three distinctive modes from the results reported in table 8. A fundamental mode in the longitudinal (x) direction; a second mode in the transversal (y) direction; and a third rotational mode (around z). This clearly shows the structure tendency to a box-like behavior, enhanced by the presence of the rigid diaphragm. The displacements of the barycenter of each floor were taken from the first mode of vibration to calculate the modal profile for the pushover analysis, reported in table 9.

Table 9. Lateral force distribution

Floor	ϕ_i	Norm. ϕ_i	Mass	Force	Norm. Force
3	3.217	1	314.60	314.604	1
2	2.442	0.759	410.07	311.287	0.989
1	1.216	0.378	669.99	253.338	0.805

These force's magnitudes were used for both positive and negative pushover analysis. The analysis was carried out on the entire aggregate and results on units were extracted from it. The reaction at base was taken from the longitudinal walls to avoid duplication of the magnitudes measured in shared walls. Results are reported in figure 54.

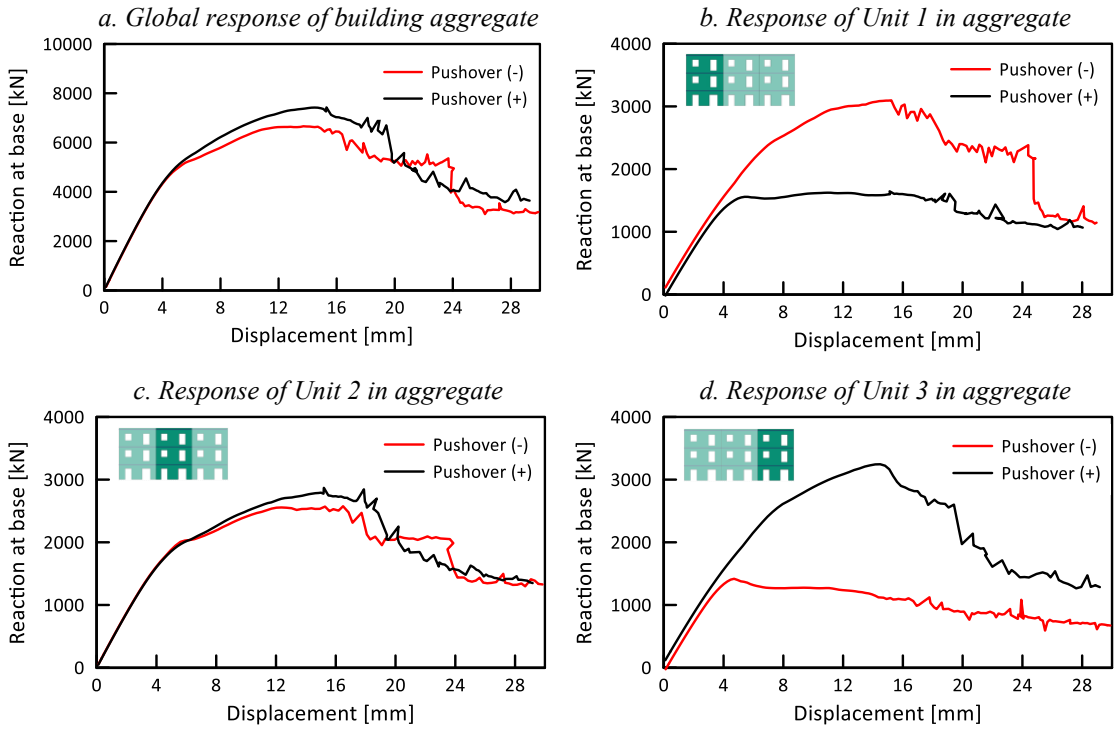

Figure 54. Pushover results, Rigid Diaphragm case. a) results on aggregate building. b), c), d) results on units taken from the aggregate analysis.

The aggregate building behaved in a similar way in both directions, reaching a peak resistance of 8000 kN. Based on the results, we can clearly see a symmetry between the external units (Unit 1 and Unit 3) when subjected to forces in both directions. When pushed in the positive direction, Unit 3 exhibits a doubled resistance compared to the pushover in the negative direction, whereas Unit 1 demonstrates this increment when the aggregate is pushed in the negative direction. The middle unit (Unit 2), on the other hand, does not experience a significant change between the two analyses, yet its peak resistance (3000) is slightly lower that the peak resistance of external units.

The 3D view reported in Fig. 55 shows the shear failure of the base pillars, as well as the damage in the spandrels with thinner section, located between the openings. The transverse walls do not present major damages except for the diagonal cracks developed from the corner of the openings towards the location of the rigid diaphragm. There is also a presence of some flexural mechanism at the base an at the second floor.

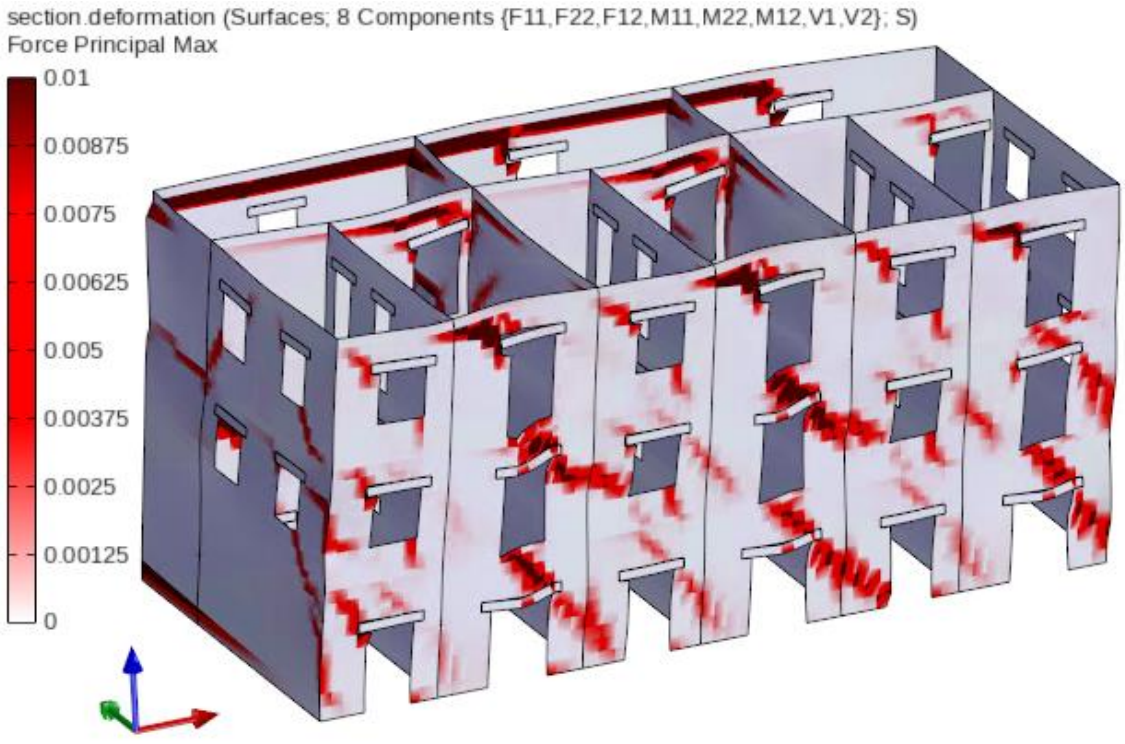

Figure 55. RD Aggregate 3D, pushover X+ direction, crack pattern.

The damage correspondent to both directions is reported in Fig. 56.

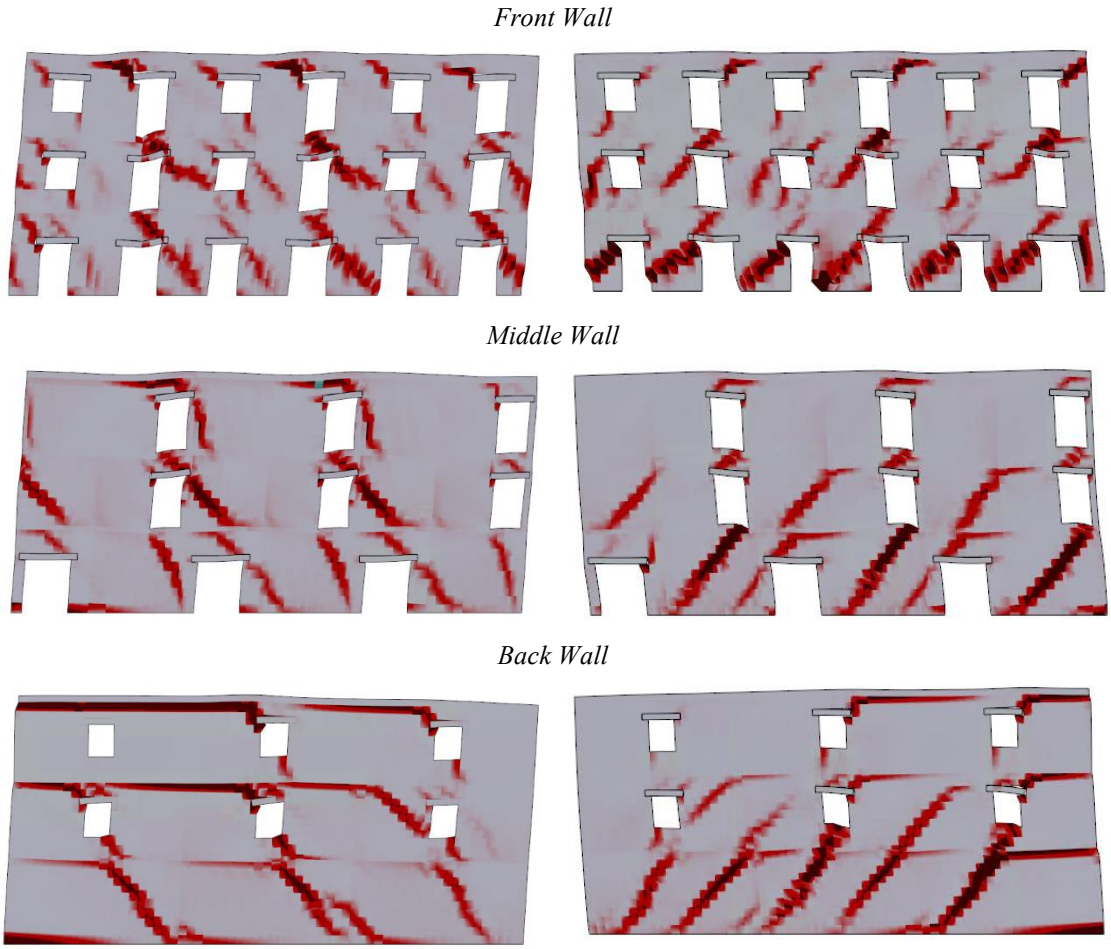

Figure 56. RD Aggregate, Pushover crack pattern. a) X+ direction; b) X- direction.

The images show how the application of forces influences the damage results. Due to the presence of the rigid diaphragm, horizontal cracks open at the floor levels. The presence of the rigid diaphragm distributes the forces according to the stiffness of the wall, incrementing the damage on the Back Wall instead of concentrating it on the Front Wall.

7.2.2 Isolated Units pushover

For the sake of simplicity, and due to the similarity between all three units, the modal analysis to obtain the lateral force distribution was performed only on Unit 2.

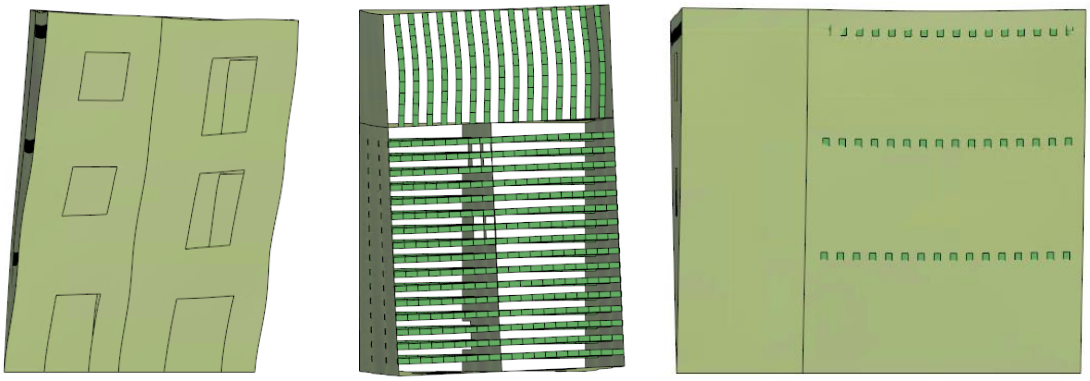

Front View *Top view* *Left side view*

Figure 57. RD Isolated Unit fundamental mode shape

The results from the modal analysis showed that the fundamental modal shape (figure 57) was mainly a displacement along the longitudinal (x) axis with a slight rotation around z. The dynamic properties obtained from the eigenvalue analysis are reported in table 10 and 11.

Table 10. Isolated Unit, modal properties

MODE	OMEGA $[rad/s]$	FREQUENCY $[1/s]$	PERIOD $[s]$
1	32.462	5.166	0.193
2	44.952	7.154	0.139
3	57.892	9.213	0.108
4	87.471	13.921	0.071
5	91.409	14.548	0.068

Table 11. Isolated Unit, modal participation mass ratios [%]

MODE	M_X	M_Y	M_Z	RM_X	RM_Y	RM_Z
1	68.9860	0.0032	0.0002	0.00004	19.4099	3.8553
2	0.0128	67.9467	0.0115	20.5434	0.0029	0.0265
3	1.2092	0.0444	0.00002	0.0243	4.7051	70.8300
4	15.3005	0.1865	0.7335	0.0369	27.5474	0.1113
5	0.0109	0.0001	0.0001	0.0006	0.0157	0.0008

Similarly, to the aggregate, it is possible to observe three distinctive modes from the results reported in table 11. A fundamental mode in the longitudinal (x) direction; a second mode in the transversal (y) direction; and a third rotational mode (around z). This shows the structure's tendency to a box-like behavior, enhanced by the presence of the rigid diaphragm. The displacements of the barycenter of each floor were taken from the first mode of vibration to calculate the modal profile for the pushover analysis, reported in table 12.

Table 12. Lateral force distribution

Floor	ϕ_i	Norm ϕ_i	Mass	Force	Norm. Force
3	5.426	1	104.87	104.868	1
2	3.756	0.692	136.69	94.618	0.902
1	1.721	0.317	223.33	70.862	0.675

The analysis on isolated units was performed applying the normalized force obtained divided by the area of the wood slab as a distributed force. Results are reported in Fig. 58.

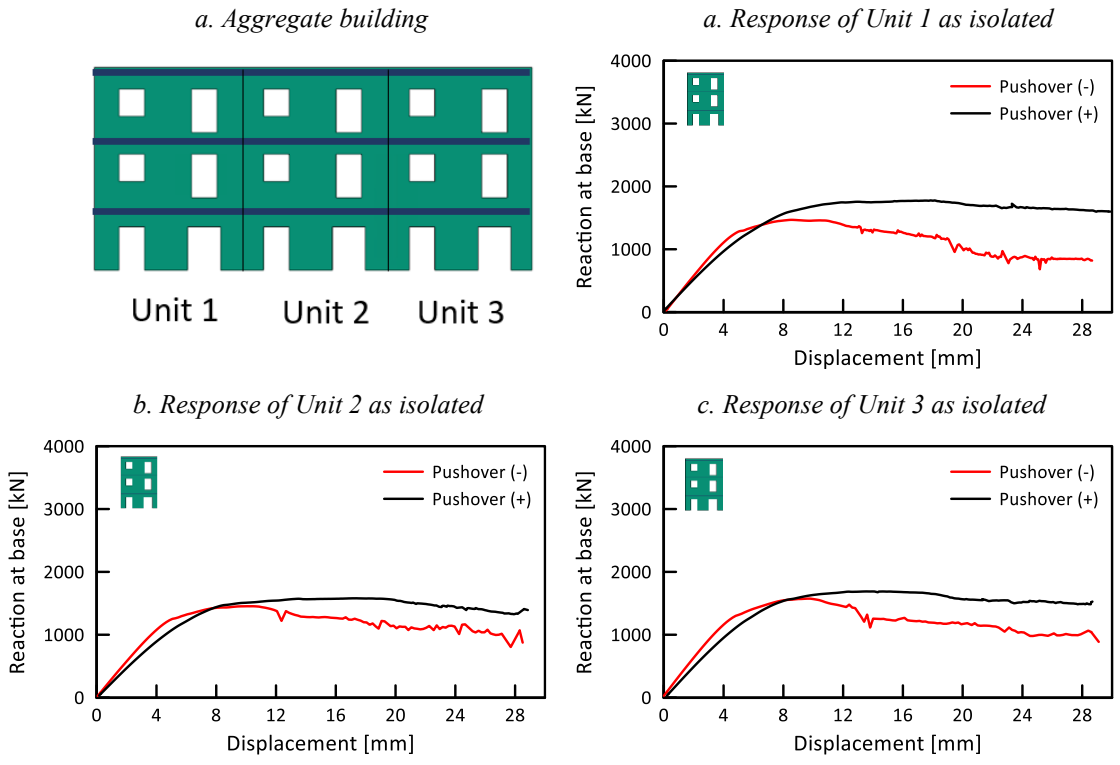

Figure 58. RD Isolated Units, pushover curves

As we can observe in the Fig. 58 both analyses provided ductile curves with similar resistance and behavior. The difference between the negative and positive pushover relies on the asymmetry of the openings present in the front and middle wall.

The damage in all longitudinal walls from the positive Pushover analysis is reported in figure 59, represented by the maximum principal force.

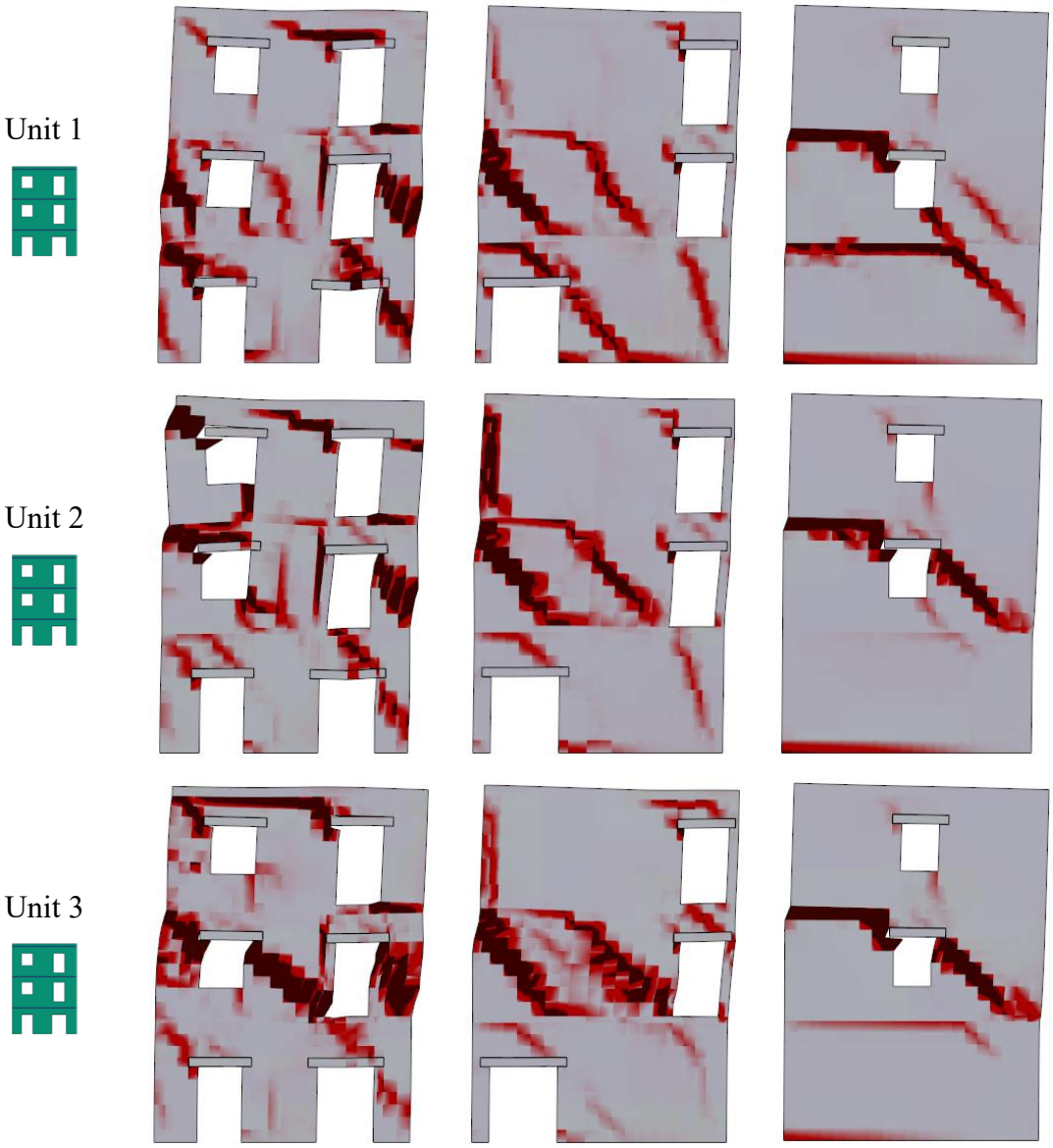

Figure 59. RD Isolated Units, Pushover crack pattern. X+ direction.

The similarity between the three units resulted in almost identical failure mechanisms. It is also worth noticing that some of the cracks that opened in the third and second floor did not continue at the base due to the increment in thickness of the first story wall.

The damage in all longitudinal walls from the negative Pushover analysis is reported in figure 60, represented by the maximum principal force.

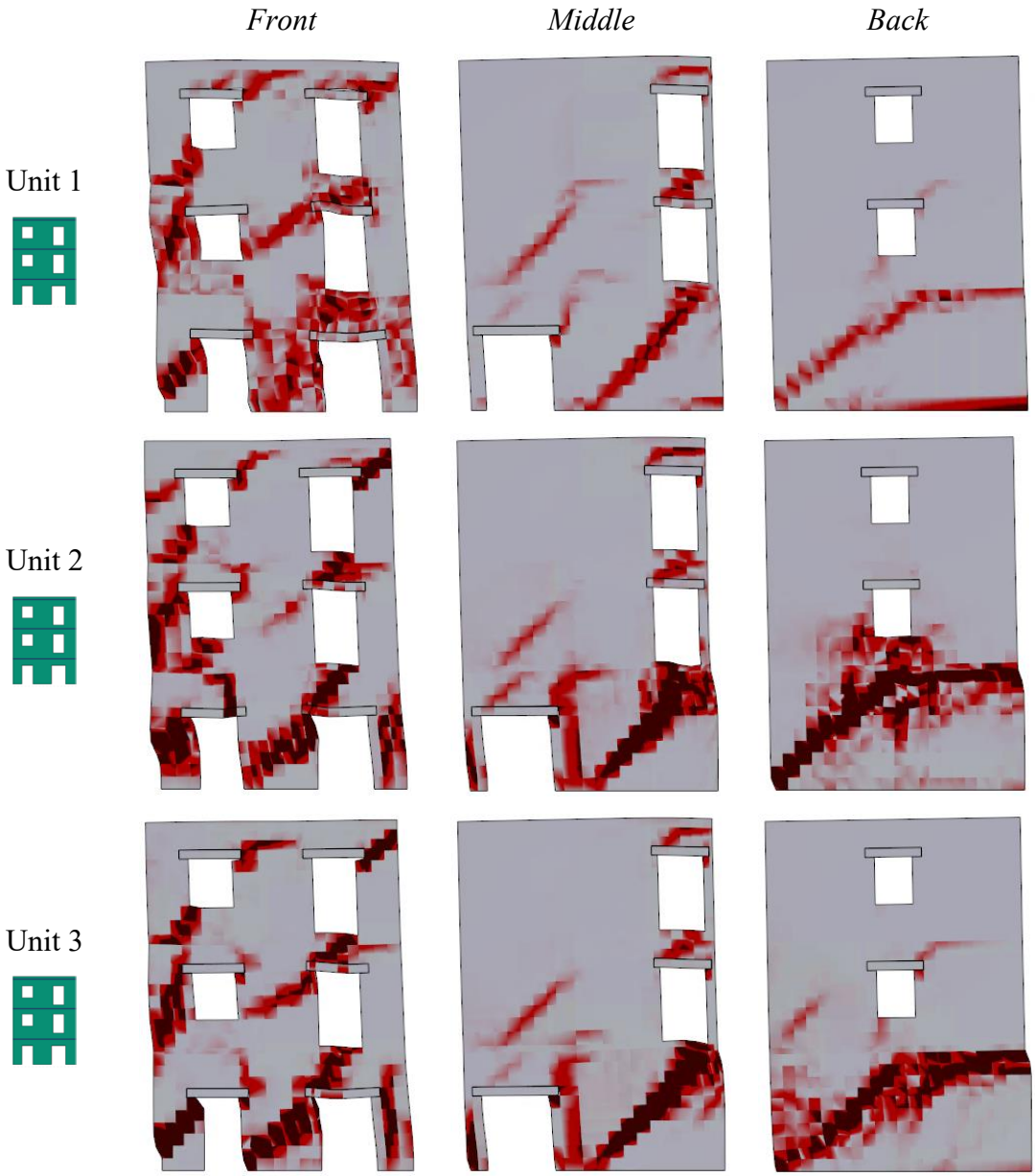

Figure 60. RD Isolated Units, Pushover crack pattern. X- direction

In the case of the negative pushover, the cracks opened at the base of the buildings. This can be explained by the positioning of the openings of the Middle Wall, which has a weak support at the left of its base. The loss in resistance of that pier activates the overturning and, therefore, the opening of the diagonal crack at the base observed in the figure.

7.2.3 Aggregate fully connected non-linear dynamic analysis.

As mentioned at the beginning of the chapter, the non-linear dynamic analysis was carried out in the aggregate's longitudinal direction. The damping was introduced in the model using an automatic calculation of the Rayleigh coefficients available in STKO, using the first and second frequencies.

The time-displacement relationship of the top right node of the Front Wall was measured to assess the response, reported in Fig 61.

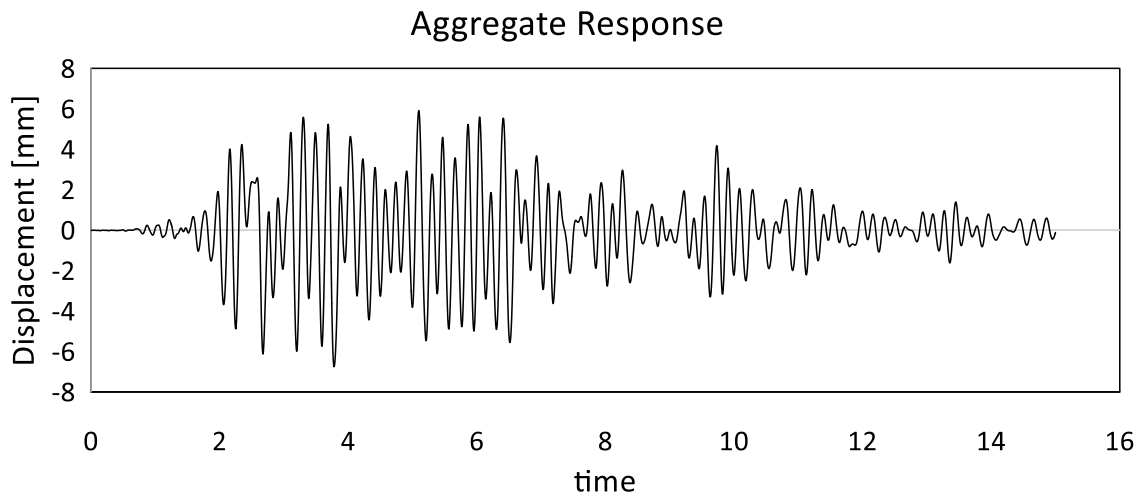

Figure 61. RD Aggregate Time-Displacement response.

The graphic shows a maximum displacement of 7 mm, achieved between the first 2,5 to 4 seconds of the analysis.

In figure 62 the displacement was correlated with the reaction at base of the aggregate, showing a maximum resistance of 6000 kN. The response of the units in the aggregate configuration was also extracted from the analysis, using as control node the top left node of the Front Wall of each unit. As before, the reaction was measured only in the longitudinal walls to avoid duplication in shared walls.

We can observe different magnitudes of peak resistance for the same unit when pushed in negative and positive direction. This resembles the results previously obtained in the pushover, indicating that the presence of the adjacent buildings incremented the resistance of the examined unit.

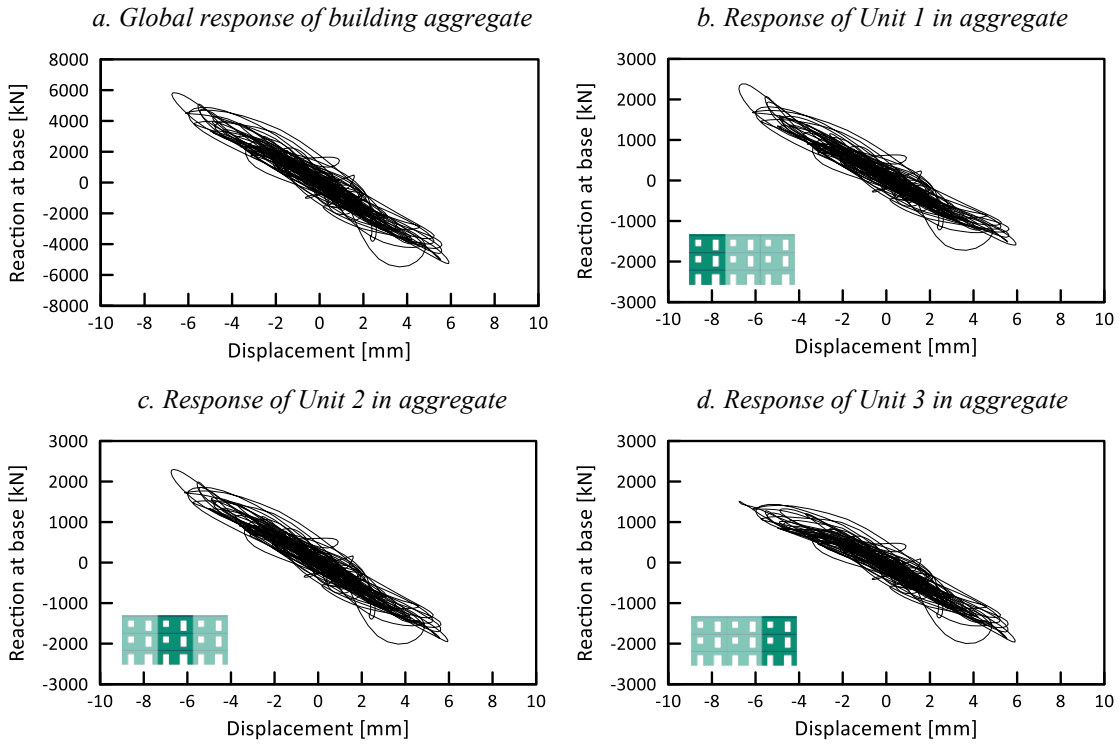

Figure 62. RD Aggregate, non-linear dynamic analysis, displacement-reaction curves

The fig 63 shows a 3D view of the dynamic analysis during one of the oscillations. Using the maximum principal force plot, it is possible to observe the opening of the cracks.

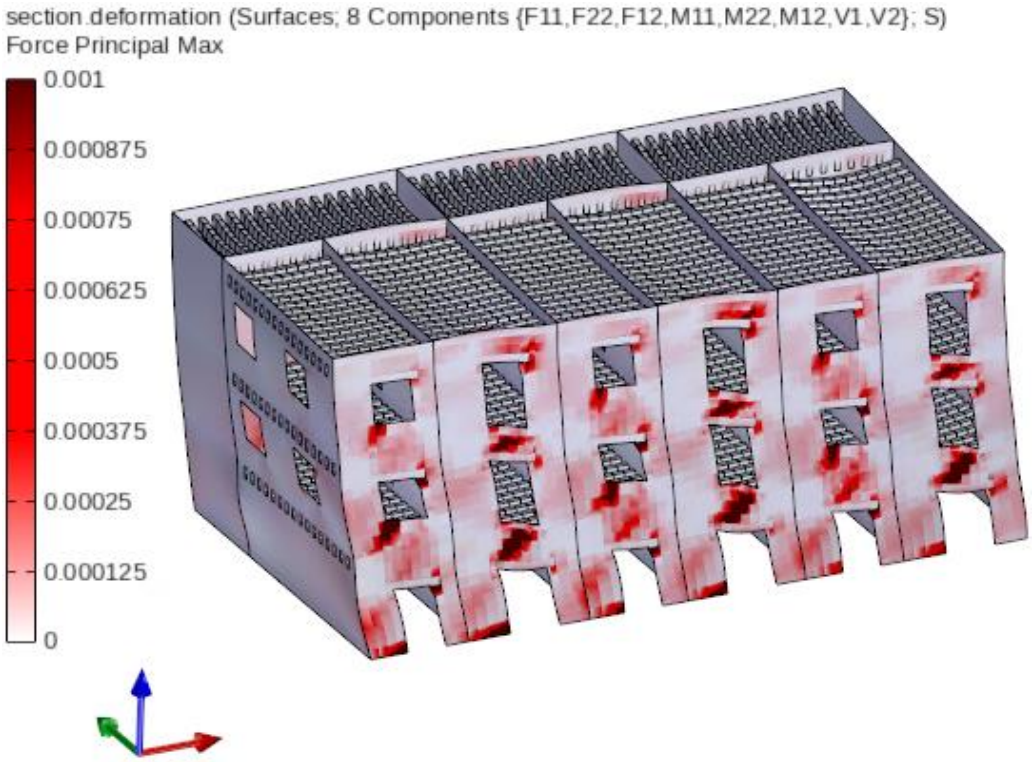

Figure 63. RD Aggregate, non-linear dynamic analysis, 3D crack pattern

Additionally, the opening of the cracks due to the dynamic analysis is represented with the maximum principal force and the damage plot in Figure 64.

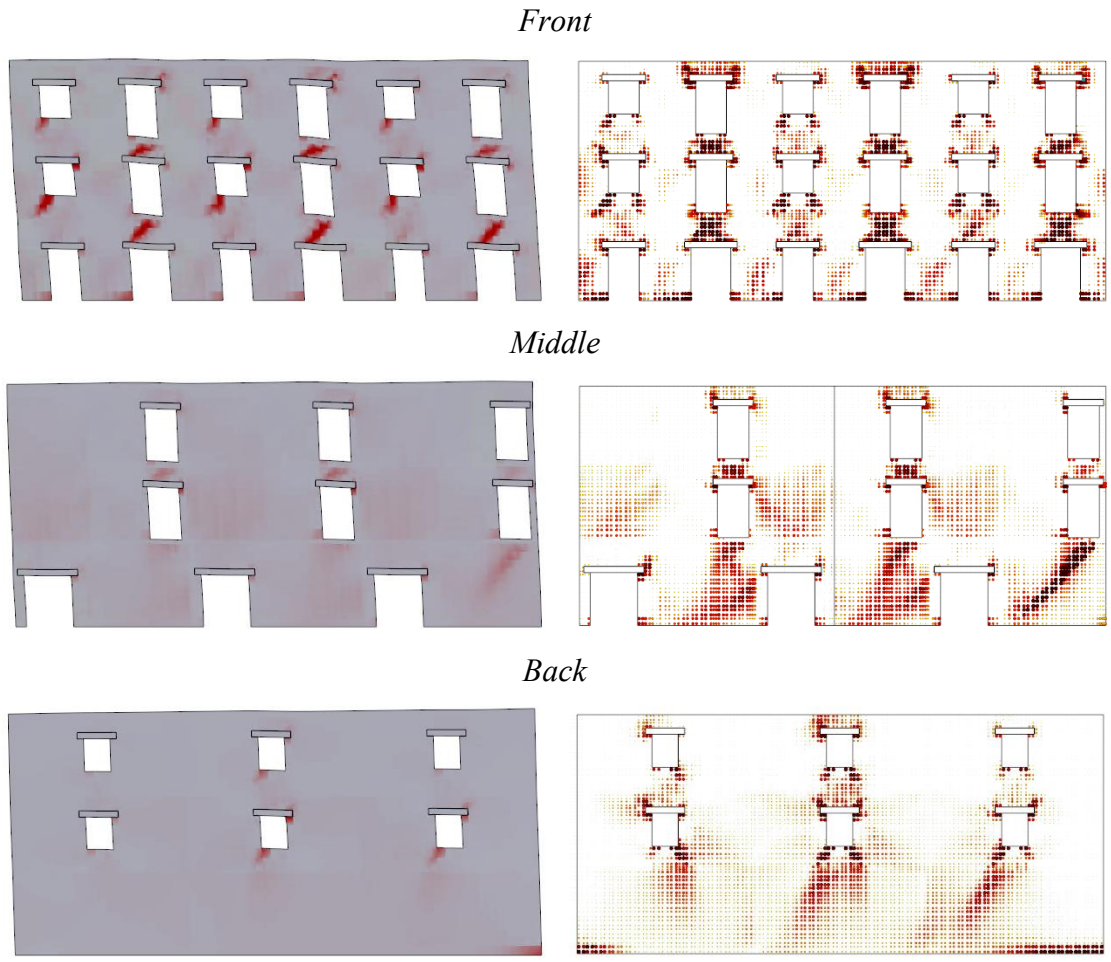

Figure 64. RD Aggregate, non-linear dynamic analysis a) maximum principal force; b) damage

We can observe some tensile cracks at the lateral base of the Back Wall and the bottom of the piers. Additionally, it is possible to notice the shear cracks in the spandrels between openings, especially those with a thinner section. The damage plot on the right, instead, shows the total damage accumulated during the analysis including compressive damage.

7.2.4 Isolated non-linear dynamic analysis

The analysis settings were the exact same as the ones used in the aggregate model except for the damping, which used the first two frequencies of the modal analysis of the isolated unit model. The analysis did not last as long as expected, only lasting 2.5 seconds before failing to converge due to building failure. In this case, the high demand on the displacement caused damage to a part of the wall, resulting in detachment. When this happens, numerically speaking, the displacement tends toward infinity, causing the analysis to fail.

The displacement-reaction at base curves for each unit are reported in figure 65.

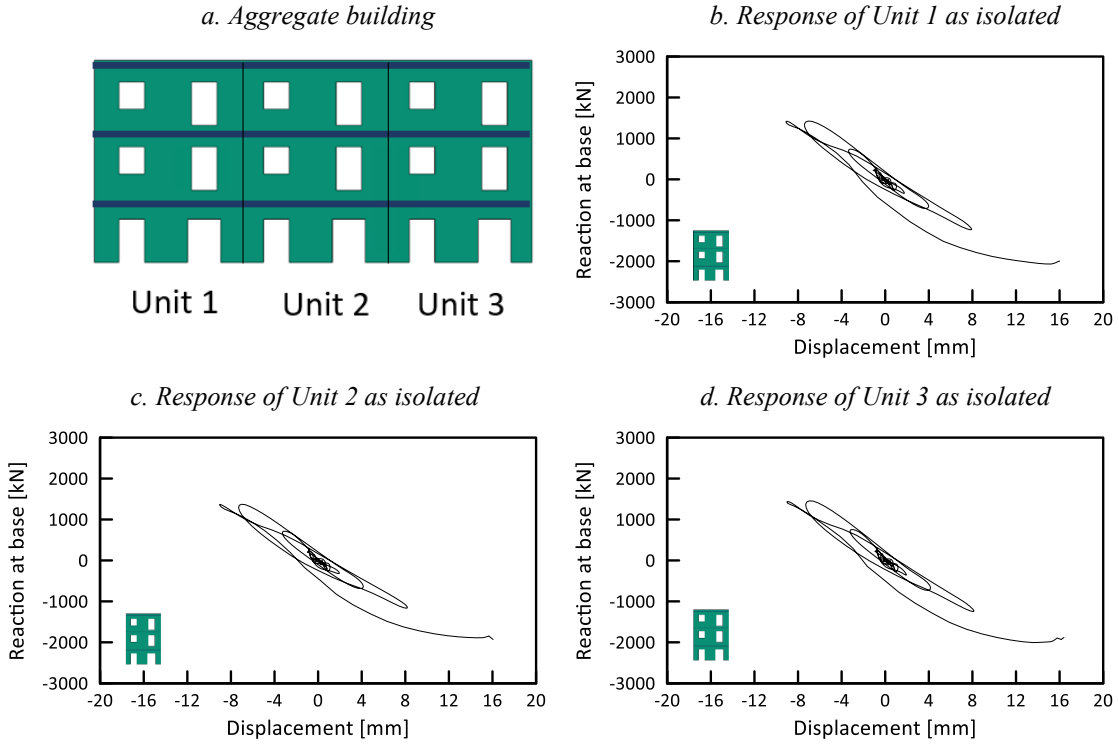

Figure 65. RD Isolated Units, non-linear dynamic analysis results

When analyzing the units as isolated, it can be observed a drastic difference with respect to the results obtained in the aggregate configuration. The rising acceleration imposed produced a displacement demand 2 times higher in the isolated units. A priori, it seems evident that the presence of the adjacent units provided a constrain, not necessarily increasing resistance but limiting the displacements, which is what ultimately caused the collapse.

The following figures (Fig. 66) show a comparison between the response of the units in aggregate configuration (black) and when isolated (red). The difference in displacement demand between both configurations is explicitly shown. All three units failed to converge around the same step, as they were very similar. A priori, it can be said that the aggregate configuration limits the displacement demand of the individual units, reducing the damage and risk of collapse.

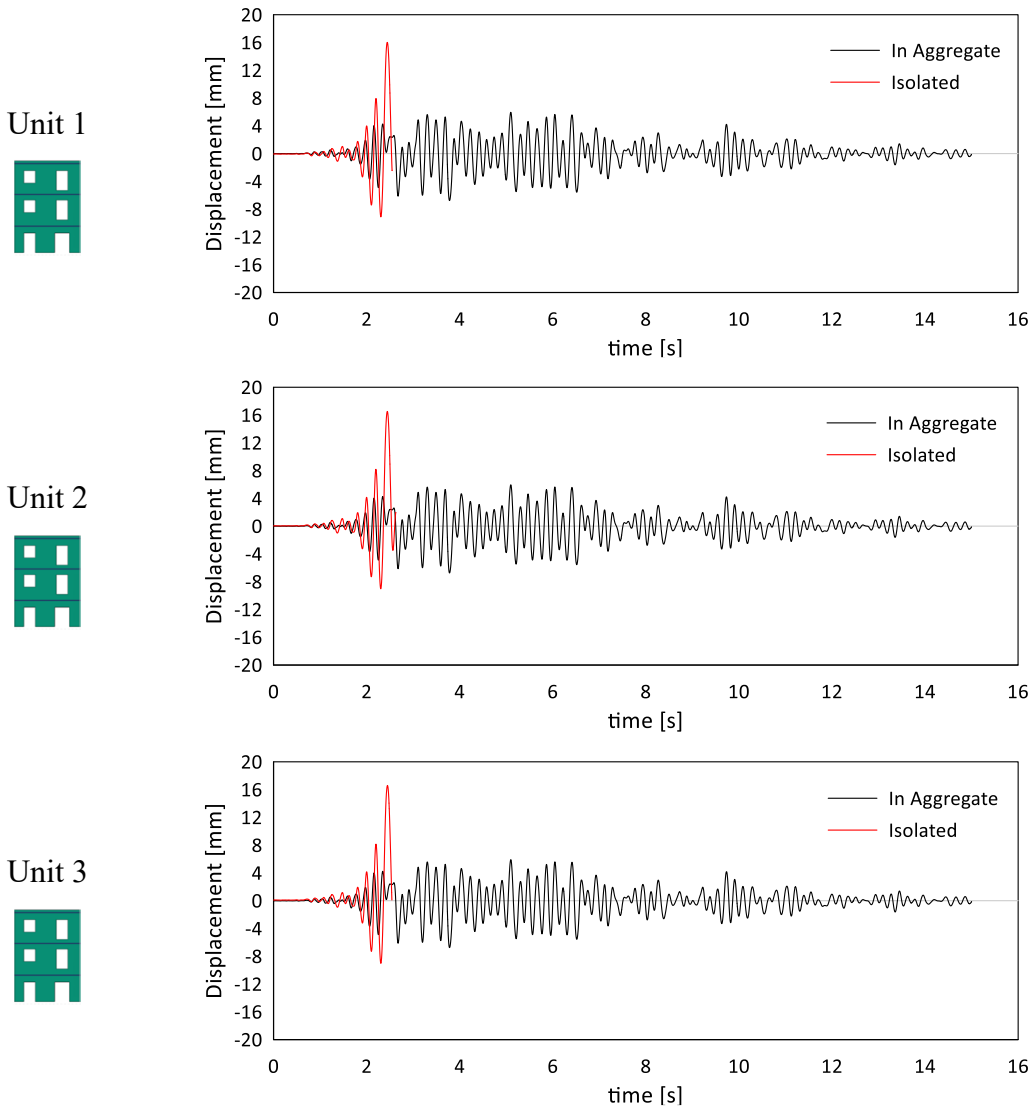

Figure 66. RD In-Aggregate and Isolated Units Time-Displacement response comparison

The images Fig. 67 and Fig. 68 are taken at the last oscillation before collapse, it is possible to observe a more pronounced damage compared to the aggregate configuration. The Front Wall presented the largest displacement, as predicted from the modal analysis. The spandrel between the left side openings were the most damaged and were the cause

of the building collapse and convergence failure. On the other hand, the Back Wall experienced tensile cracks at the base and minimum cracks developing from the openings.

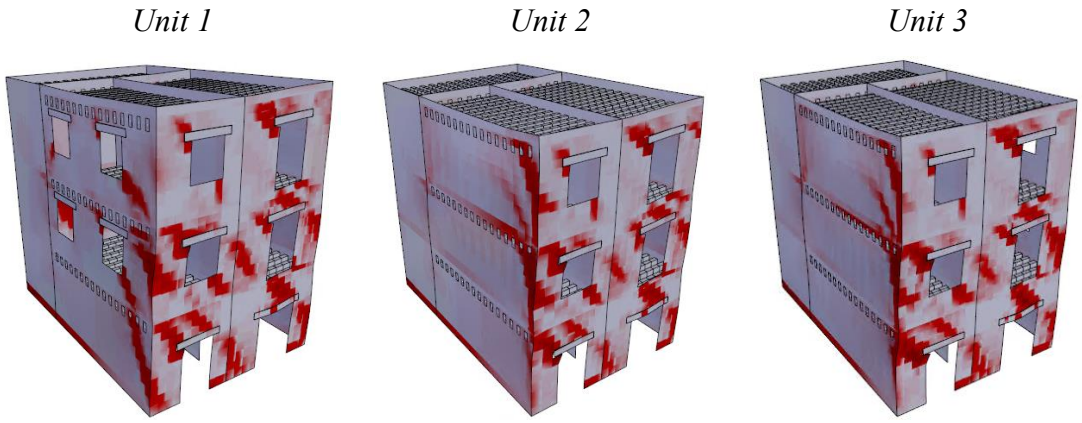

Figure 67. RD Isolated Units dynamic analysis crack pattern 3D. a) Unit 1; b) Unit 2; c) Unit 3.

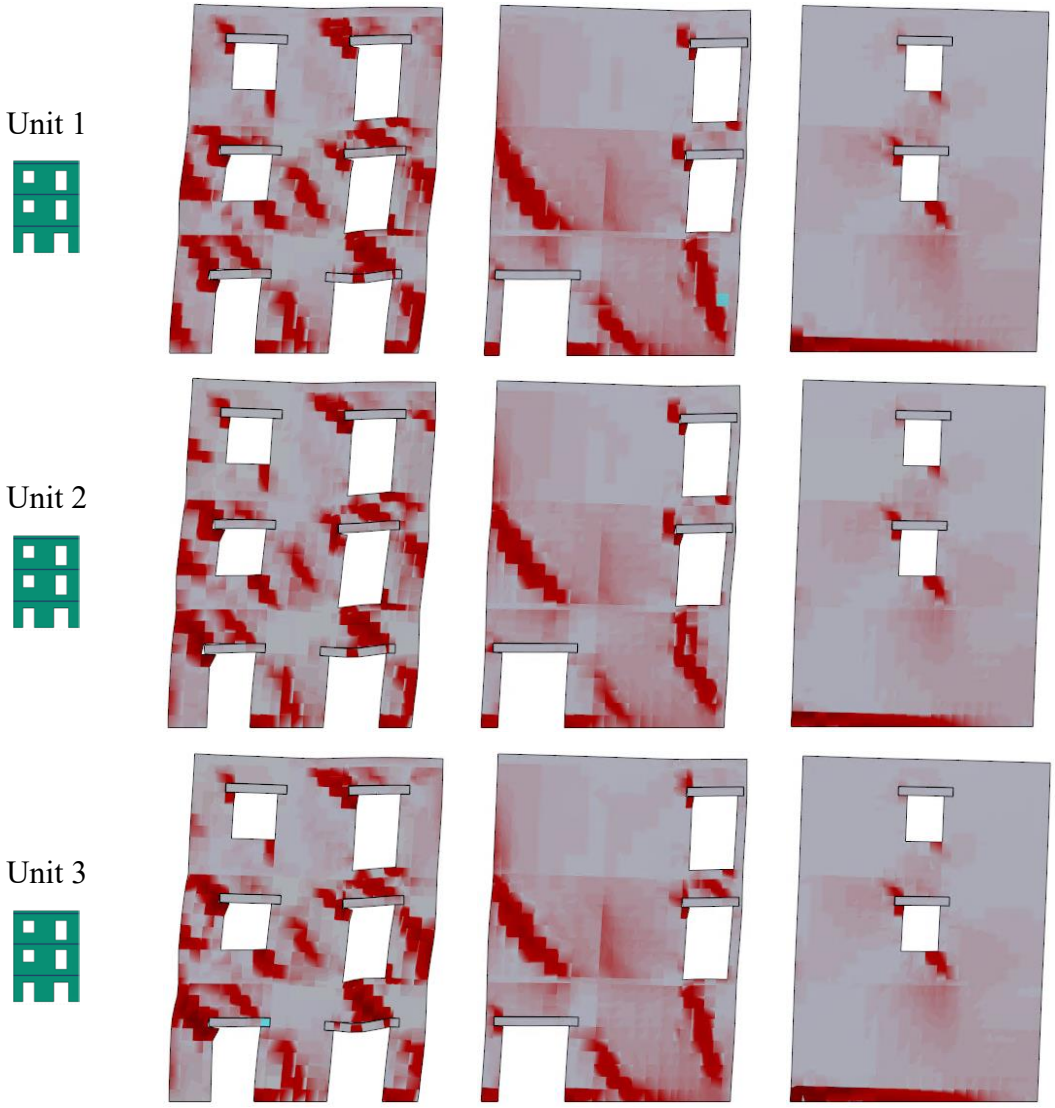

Figure 68. RD Isolated Units, non-linear dynamic analysis, crack pattern on walls

7.2.5 Aggregate semi-connected Pushover

Since Units are Semi-connected, it is not possible to consider 1 rigid diaphragm per floor with the master node located in the barycenter of the aggregate. For this reason, each unit had its own rigid diaphragm independent from the adjacent. The pushover forces applied on each unit for a given floor was the total load that should be applied in the aggregate's barycenter of that floor divided by 3.

The curves belonging to each unit were extracted and are reported in figure 69.

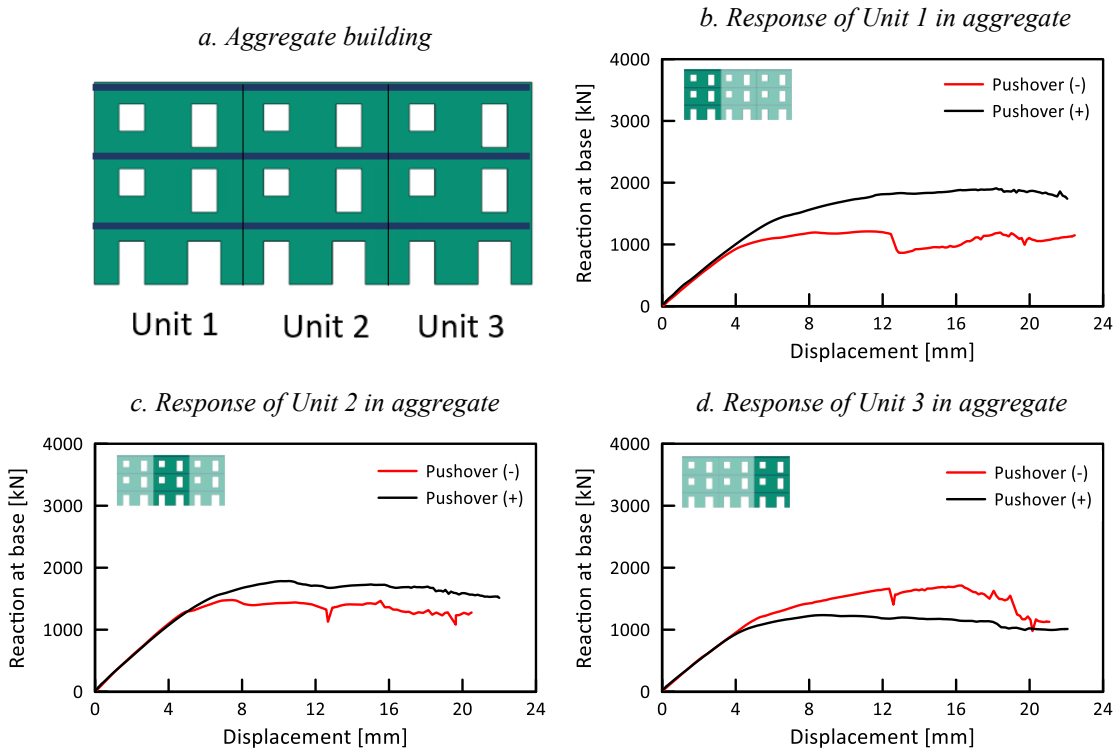

Figure 69. RD Semi-connected Units, Pushover curves

From Fig. 69 it is possible to notice that there is an increment in the resistance for Unit 1 when pushed in a positive direction and in Unit 3 when pushed in a negative direction. However, the increment is much less than that obtained when the aggregate is fully merged. It should be noted, however, that once the friction forces are overcome and the walls begin to slide against each other, the nodes located as control points tend to move upwards, reducing the reliability of the analysis.

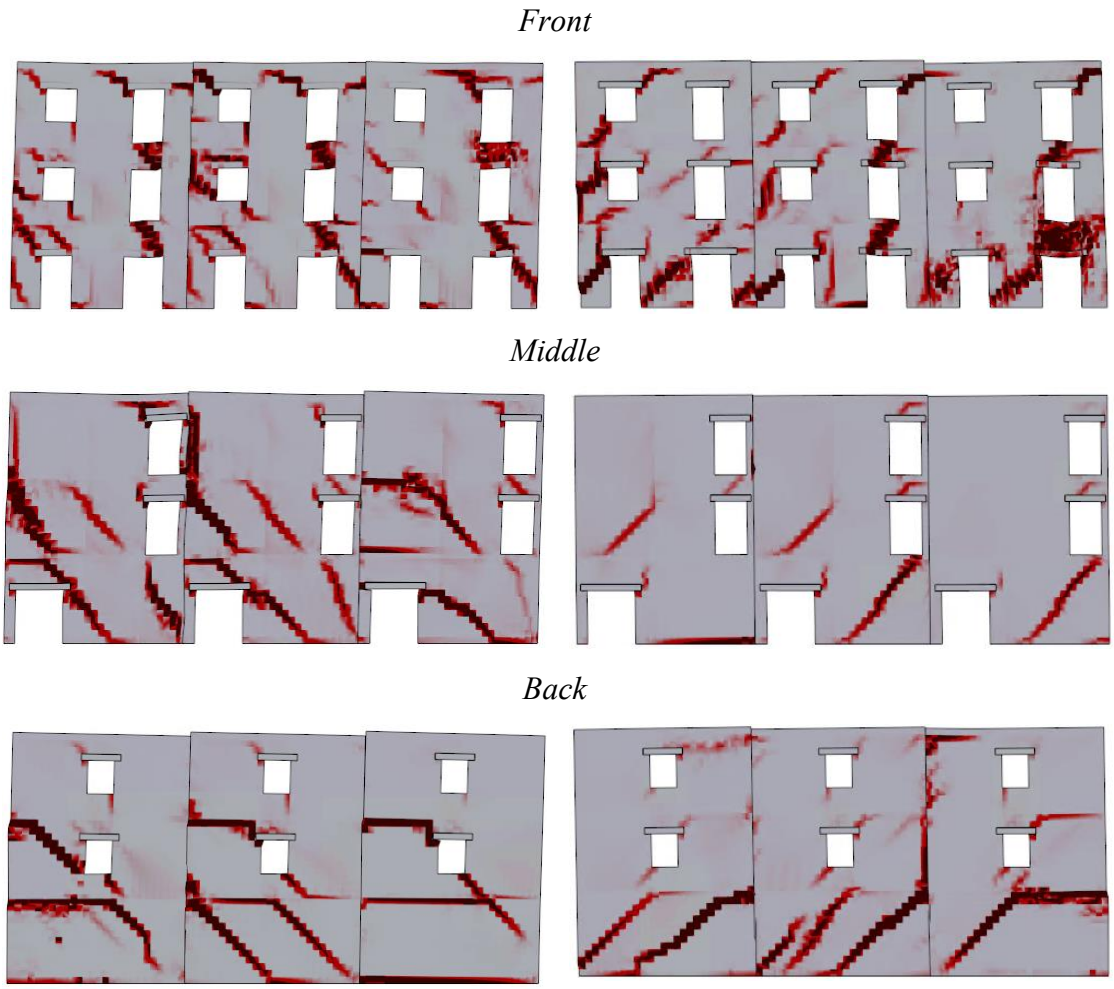

Figure 70. RD Semi-connected Units, pushover crack pattern. a) X+ direction; b) X- direction

In both positive and negative pushover, it was registered a large damage of the spandrels between the left side openings of all three units, being the principal cause of collapse under large displacement demand.

Additional damage was observed along the contact between adjacent units, especially in the third story where the displacement demand is higher.

7.2.6 Aggregate semi-connected non-linear dynamic analysis

For the Semi-connected case, it was not possible to perform a modal analysis because all first modes where predominantly local, and there was no clear global behavior. For this reason, the frequencies adopted were the same used in the "Fully Connected" case.

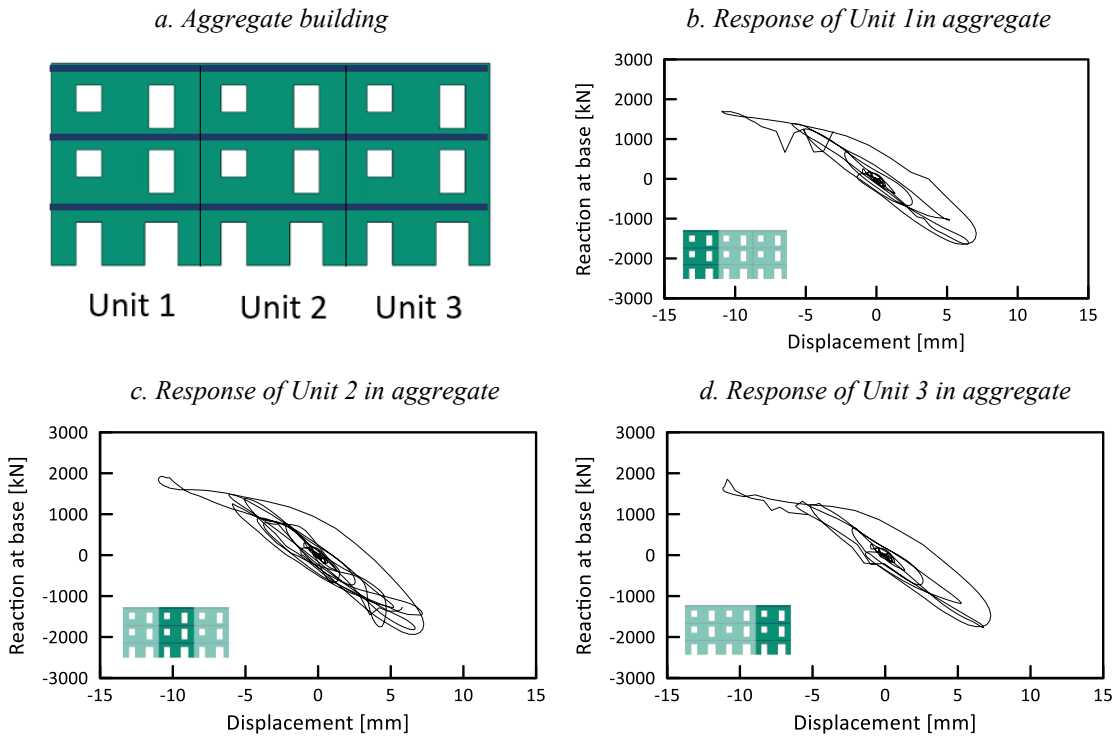

Figure 71. RD Semi-connected Units, non-linear dynamic analysis results

The dynamic analysis had convergence issues around step 600/3000 (about 3 seconds). As before, from 2.3s to 4.5s is where the major displacement was registered in previous cases. The displacement registered on all three units surpassed the 10mm, which is less than the obtained for the isolated case. It should be noted that there are additional stresses along the contact between adjacent walls that are not considered in the previous cases.

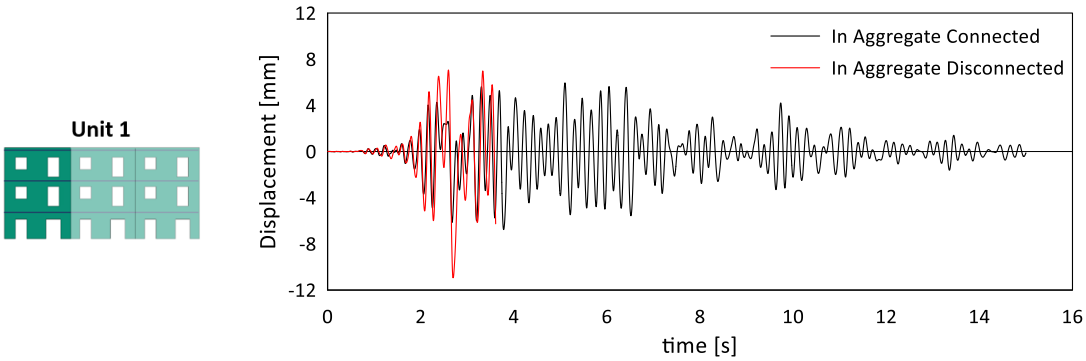

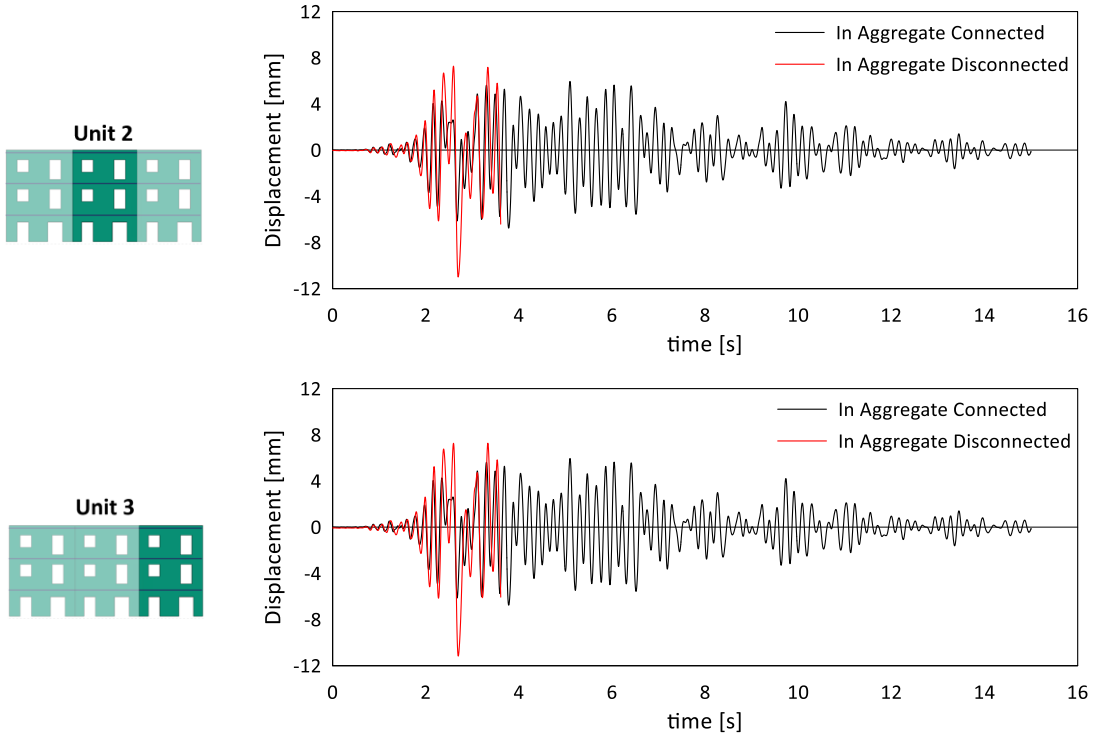

Figure 72. RD In Aggregate Connected and Semi-connected case, response comparison.

In Fig. 73 we can observe how the walls from Unit1 and Unit 2 are uplifted when the aggregate is oscillating. It is also noticeable that the model did not develop major damage in piers and spandrels before failing the analysis due to detachment of elements because of localized damage.

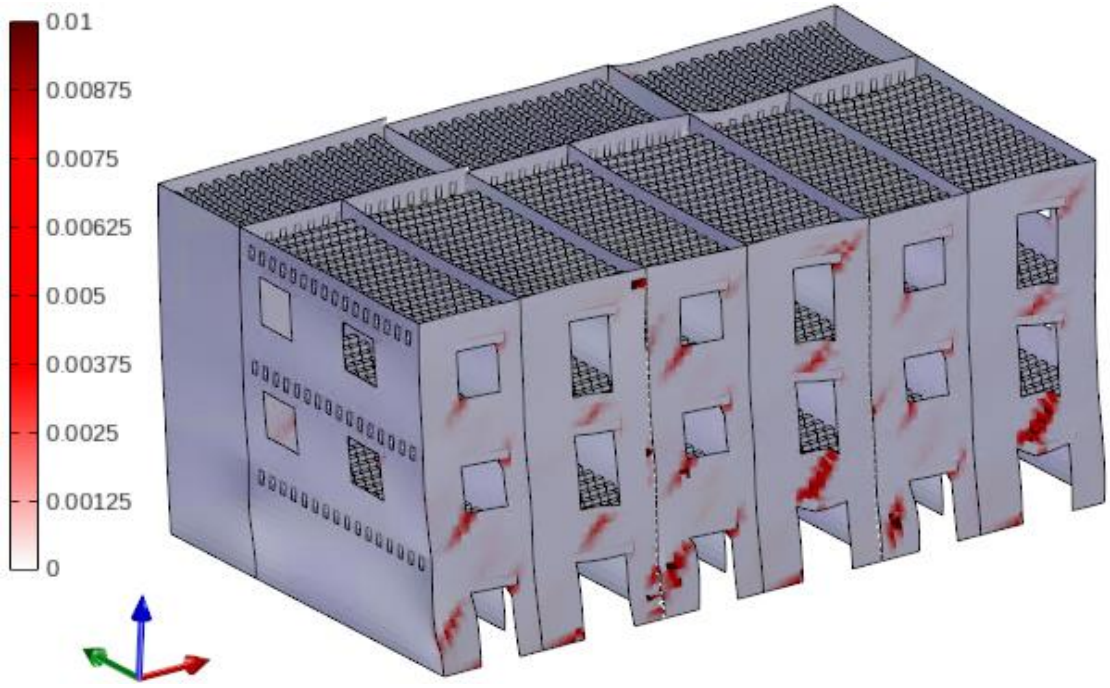

Figure 73. RD, Semi-connected Units, non-linear dynamic analysis 3D crack pattern

7.3 Flexible Floor case

The Flexible Floor case was the most complex to evaluate, as it required careful consideration during the modeling phase, such as the addition of the wood plate and the proper method of linking it with the rest of the structure. These considerations were necessary to ensure that the push forces were applied in the most accurate manner possible, as the method of force application can ultimately impact the pushover analysis outcome.

The analysis was also more unstable, requiring in some cases more steps to reach a softer curve. This was mainly due to the out-of-plane failure mechanisms developed due to the lack of slab stiffness.

The analysis procedure was the same adopted in section 7.2.

7.3.1 Aggregate fully connected Pushover.

As before, an initial Modal Analysis was performed to identify the fundamental mode.

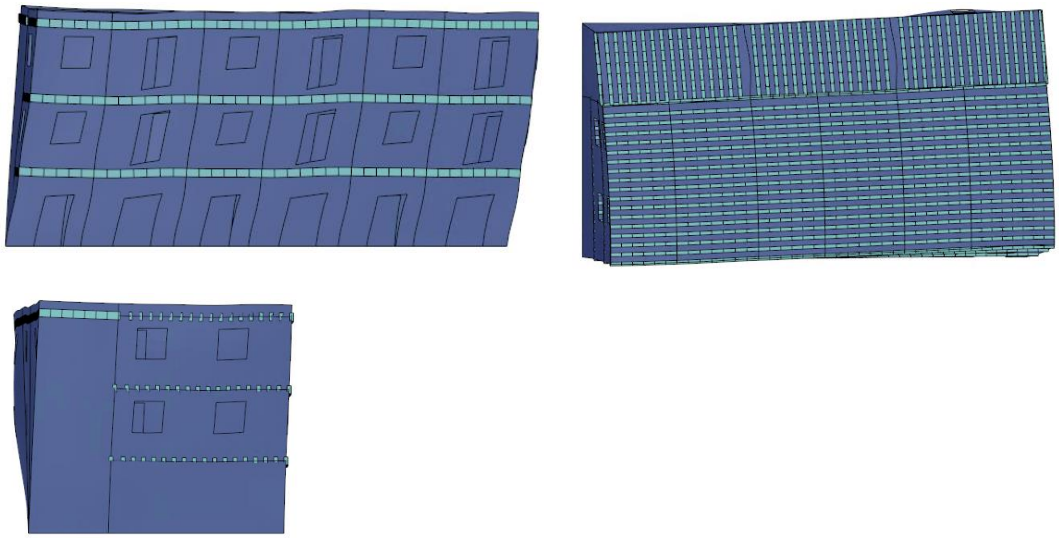

Figure 74. FF Aggregate, fundamental mode shape.

The images show some out-of-plane behavior of the walls, yet it is significantly reduced by the presence of the wood plate, which provides some stiffness. The fundamental mode presents a global longitudinal displacement.

Table 13. Flexible Floor modal properties

MODE	OMEGA $[rad/s]$	FREQUENCY $[1/s]$	PERIOD $[s]$
1	36.757	5.850	0.170
2	39.037	6.213	0.160
3	43.621	6.942	0.144
4	45.219	7.196	0.138
5	53.615	8.533	0.117

Table 14. Flexible Floor modal participation mass ratios [%]

MODE	M_X	M_Y	M_Z	RM_X	RM_Y	RM_Z
1	68.5296	0.3508	0.0006	0.0694	4.3817	9.6776
2	0.4387	69.4257	0.0053	14.6880	0.0243	0.0062
3	0.0118	0.9551	0.0017	0.6105	0.0008	0.0947
4	4.4660	0.0111	0.0000	0.0023	0.3530	30.2817
5	3.3521	0.0011	0.0001	0.0062	1.0040	32.3232

Tables 13 and 14's data indicate a fundamental mode that is characterized by a longitudinal displacement in the X direction. Although the mobilized mass ratio data exhibits a second mode with a displacement in the transverse (Y) direction, the absence of the r box-like rotational behavior is what distinguishes it from the Rigid Diaphragm case. This demonstrates the main distinction between the two floor types and the way that the lack of a stiff slab facilitates the activation of local mechanisms.

The lateral force distribution is obtained from the fundamental mode, reported in table 15.

Table 15. Lateral force distribution

Floor	ϕ_i	Norm. ϕ_i	Mass	Force	Norm. Force
3	4.268	1	314.60	314.604	0.953
2	3.434	0.804	410.07	329.942	1
1	1.765	0.413	669.99	277.176	0.840

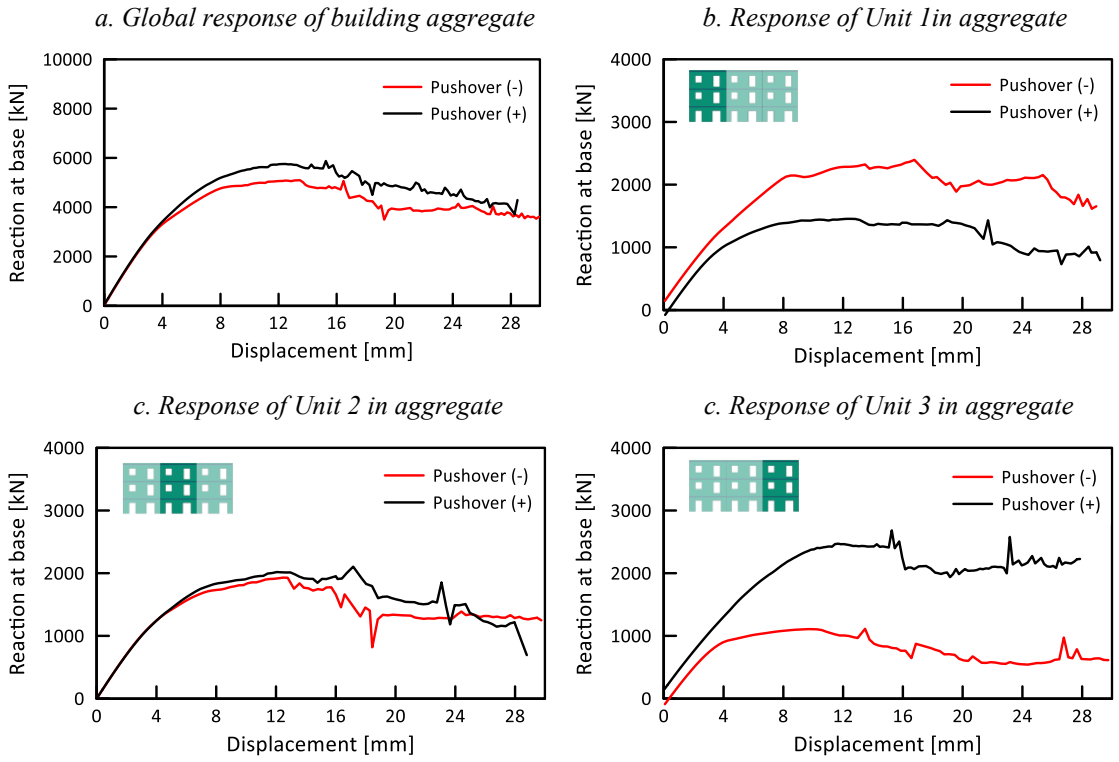

Figure 75. FF Aggregate, Pushover curves.

The curves in Figure 75 show that the aggregate building exhibits a similar response in both directions, with a peak resistance of 6000 kN. Like the rigid diaphragm case, the external units (Unit 1 and Unit 3) exhibited different behavior depending on the pushover direction, with an increase in resistance when adjacent units are present. The central unit (Unit 2), with one unit on each side, presented a similar behavior in both directions.

The damage obtained from the pushover analysis is reported below (Fig. 76) using the maximum principal force measured to represent the crack openings.

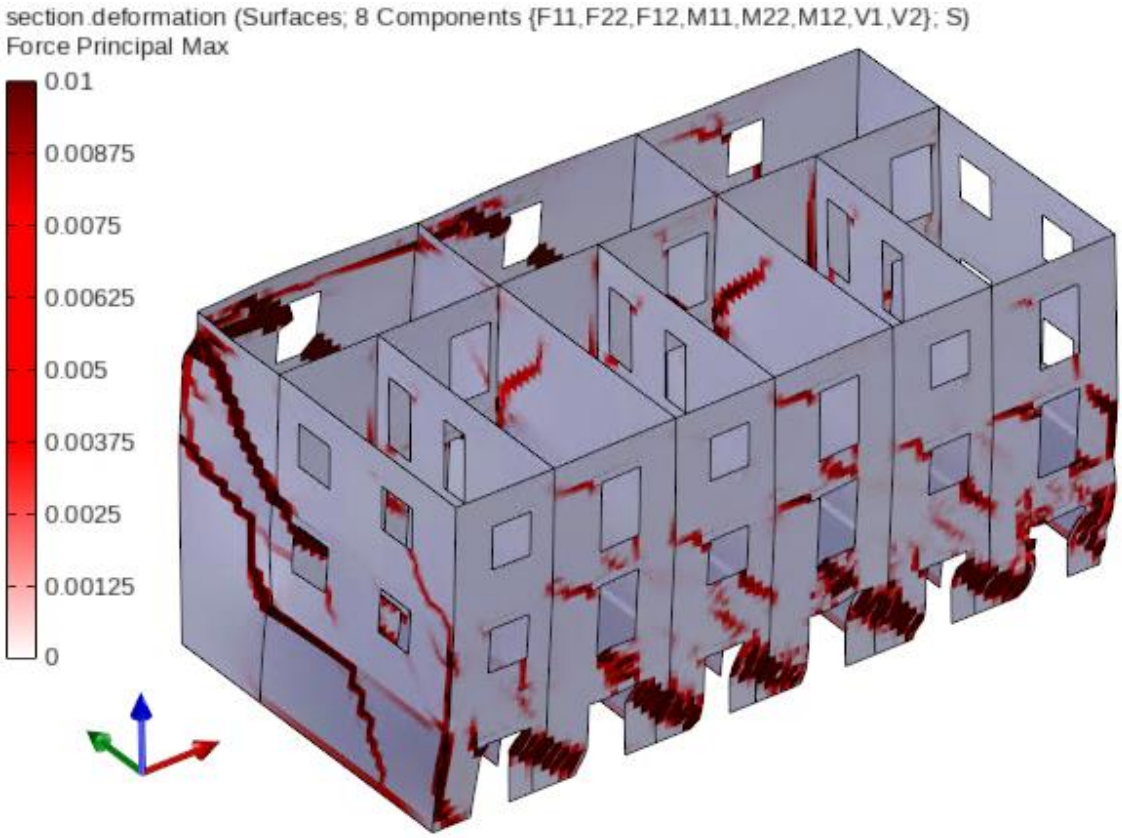

Figure 76. FF Aggregate, Pushover crack pattern 3D

From the figure, it can be observed that the base piers have suffered complete damage due to a clear shear failure mechanism. This, in combination with the push applied on the first story, resulted in the clear flexural failure that can be observed on the left transverse wall at the first level. Furthermore, the difference in stiffness between the back and front wall caused a larger displacement of the front wall, leading to the opening of diagonal cracks that can be seen on the left transverse wall.

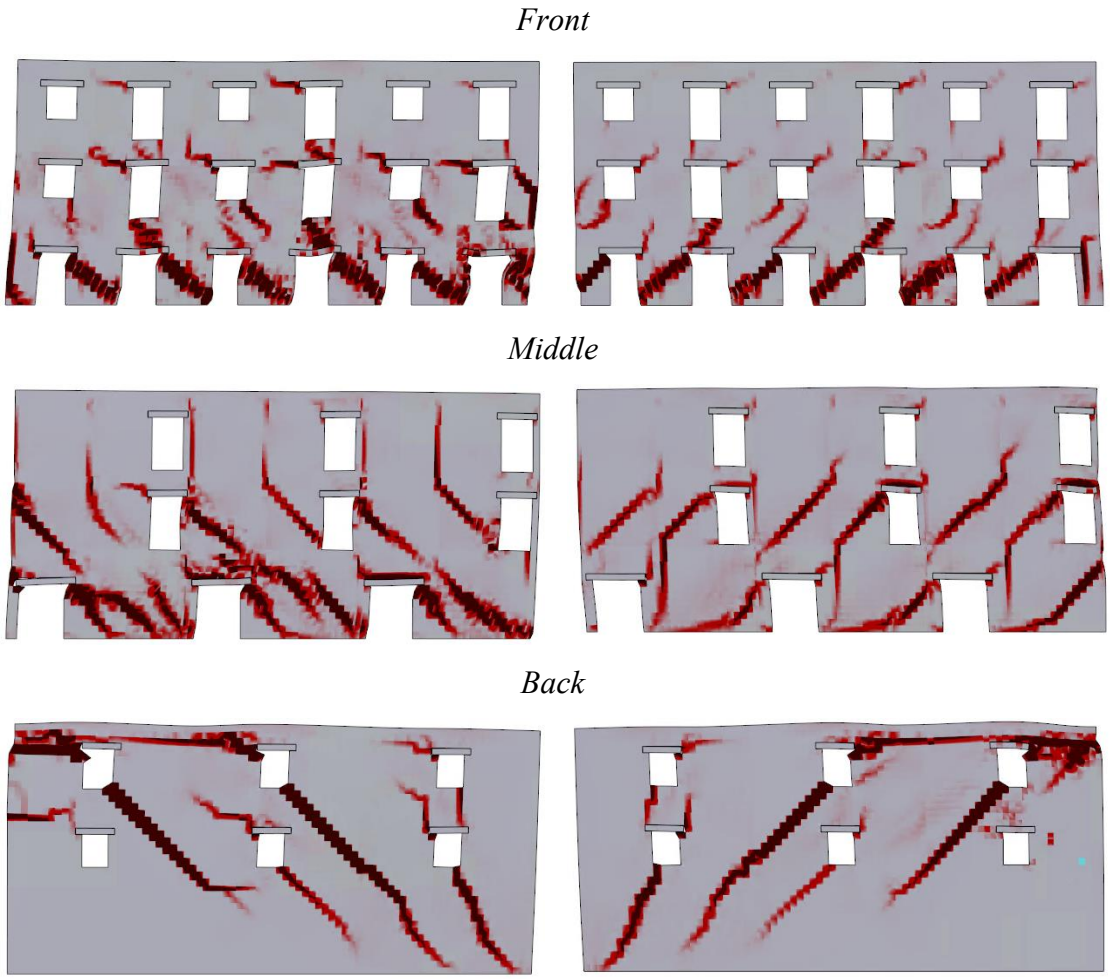

Figure 77. FF Aggregate, pushover crack pattern on walls a) X+ direction; b) X- direction..

The pictures (Fig. 77) clearly show the shear mechanism developed as well as the vertical cracks that are formed where the central wall and transverse walls meet. Also, the sliding that the flexible floor causes when forces are applied can be seen at the top of the back wall. This is often a byproduct of the pushover analysis since forces are applied through the flexible plate instead of manifesting as inertial forces in the walls. This impact is only noticeable at the third level because the plate is absent from the second and first floors (and hence no force is directly applied).

Additionally, it can be noted that the Front Wall has the largest longitudinal displacement among all others and that the Back Wall remains quasi unchanged, accurately reproducing the walls' displacement shown in the fundamental mode shape.

7.3.2 Isolated Units pushover

For the sake of simplicity, and due to the similarity between all three units, the modal analysis was performed only on Unit 2.

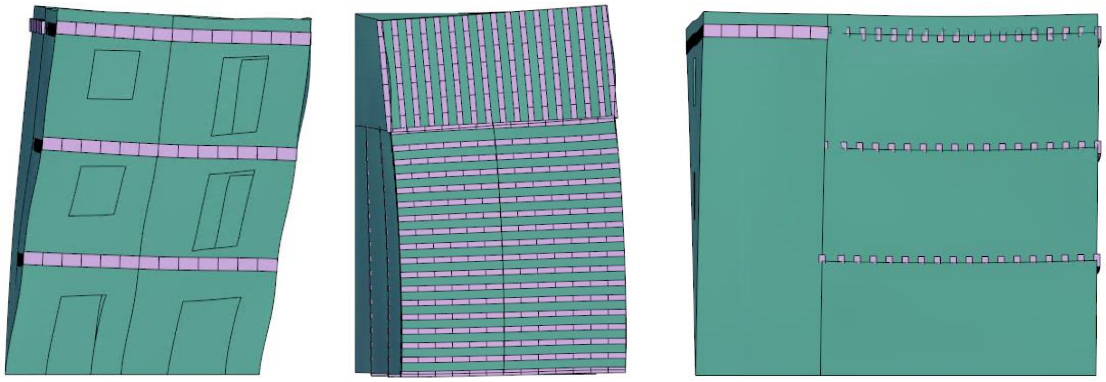

Figure 78. FF Isolated Units fundamental mode shape.

From the mode shape (Fig. 78) it can be noted that the slab is not behaving perfectly rigidly. The top view shows how the wall is curved. However, the presence of the wood slab provides it with minimum stiffness to avoid a complete out-of-plane behavior of the walls.

Table 16. Isolated Unit, modal properties

MODE	OMEGA $[rad/s]$	FREQUENCY $[1/s]$	PERIOD $[s]$
1	30.093	4.789	0.208
2	39.569	6.297	0.158
3	48.043	7.646	0.130
4	54.494	8.673	0.115
5	69.134	11.003	0.090

Table 17. Isolated Unit, modal participation mass ratios [%]

MODE	M_X	M_Y	M_Z	RM_X	RM_Y	RM_Z
1	69.2108	0.0059	0.0001	0.0001	18.1522	4.0973
2	0.0144	47.0535	0.00002	7.8268	0.0012	0.0045
3	0.0043	20.6180	0.0441	14.4694	0.0007	0.0169
4	0.8799	0.0174	0.0002	0.0195	6.3325	68.8347
5	12.2302	0.0238	0.1305	0.0010	21.5062	1.2979

For this case it is possible to distinguish a first mode characterized by a global displacement in the x direction. However, there is a considerable amount of mass rotating round the y axis, which is indicator of the out-of-plane behavior of the transverse walls. Another difference observed with respect to the Rigid Diaphragm case is that the rotational mode is the 4th instead of the 3rd , and the 2nd mode mobilizes less mass, which indicates a greater predominance of local modes.

Table 18. Lateral force distribution

Floor	ϕ_i	Norm ϕ_i	Mass	Force	Norm. Force
3	7.450	1	104.87	104.868	1
2	5.346	0.717	136.69	98.087	0.935
1	2.461	0.330	223.33	73.795	0.703

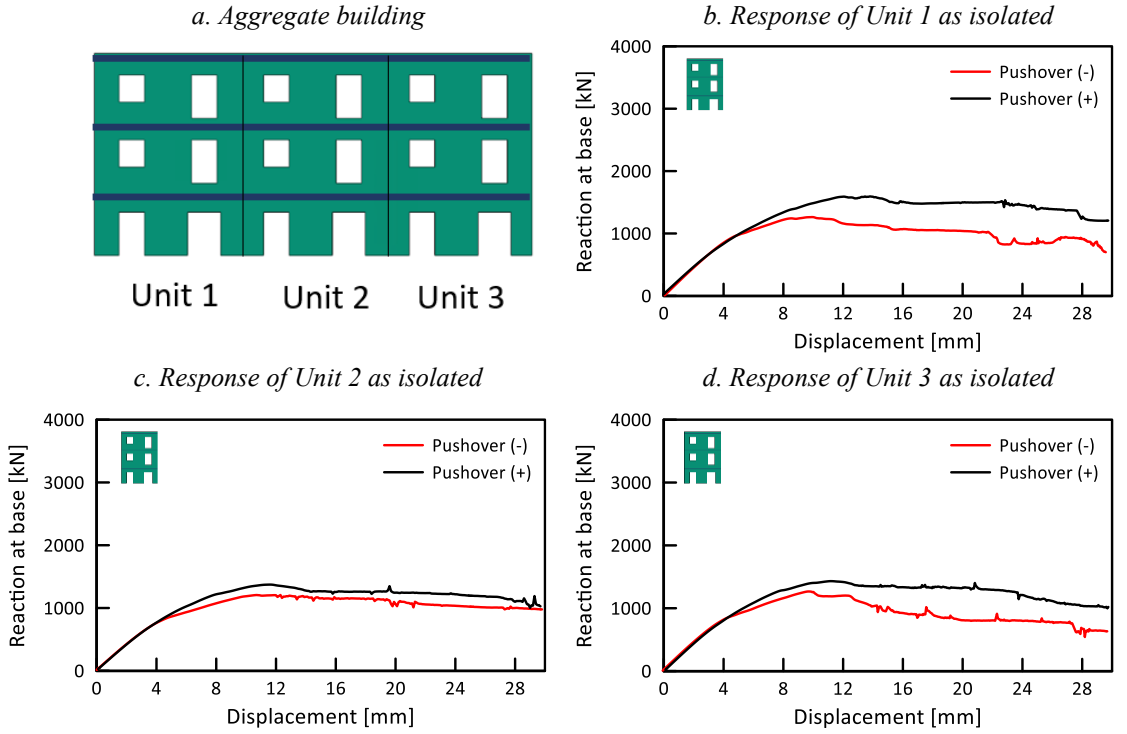

Figure 79. FF Isolated Units, pushover curves.

Outcomes, particularly in Unit 2, demonstrate behavior that is similar in both positive and negative directions. The position of the openings, which weakens the right side of each unit, especially the Middle Wall, may be the cause of the reduction in resistance in the negative analysis. Because the transverse perimetral walls have openings, units 1 and 3 can undergo a bigger difference.

To highlight the crack openings, the damage on walls was depicted by plotting the maximum principal force (Fig. 80).

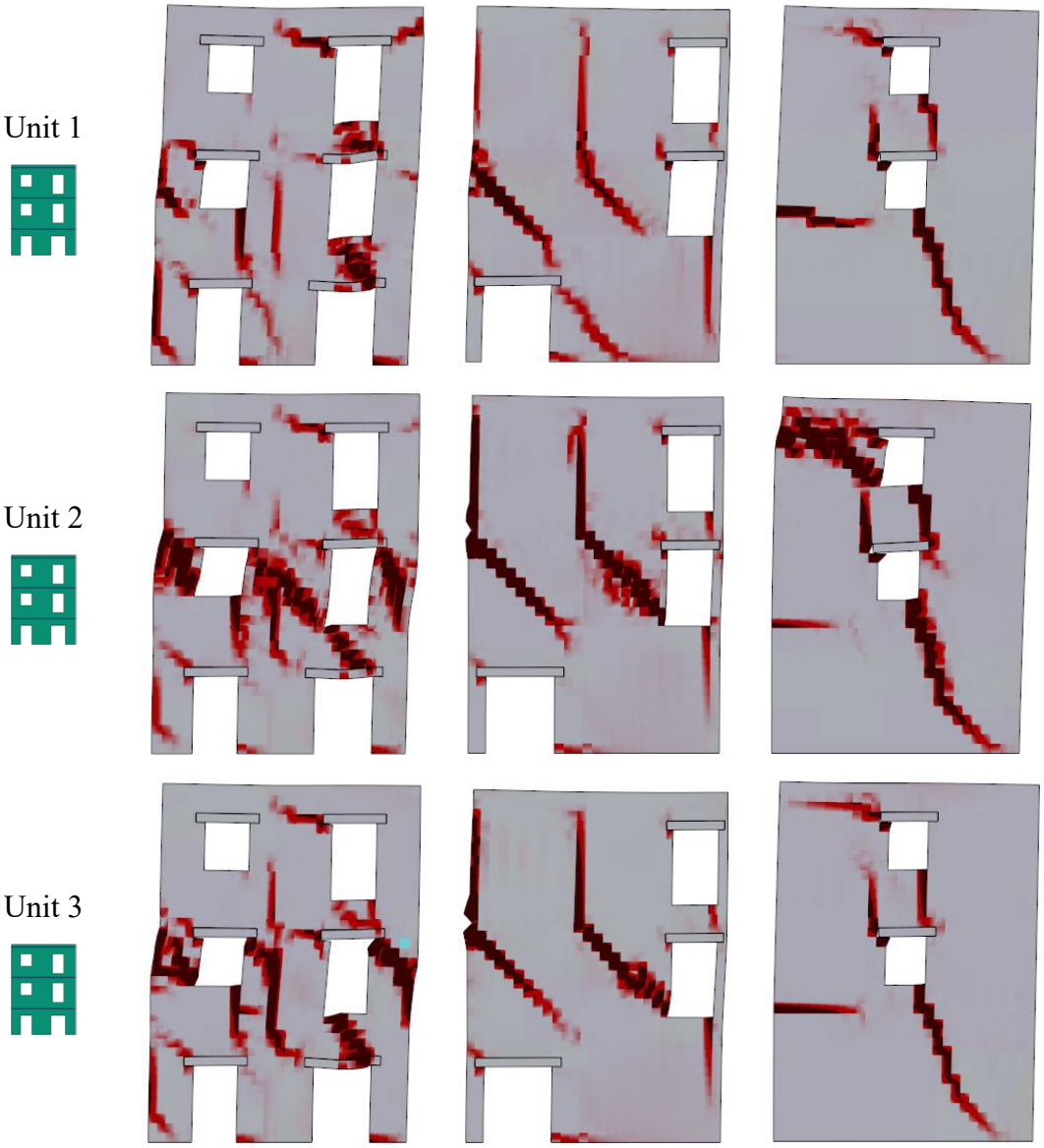

Figure 80. FF Isolated Units, pushover crack pattern X+ direction

The image clearly demonstrates damage to all unit front walls at the second-floor piers. Also, as seen in earlier analyses, the front wall's spandrel between the right-side openings was damaged. Two shear cracks at the middle wall's second level are connected to the vertical cracks created where the middle wall and transverse walls intersect. The back wall consistently displayed both the damage from the flexible plate at the third level (which is not present at the second and first floors) and the shear crack that had developed from the second-floor opening.

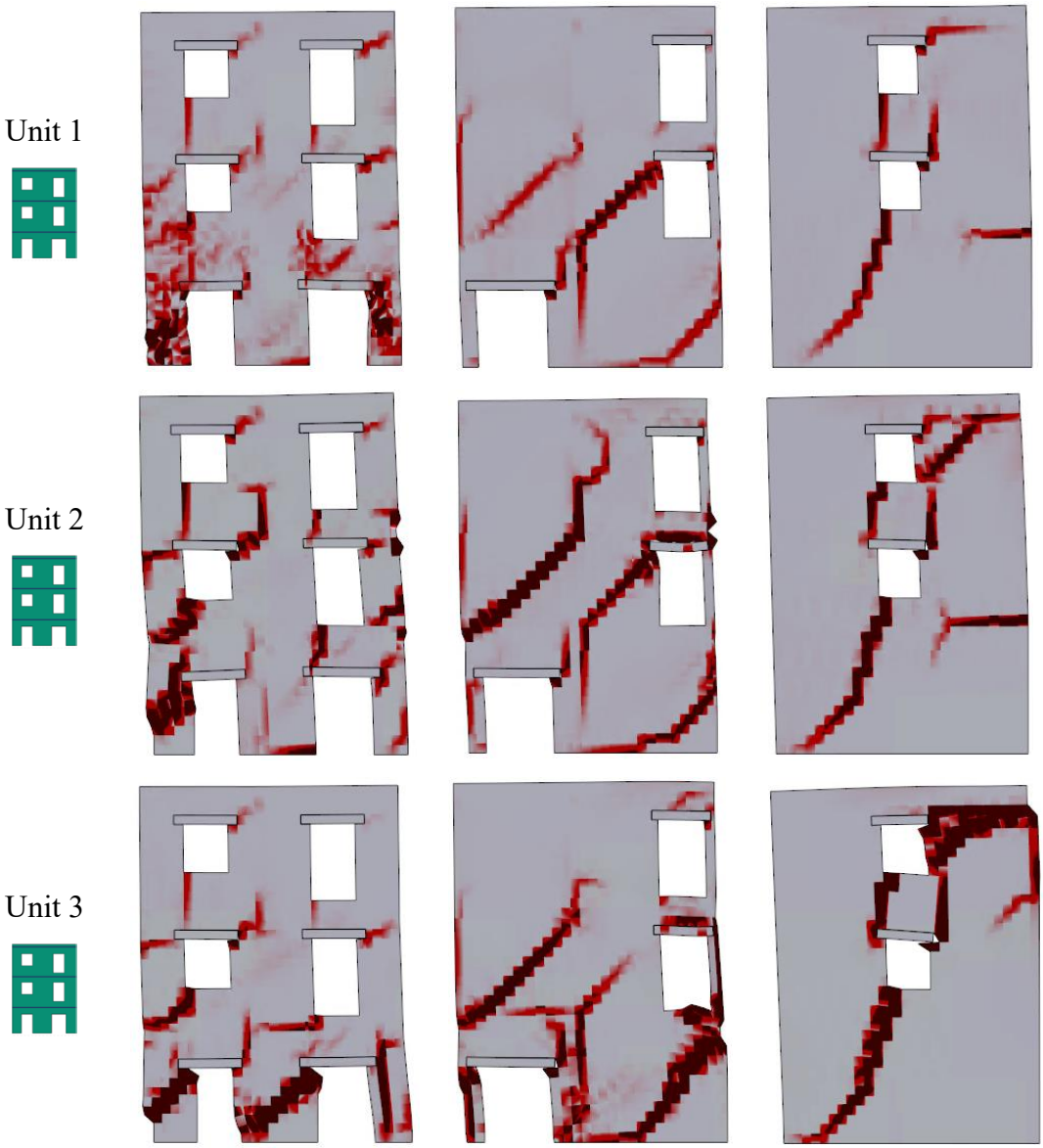

Figure 81. FF Isolated Units, pushover crack pattern X- direction

Comparing the negative pushover to the positive pushover reveals a difference in the front wall's failure mechanism. In this instance, the base piers rather than the second story developed the shear collapse. In fact, Unit 1's external piers completely failed. This explains the difference in resistance between the positive and negative curves. The middle wall also had two shear cracks at the second level that were visible in the positive pushover results, as well as a third crack brought on by the left base pier failing, which caused the overturning of the wall. The Back wall behaved similarly as in the positive pushover.

7.3.3 Aggregate fully connected Dynamic.

As mentioned at the beginning of the chapter, the non-linear dynamic analysis was carried out in the aggregate's longitudinal direction with the L'Aquila earthquake's "X" component as dynamic input. The damping was introduced in the model using an automatic calculation of the Rayleigh coefficients available in STKO, using the first and second frequencies

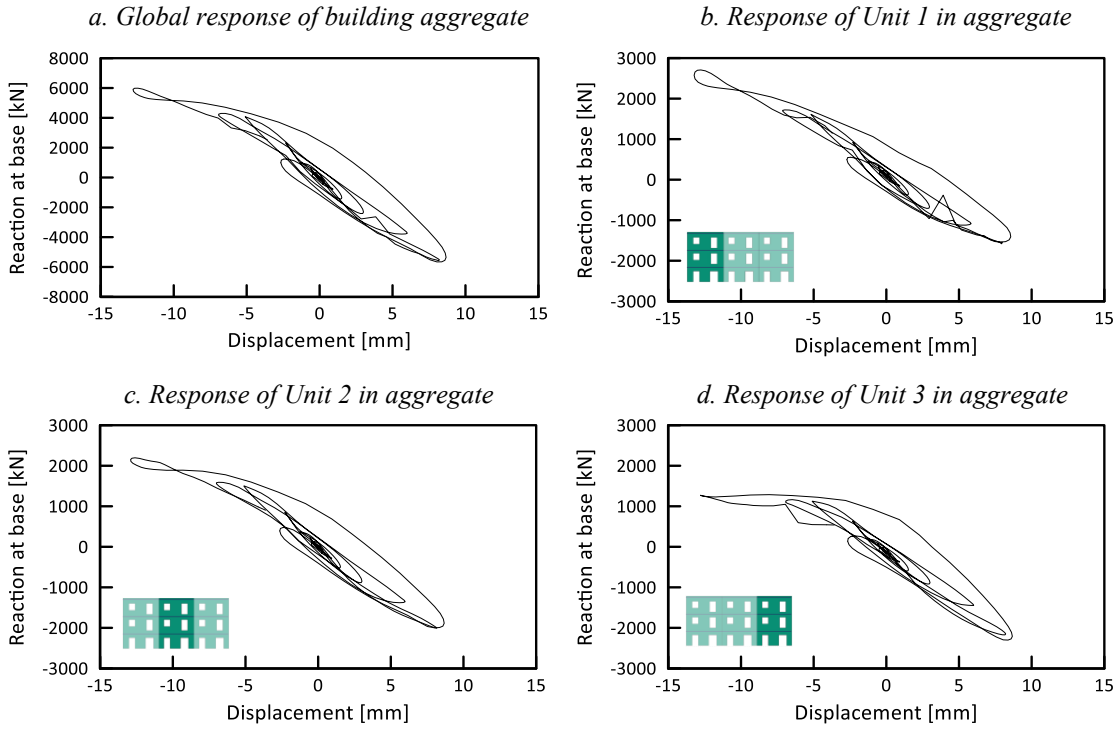

Figure 82. FF Aggregate, non-linear dynamic analysis results

In figure 82, the displacement was correlated with the reaction at the base of the aggregate, showing a maximum resistance of 6000 kN. The response of the units in the aggregate configuration was also extracted from the analysis, using as the control node the top left node of the Front Wall of each unit.

As before, the reaction was measured only in the longitudinal walls to avoid duplication in shared walls. All three units showed very different resistance values in both positive and negative directions. Unit 1 reached a maximum of 2700 kN in the negative direction, while Unit 2 registered 2100 kN and Unit 3 reached 1300 kN in the same direction. When moving in the positive direction, this order was inverted, with Unit 3 being the one with the maximum reaction at base (2500 kN). It can be observed a higher displacement

reached in the negative direction; this is because the oscillation was not completed as the analysis failed when moving towards the positive.

Figure 83 shows the crack opening at the maximum displacement reached and shear failures on the spandrels between the openings of the first and second floor. The tensile cracks at the base piers are also visible.

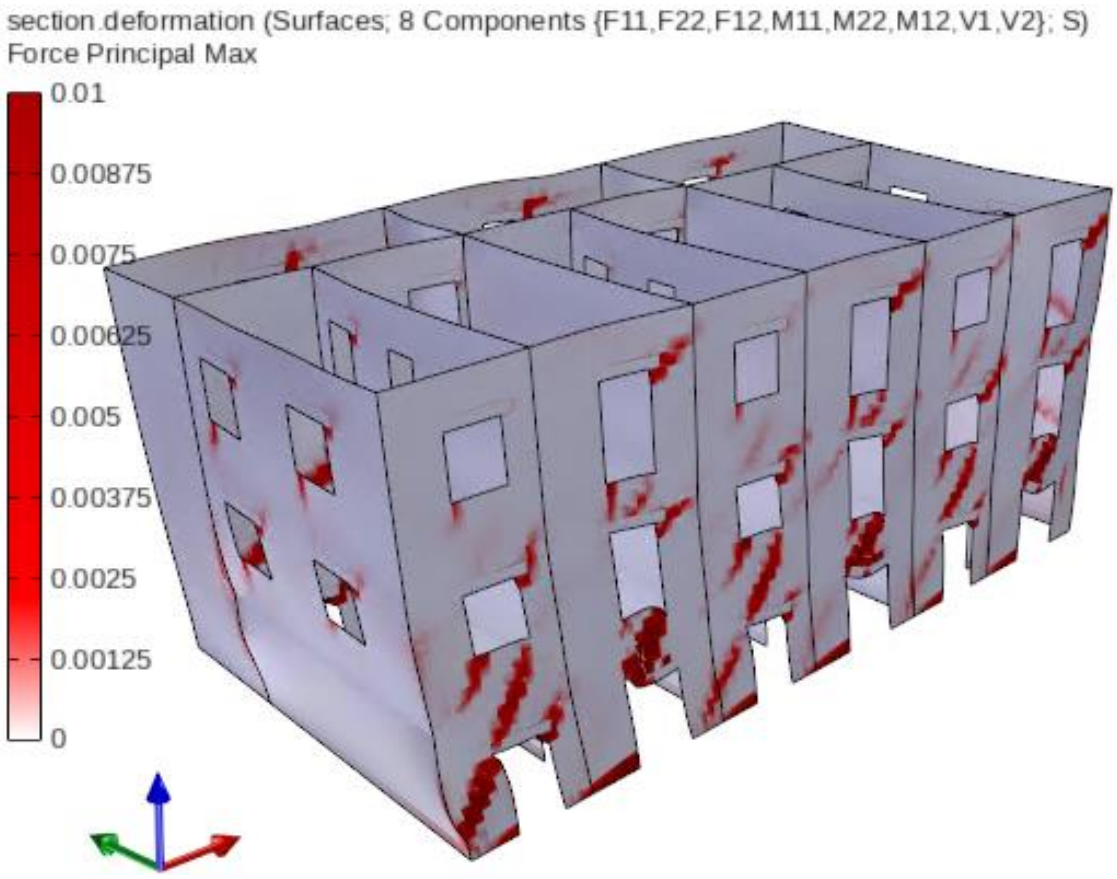

Figure 83. FF Aggregate, non-linear dynamic crack pattern 3D.

In Fig 84, it is possible to observe the shear mechanism on the second floor in the Middle Wall, which is very similar to that obtained in the pushover analysis. The back wall also presented shear cracks at the openings and a tensile crack on the right side of its base. On the right, the total damage, is reported from the step before the collapse.

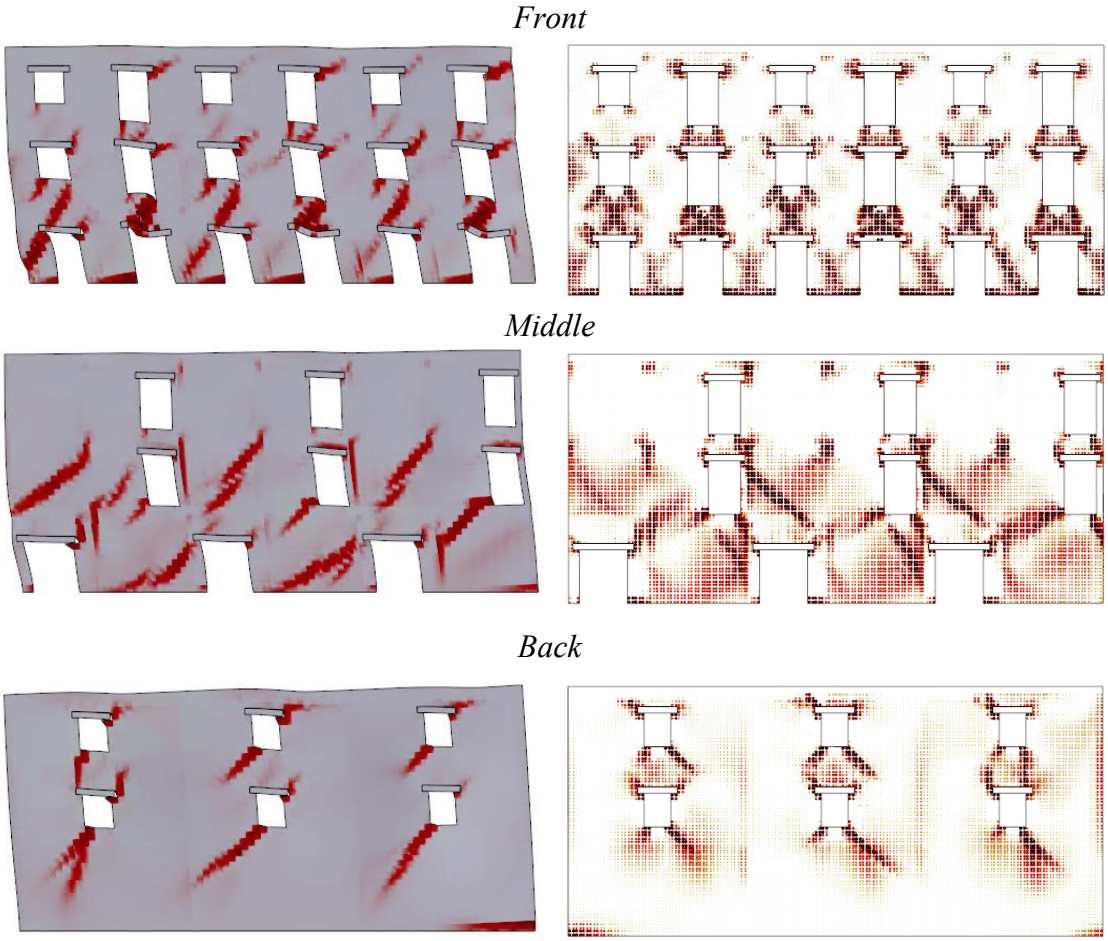

Figure 84. FF Aggregate, non-linear dynamic analysis. a) maximum principal force; b) damage

7.3.4 Isolated non-linear dynamic analysis

The analysis settings were the exact same as the ones used in the aggregate model except for the damping, which used the first two frequencies of the modal analysis of the isolated unit model. The analysis did not last as long as expected, only lasting 2.3 seconds before failing to converge due to building failure. In this case, the high demand on the displacement caused damage to a part of the wall, resulting in detachment. When this happens, numerically speaking, the displacement tends toward infinity, causing the analysis to fail. The displacement-reaction at base curves for each unit are reported in figure 85.

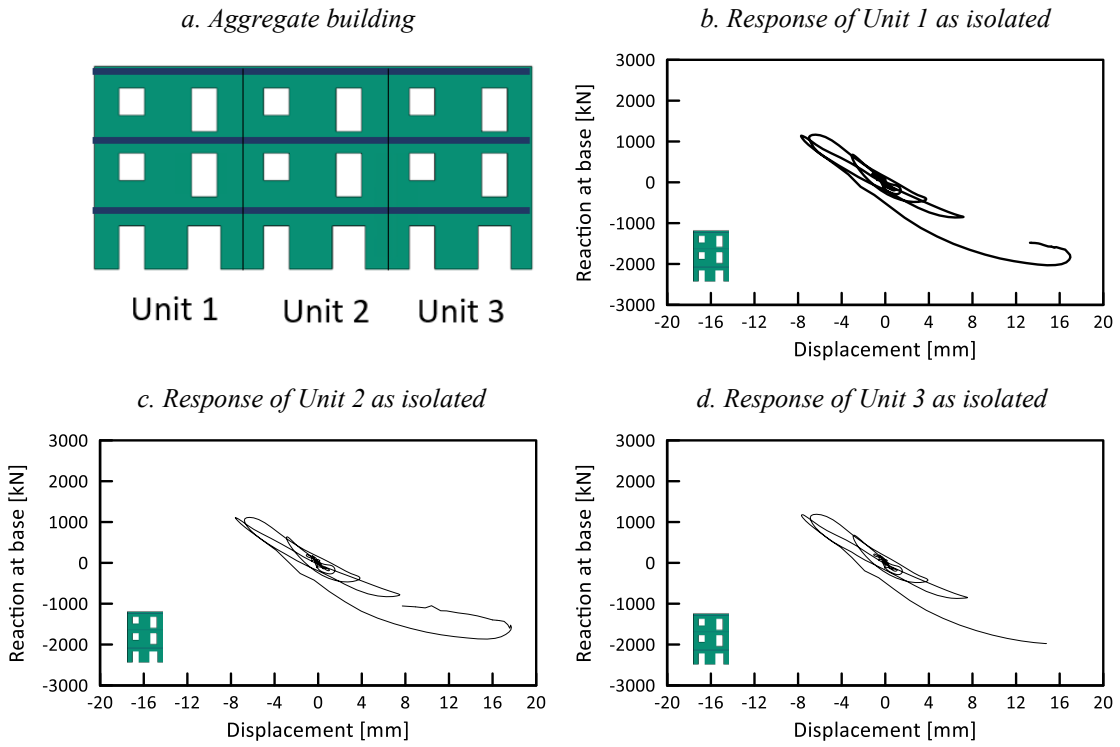

Figure 85. FF Isolated Units, non-linear dynamic analysis results

The curves show that all three units behave the same way, reaching almost the same maximum displacement (Unit 1 reached 17 mm and Unit 2 reached 18 mm). Unit 3 failed convergence before (at 15.7 mm). In all cases, all three units reached the same maximum reaction at base of 2000 kN in the last half oscillation. All three units presented similar failure mechanisms (Figs. 86, 87)

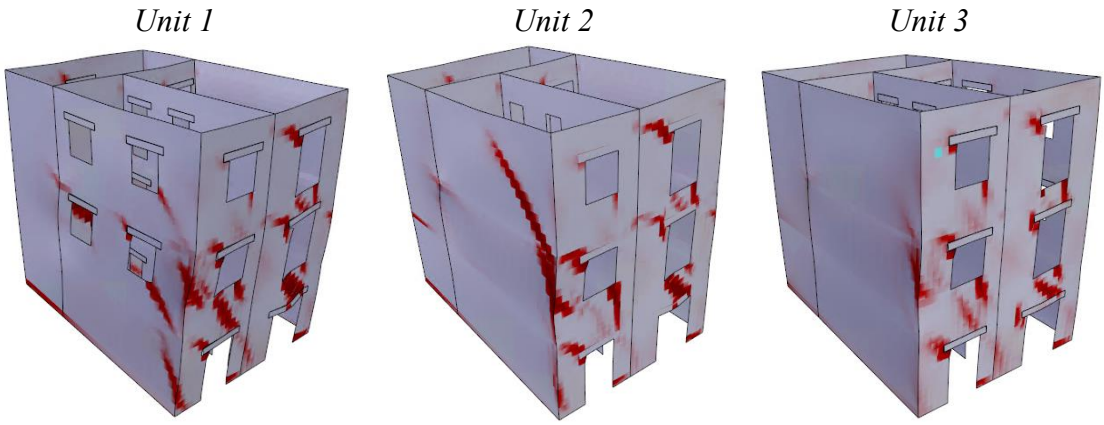

Figure 86. FF Isolated Units, non-linear dynamic analysis crack pattern 3D.

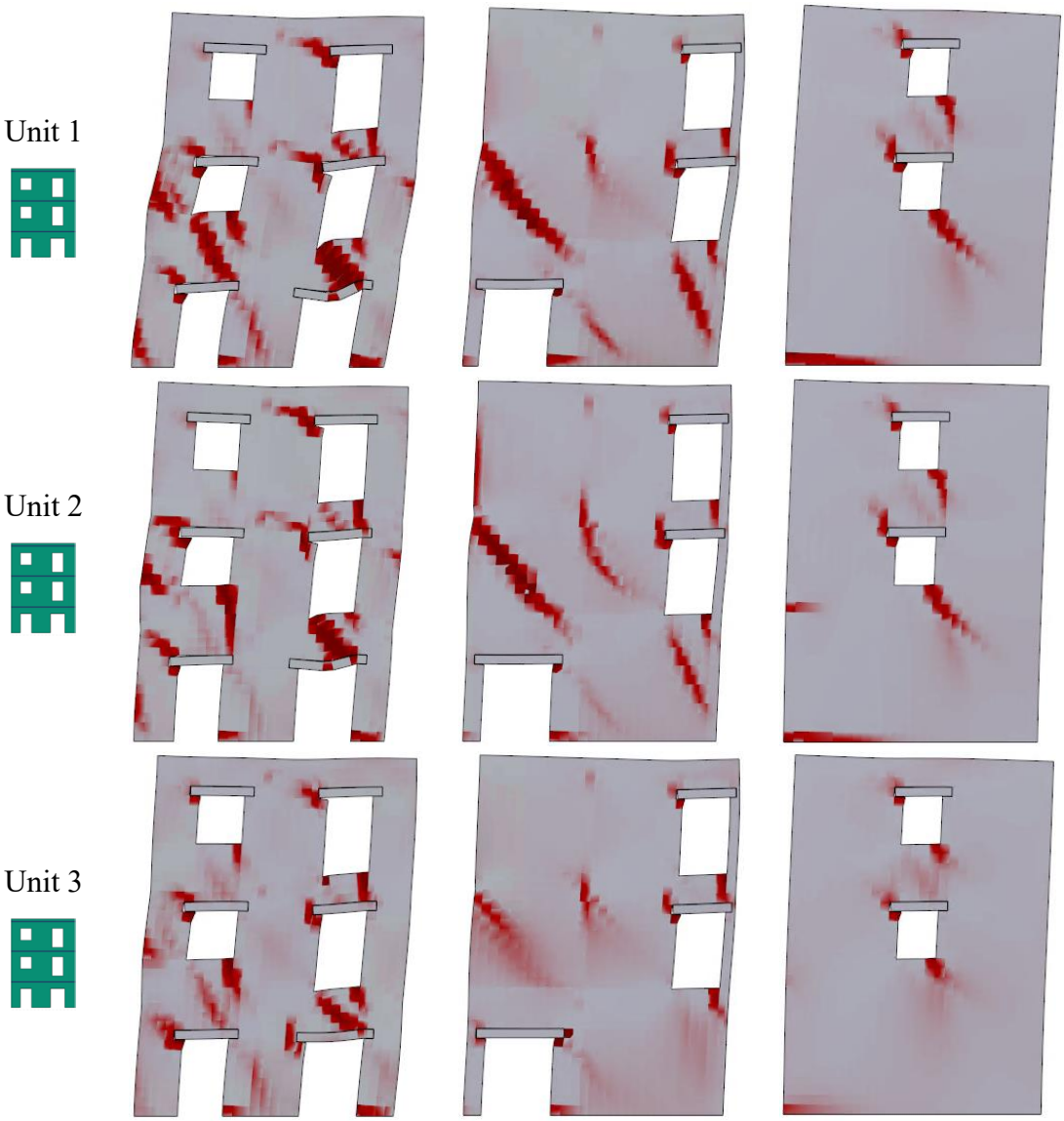

Figure 87. FF Isolated Units, non-linear dynamic analysis crack pattern on walls.

7.3.5 Aggregate semi-connected Pushover

For the Semi-connected case, it was not possible to perform a modal analysis to assess the fundamental mode because all first modes where predominantly local, and there was no clear global behavior. For this reason, the forces applied were the same used in the fully connected case, again applied as a distributed face force.

The curves belonging to each unit were extracted and are reported in figure 88.

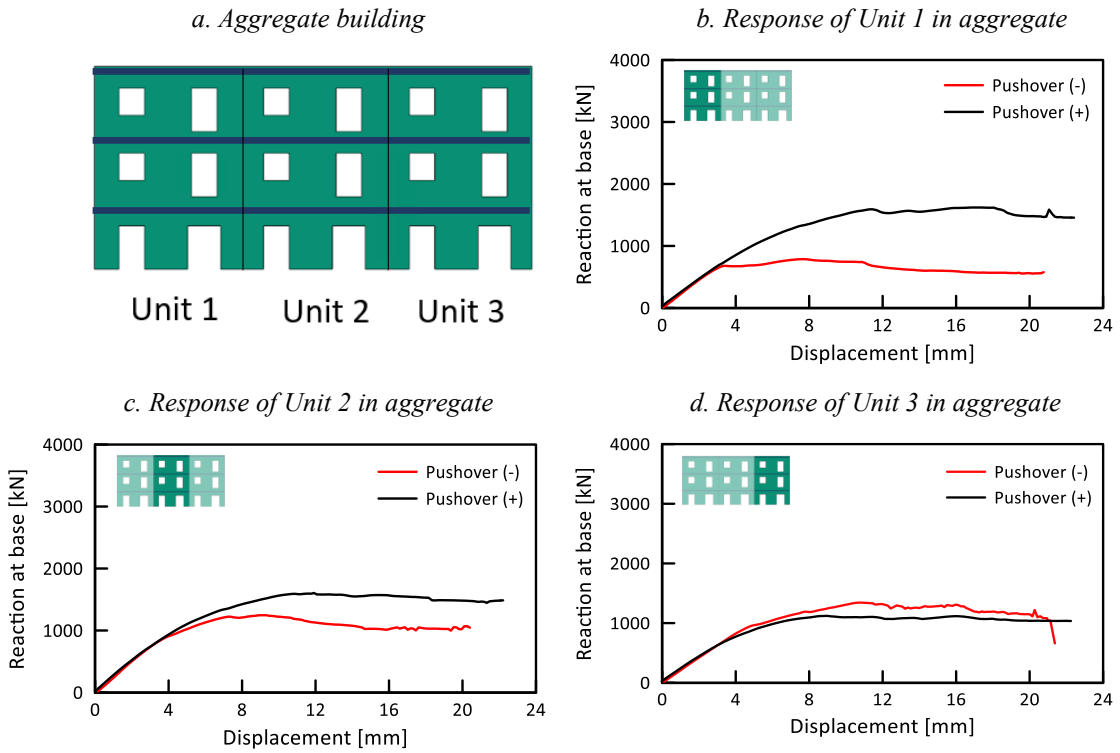

Figure 88. FF Semi-connected Units, pushover curves

Similarly, to the Rigid Diaphragm case, after reaching 21mm, the friction forces are overcome, and the buildings start to slide against each other. As it can be observed, when pushed to the negative direction, after 21mm, only the Unit 3 shows softening whereas Unit 1 and 2 have an increment in resistance. The sliding also causes the top nodes to uplift, compromising the reliability of the displacement measure.

Figure 89 shows a predominantly shear failure at he the second story of the front wall and multiple flexural failures at the transverse wall. It is possible to observe the front wall of Unit 1 sliding forward the front wall of unit 2, while the Back Wall mirrors that action. The middle wall, being trapped is the one that damages the most due to crushing.

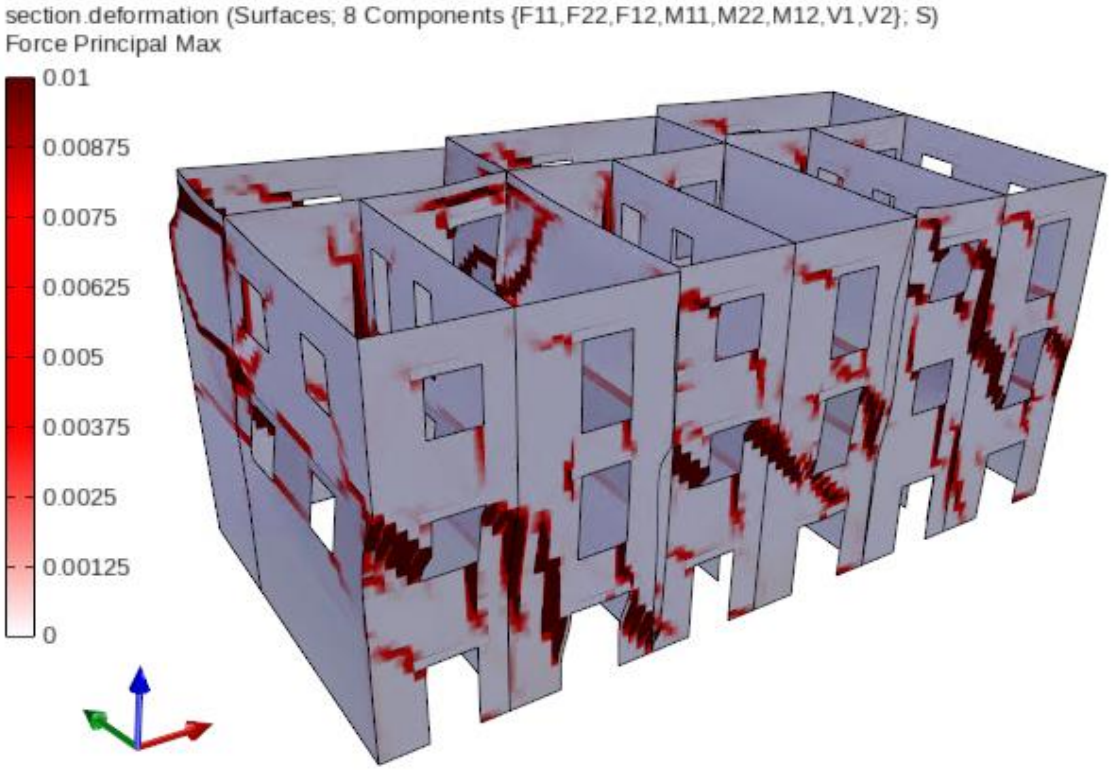

Figure 89. FF Semi-connected Units, pushover crack pattern 3D

Figure 90 shows a detailed plot of the damage using the maximum principal force.

Front

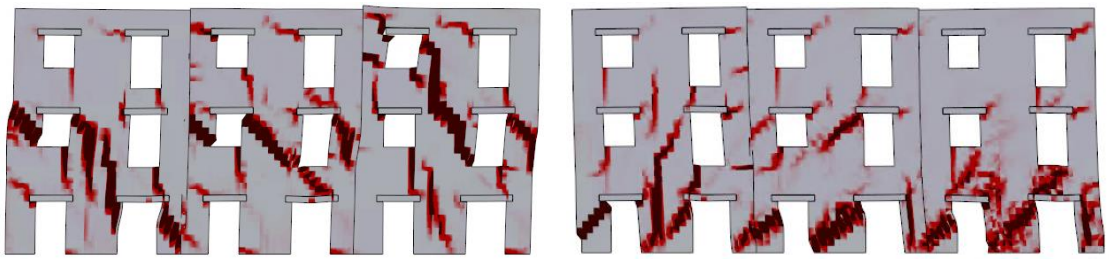

Middle

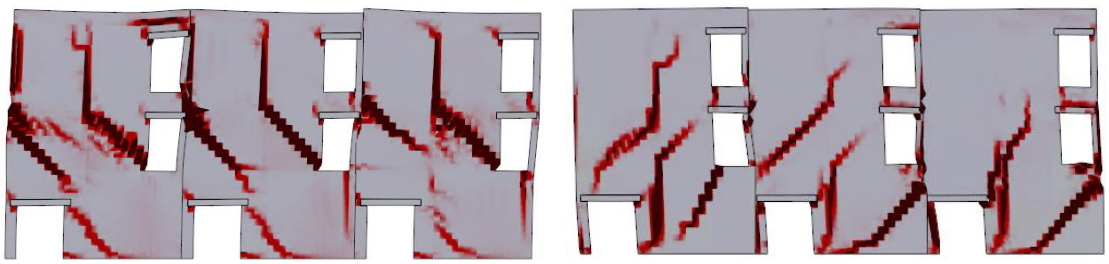

Back

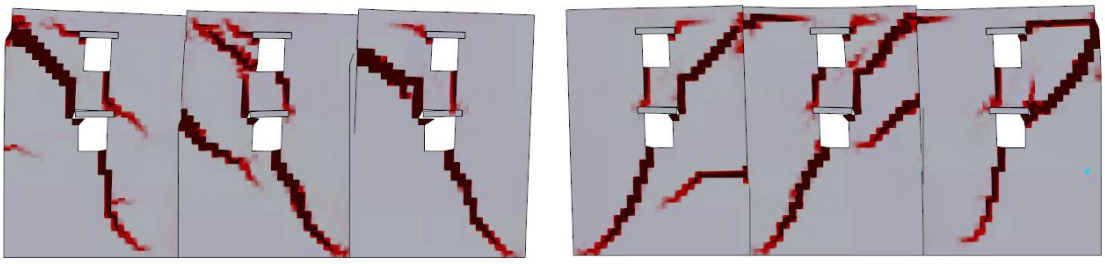

Figure 90. FF Semi-connected Units, pushover crack pattern a) X+ direction; b) X- direction

Figure 90 makes it easier to see the crushing that occurred between the left openings and the intersection of the walls, which is one of the middle wall's weak areas. Like earlier analyses, a pushover in a positive direction tends to heighten the damage in the second story while a pushover in a negative direction tends to raise the damage at the base piers. This demonstrates how the location and size of openings have a direct impact on the failure mechanism in masonry structures. The Back wall, being symmetric, behaved the same way in both analyses.

7.3.6 Aggregate semi-connected non-linear dynamic analysis

For the Semi-connected case, it was not possible to perform a modal analysis to assess the frequencies to be used for the Rayleigh damping model because all first modes where predominantly local, and there was no clear global behavior. For this reason, the frequencies adopted were the same used in the "Fully Connected" case.

The curves belonging to each unit were extracted and are reported in figure 91.

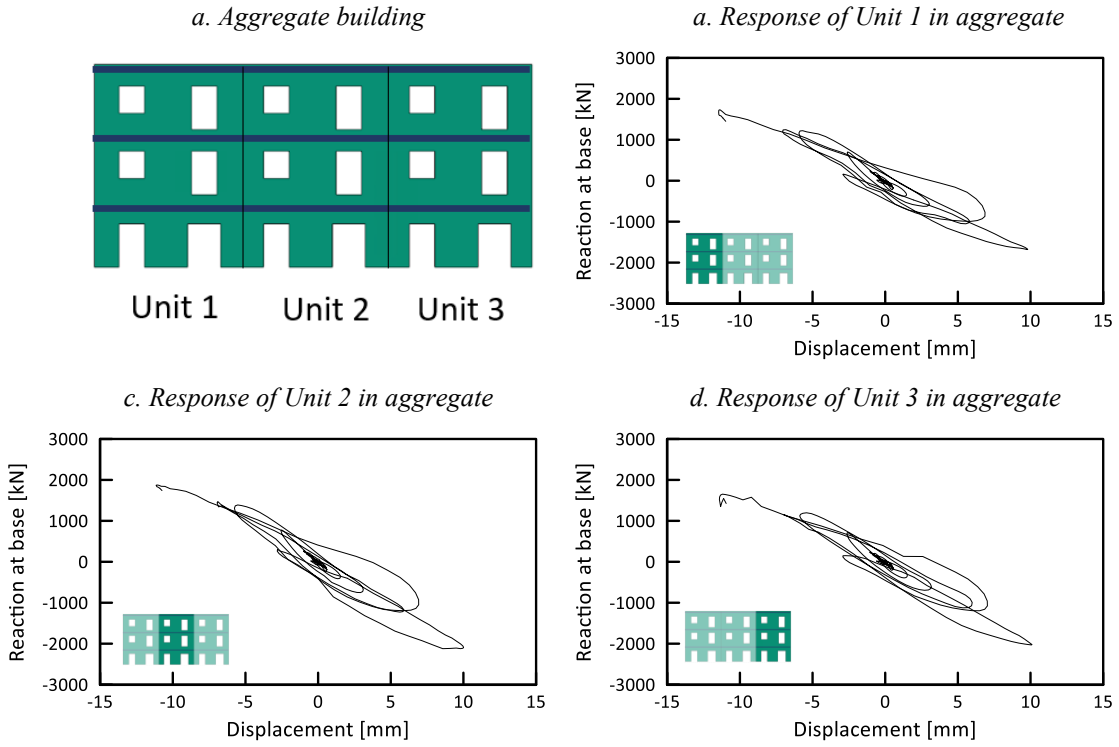

Figure 91. FF Semi-connected Units, non-linear dynamic analysis results

The dynamic analysis had convergence issues around step 555/3000. Which is about 2,8 seconds. As before, the range from 2.3s to 4.5s is where the major displacement was registered in both Fully Connected and Isolated Units cases. The displacement registered on all three units surpassed the 11.5 mm in the negative direction and reached 10 mm in the positive direction, which is less than the one obtained when analyzing the units as isolated. It should be considered that there are additional stresses along the contact between adjacent walls that are not taken into account in the previous cases.

It can be seen from Figure 92 that the front and back walls of Unit 1 and Unit 3 lift as the aggregate oscillates. The model showed significant damage to the piers and spandrels prior to the analysis being terminated due to the large displacement demand in the last oscillation.

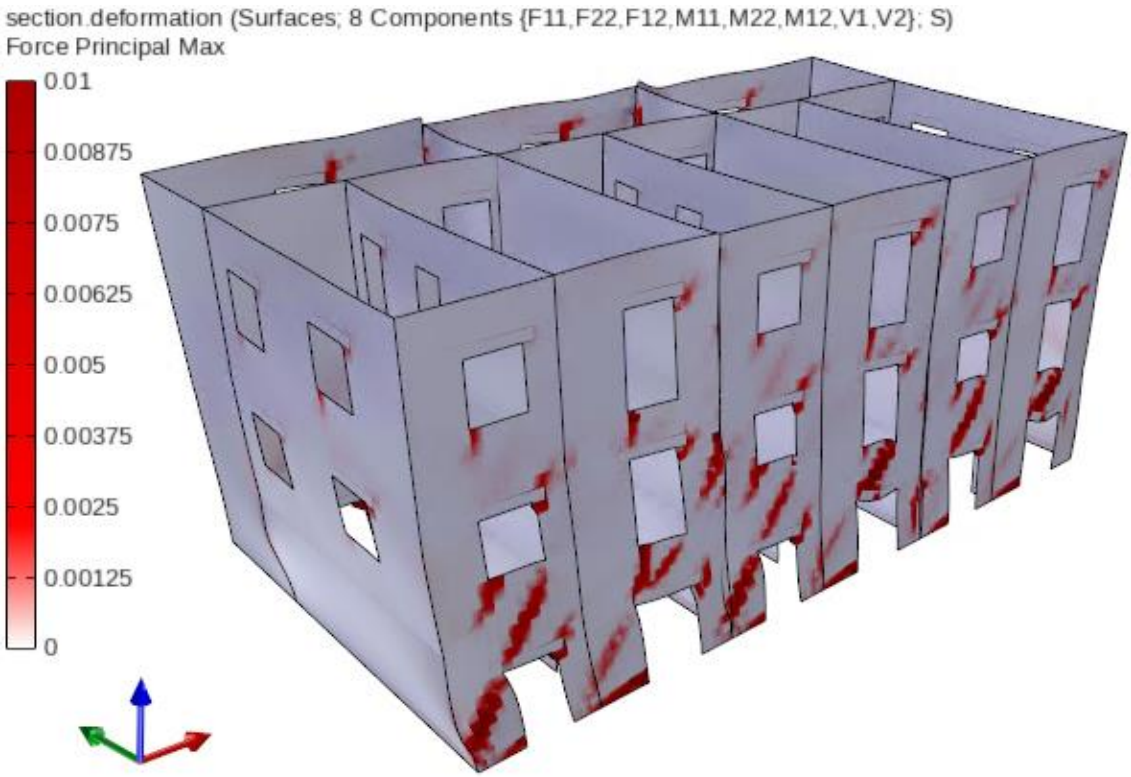

Figure 92. FF Semi-connected Units, non-linear dynamic analysis crack pattern 3D.

7.4 Discussion

In this paragraph, the results of the analyses are discussed and compared to assess the influence of the "aggregate effect" in all the configurations studied.

Results of fully connected aggregate with rigid diaphragm

The curves belonging to the Fully Connected Aggregate and Isolated Units analyses from the Rigid Diaphragm case are reported in figure 93.

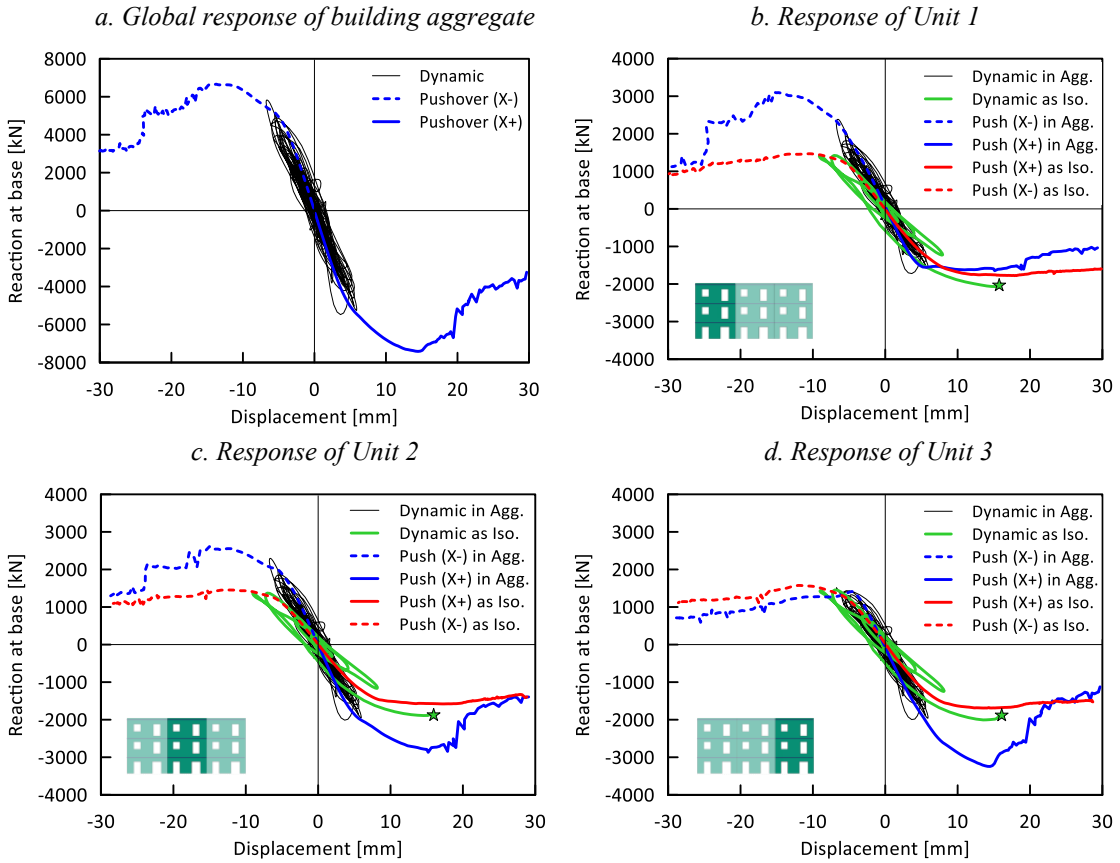

Figure 93. Comparison of numerical response: "Fully Connected" and "Isolated Units" cases with Rigid Diaphragm

Observing the pushover curves from Unit 1, it can be noted that when pushed to the negative direction in aggregate configuration (blue), there is an increment in the resistance that almost triplicates the one obtained when analyzing the unit as isolated (red). The same effect occurs when analyzing Unit 3 when pushed in the positive direction. Instead, when Unit 1 is pushed in the positive direction, there is almost no difference between the aggregate and the isolated configuration. The same occurs in Unit 3 in the negative direction. Unit 2, however, presents very similar results in both directions yet the

increment of resistance with respect to the isolated configuration is less than the measured for external units.

Results of fully connected aggregate with flexible floor

The curves belonging to the Fully Connected Aggregate and Isolated Units analyses from the Flexible Floor case are reported in Figure 94.

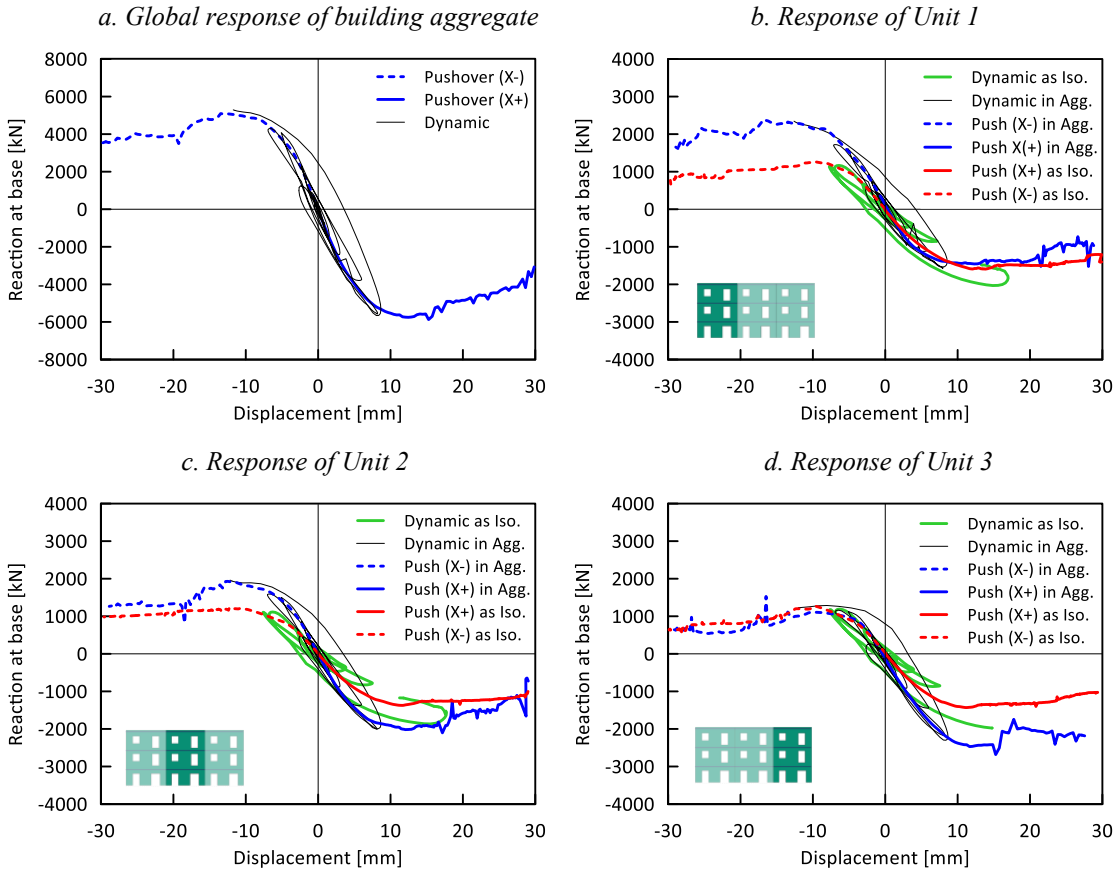

Figure 94. Comparison of numerical response: "Fully Connected" and "Isolated Units" cases with Flexible Floor

As observed in the Rigid Diaphragm configuration results, the same effect on the external units is observed. When the aggregate is pushed in the positive direction, Unit 1 behaves as if it was isolated from the aggregate. Unit 3, on the other hand, experiences this effect when the aggregate is pushed in the negative direction. Although these results are comparable in that sense, it is essential to take into consideration the lower increase in resistance, which could be the root cause of the premature failure of the aggregate dynamic analysis. In fact, it can be said a priori that the degree of slab stiffness potentiates the benefits of the "aggregate effect".

Results of semi-connected aggregate with rigid diaphragm

Figure 95 shows the comparison between the "semi-connected" and the "Isolated Units" configurations for the Rigid Diaphragm case.

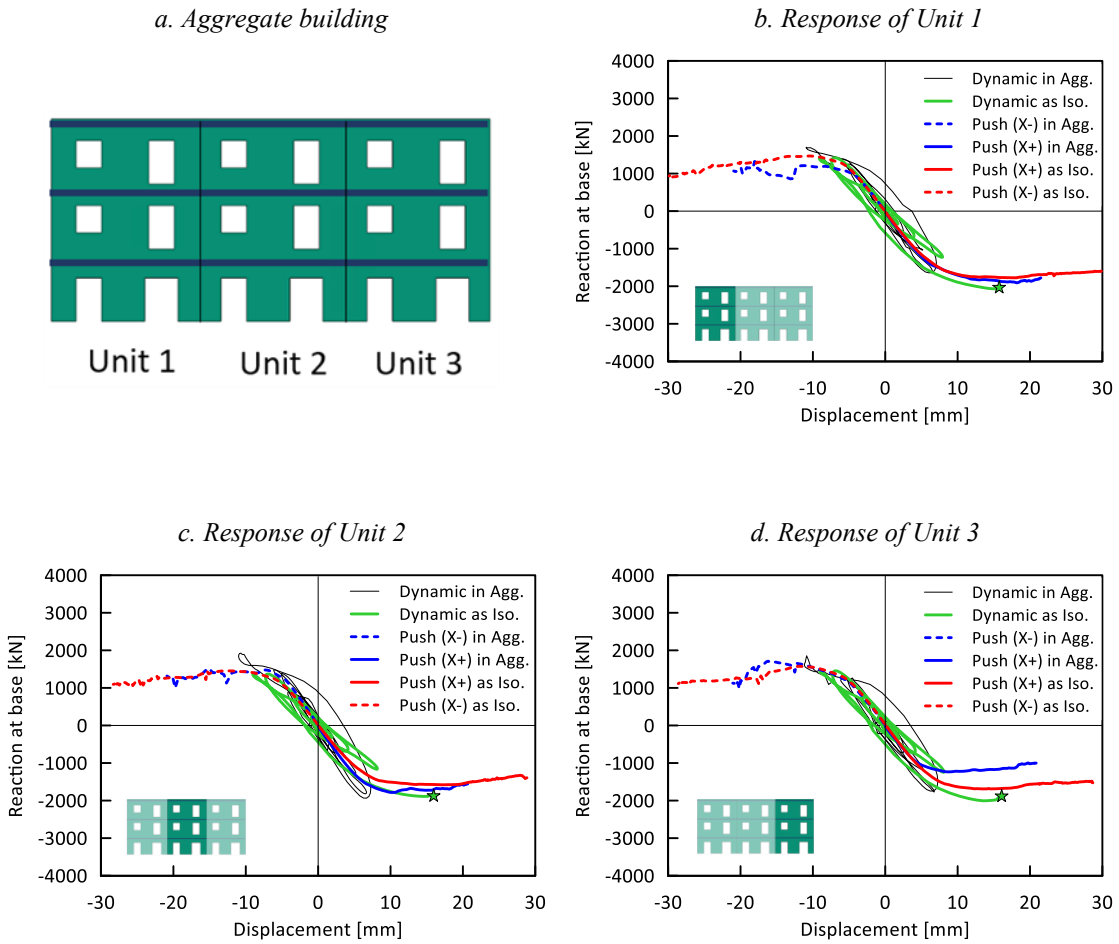

Figure 95. Comparison of numerical response: "Aggregate semi-connected" and "Isolated Units" cases with Rigid Diaphragm

The results of the dynamic test showed that the isolated units reached a larger displacement in the first cycles, compared to the Semi-connected aggregate configuration, where the displacement was limited until the friction force was overcome. Once the friction force had been overcome, the displacement demand increased, leading to a behavior that was like that of the isolated case. Comparing the pushover results with the fully connected case (both rigid and flexible configuration), it is possible to observe that the increment in resistance is no longer present. In fact, pushover curves indicate that the semi-connected units behave as isolated units, but with a possible loss in resistance due to the contact and frictional stresses.

Results of semi-connected aggregate with flexible floor

Figure 96 show the results comparison between the "Aggregate semi-connected " and the "Isolated Units" configurations for the Flexible Floor case.

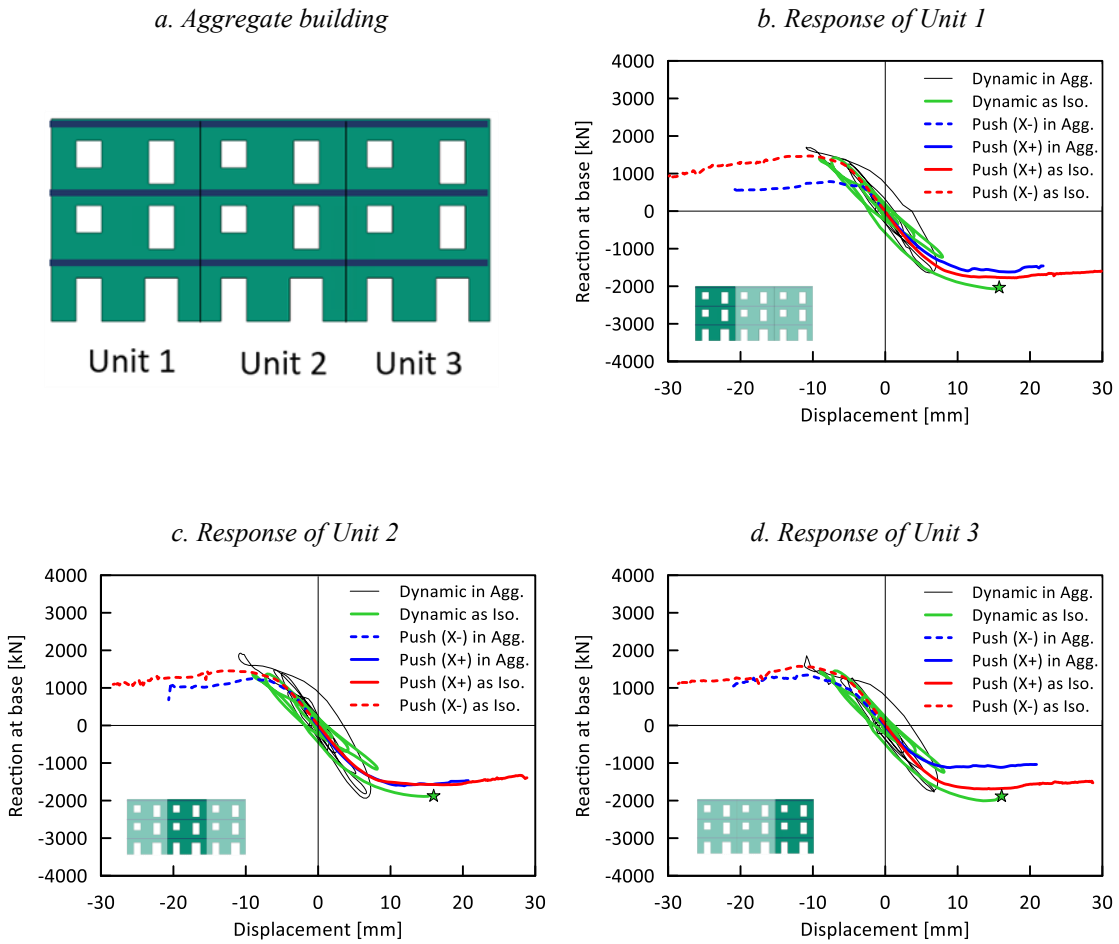

Figure 96. Comparison of numerical response: "Aggregate semi-connected" and "Isolated Units" cases with Flexible Floor

The dynamic results did not differ much with respect to those obtained for the Rigid Diaphragm case, showing that the aggregate effect seems to be present only in the first cycles. Again, the pushover curve of the semi-connected aggregate does not match the aggregate's dynamic one. Instead, it seems to follow the isolated unit one. The pushover results also evidence the lack of increment in resistance observed in the fully connected aggregate for both slab configurations.

8. Conclusions

The analysis of aggregate buildings has proven to be a challenging task due to the complexity of the interacting failure mechanisms present, the high dependency on geometrical features and the difficulty in defining constitutive models that are able to replicate masonry behavior. Over the years, conservative simplifications led to common practices such as the analysis of single structural units without considering the interaction with adjacent ones known as “Aggregate Effect”.

In this context, the present study aimed to demonstrate the potentially beneficial impact of the “Aggregate Effect” by means of static and dynamic analyses and assessed the validity of the non-linear static analysis in capturing the dynamic behavior of the structure.

With the aid of STKO, a reference aggregate model of similar single units was designed to compare responses without the influence of geometry variations. The aggregate was composed of three units of three-story each, with the central unit sharing a divisor wall with the other two. Masonry was modelled using a homogenized (continuum) approach following a calibration of the strength parameters saving valuable computational time and maintaining the quality of the outcome. It is worth noting that this was possible thanks to the efficiency of the *IMPL-EX* algorithm and the performance of the *ASDShellQ4*.

The aggregate was studied using two floor configurations: “Rigid Floor” and “Flexible Floor”. Under both, the aggregate was examined in two ways: “Fully Connected” and “Semi-connected”. In the “Fully Connected” situation, the longitudinal walls of Unit 1 and Unit 3 were rigidly connected to the transverse walls of Unit 2. In the “Semi-Connected” case, although these walls were separated, they were able to interact by creating contact and friction forces. Additionally, the units were also examined separately, referred to as “Isolated”.

The analysis procedure involved, first, a modal analysis to assess the fundamental mode of vibration, which served as input for the following analysis. Secondly, pushover analyses were carried out using a lateral force distribution proportional to the fundamental

mode. Finally, these were contrasted with non-linear dynamic analyses using a component of L'Aquila earthquake as input in the longitudinal direction of the aggregate.

Pushover curves largely matched those of non-linear dynamic analysis in the elastic phase, yet the aggregate dynamic curve does not reach softening, so comparison to the pushover curve is not possible. Consequently, the pushover's ability to capture dynamic behavior is unclear. To further evaluate the pushover's capacity to assess seismic response of masonry aggregates, additional dynamic analyses using a series of spectrum-compatible earthquakes could be considered in future developments.

The results demonstrate that the in-aggregate configuration has a considerable beneficial effect depending on the position of the individual units and the direction of displacement. The confinement effect of the adjacent units provides a considerable increment in resistance that cannot be captured by analyzing units as isolated. This effect is enhanced when a rigid diaphragm is present, displaying a substantial rise in resistance, useful during a dynamic input. Even though the aggregate effect is still evident with a Flexible Floor, there is a notable reduction in magnitude compared to the rigid case.

The tests on both rigid and flexible diaphragm cases also showed that isolated units had a larger displacement in the first cycles, compared to the Semi-connected-units configuration where the displacement was limited until the friction force was overcome. After the resistance of the friction force was surpassed, the displacement demand increased and behaved similarly to the isolated case.

It is possible to conclude that the "Aggregate Effect" is in any case beneficial and can be advantageous to consider it in the assessment of masonry buildings. The increase in resistance, regardless of slab configuration, can be fundamental in facilitating the fulfillment of seismic verifications. In this context, determining the actual degree of connection between units becomes critical when assessing these structures.

Appendix

Aggregate dimensions

Front Wall

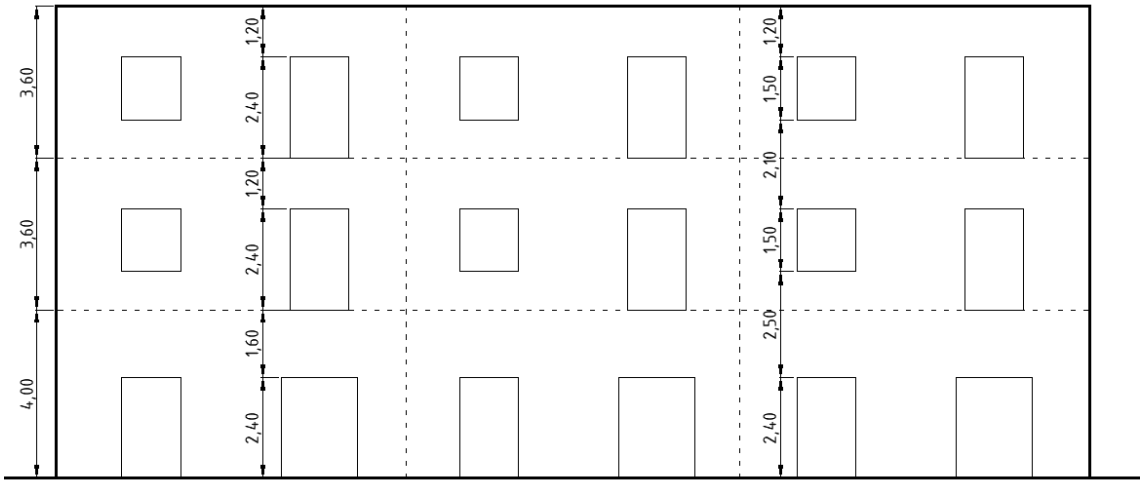

Back Wall

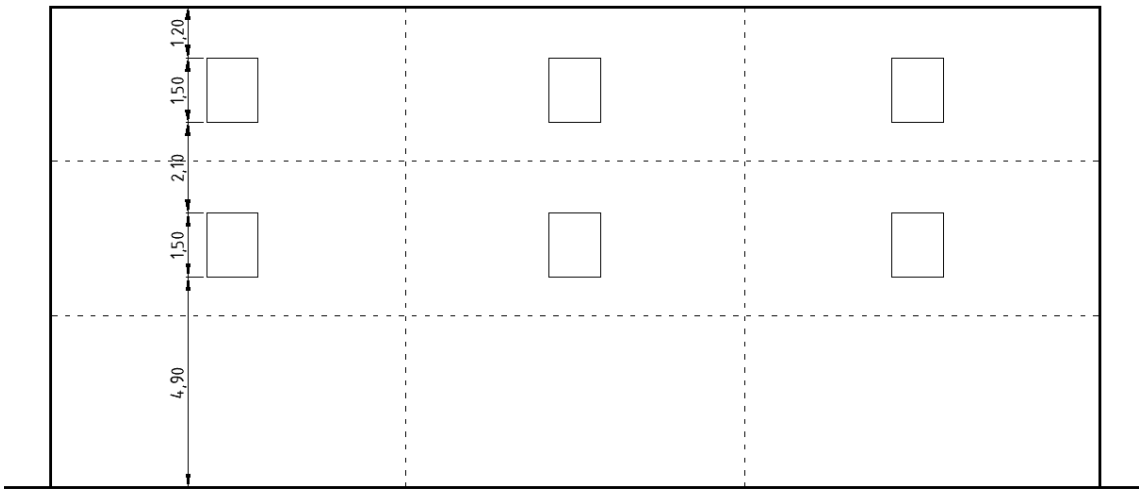

Middle Wall

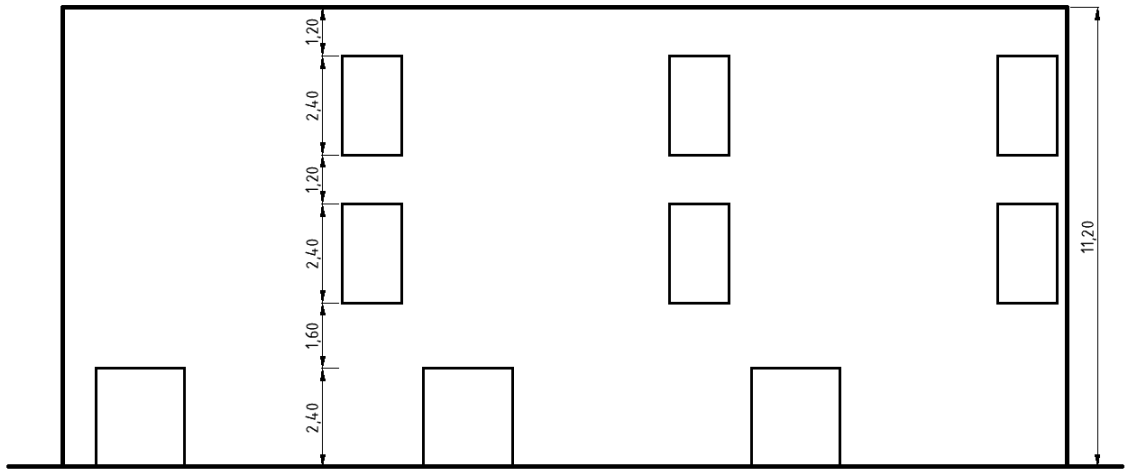

First Floor

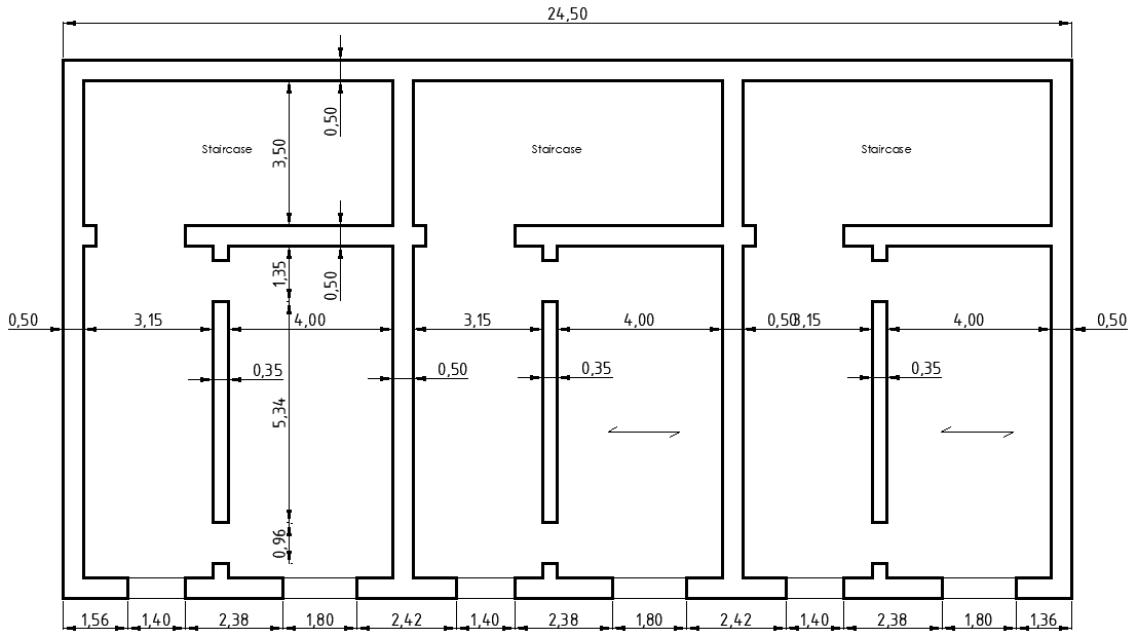

Second and Third Floor

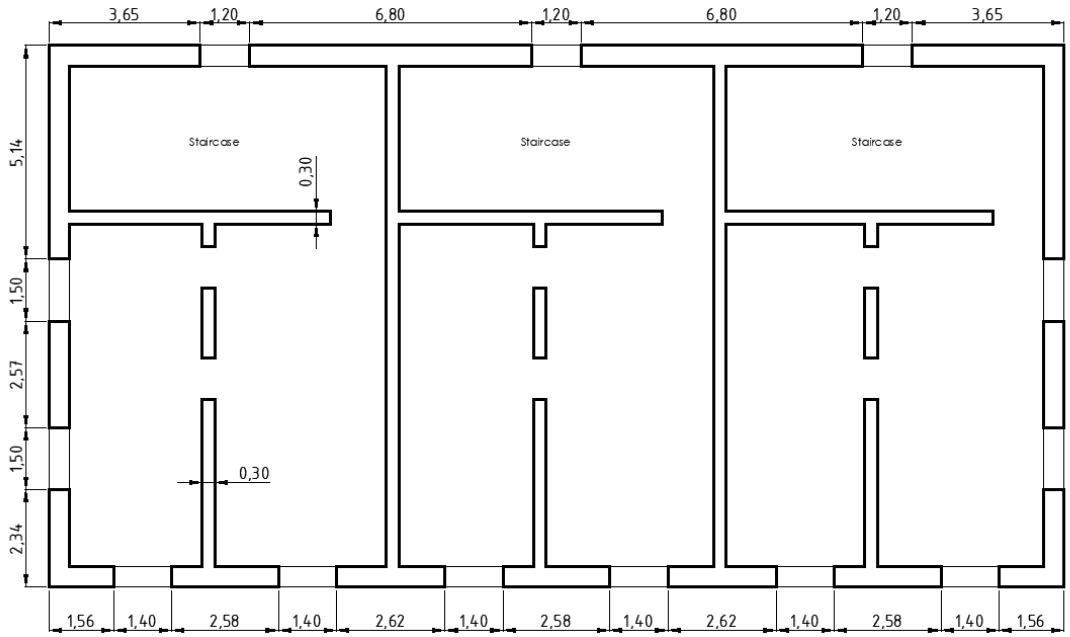

Transverse Walls

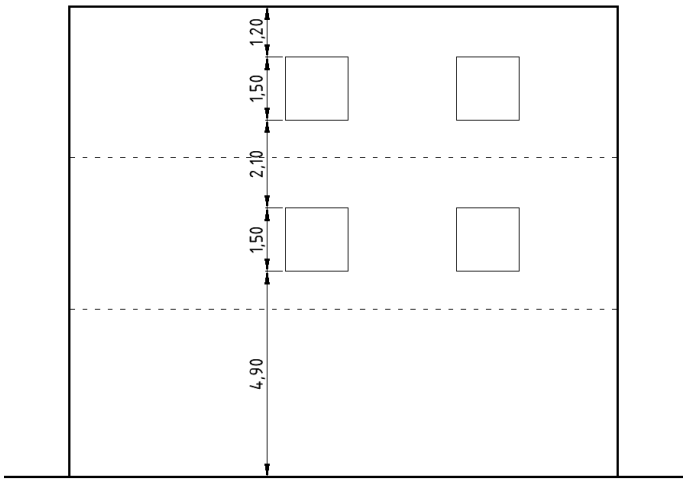

References

1. *Seismic behaviour of ordinary masonry buildings during the 2016 central Italy earthquakes.* Sorrentino, L., Cattari, S., da Porto, F., Magenes, G., & Penna, A. 1-25, 2019, Bulletin of Earthquake Engineering, págs. 1-25.

2. *Seismic assessment of interacting structural units in complex historic masonry constructions by nonlinear static analyses.* Abbati, Stefania Degli, et al. 2019, Computers & Structures, vol 213, pp. 51-71.

3. *Seismic fragility assessment of existing masonry buildings in aggregate.* Angiolilli, Michele, et al. 2021, Engineering Structures 247, pp. 0141-0296.

4. *Seismic Testing of a Full-Scale, Two-Story Masonry Building: Test Procedure and Measured Experimental Response.* Magenes, Kingsley and Calvi. 1995.

5. *Measuring masonry material Properties.* Binda, L., Roberti, G. Mirabella and Abbaneo, C. Tiraboschi e S. 1994, Proceeding of the U.S.-Italy Workshop on Guidelines for Seismic Evaluation and Rehabilitation of Unreinforced Masonry Buildings (Technical report NCEER-94-0021), pp. 6.3-6.24.

6. *Shear-compression testing and analysis of brick masonry walls.* Anthoine, A. and Guido, G. Magonette and M. 1995, Proceedings of the 10th European conference on earthquake engineering, vol 3.

7. *Experimental Research on Response of URM Building Systems.* Magenes, G. M. Calvi and G. 1994, Proceeding of the U.S.-Italy Workshop on Guidelines for Seismic Evaluation and Rehabilitation of Unreinforced Masonry Buildings (Technical report NCEER-94-0021), págs. 3.41 - 3.57.

8. Petracca, M., Candeloro, F., Camata, G. *ASDEA Software STKO user manual.* 2017.

9. McKenna, F., Fenves, G.L. and Scott, M.H. Open system for earthquake engineering simulation. University of California, Berkeley, CA. : s.n., 2000.

10. Fondo Ambiente. [Online] fondoambiente.it.

11. Donà, C. and A. De Maria. *Manuale delle murature storiche.* Roma : DEI, 2011.

12. *Comparative Seismic Assessment Methods for Masonry Building Aggregates: A Case Study.* Formisano, Antonio and Chieffo, Nicola. 2019, Built Environment, p. 5:123.

13. *On the vulnerability features of historical masonry buildings in aggregate.* Angiolilli, Michele, et al. 2023, Procedia Structural Integrity, Vol 44, pp. 2074-2081.

14. *Influence of wall-to-floor connections and poundingon pre- and post-diction simulations of a masonry buildingaggregate tested on a shaking table.* Bianchini, N., et al. 2023, Bulletin of Earthquake Engineering.

15. Mezzina, M. and Uva, G. *Edifici esistenti in muratura tra sicurezza e conservazione. Palazzo Carmelo a Cerignola.* s.l. : CittàStudi, 2022.

16. Pisani, M. *Consolidamento delle strutture. Guida ai criteri, ai materiali e alle tecniche più utilizzati.* Milan : Hoepli, 2008.

17. *Numerical investigation of non-linear equivalent-frame models for regular masonry walls.* Siano, Rossella, et al. 2018, Engineering Structures, Vol 173, pp. 512-529.

18. *Micro-scale continuous and discrete numerical models for nonlinear analysis of masonry shear walls.* Petracca, Massimo, et al. 2017, Construction and Building Materials, Vol 149, pp. 296-314.

19. *Efficient Constitutive Model for Continuous Micro-Modeling of Masonry Structures.* Petracca, M., et al. 2023, International Journal of Architectural Heritage, pp. 17:1, 134-146.

20. *Regularization of first order computational homogenization for multiscale analysis of masonry structures.* Petracca, M., L., Pelà and R., Rossi. 2016, Comput Mech 57, pp. 257–276.

21. *Numerical simulation of an adobe wall under in-plane loading.* Tarque, Nicola & Camata, et al. 2014, Earthquakes and Structures, Vol 6, pp. 627-646.

22. *Schematizzazione e modellazione degli edifici in muratura soggetti ad azioni sismiche.* Dolce, M. 1991.

23. *Uses and limits of the Equivalent Frame Model on existing unreinforced masonry buildings for assessing their seismic risk: A review.* E., Quagliarini, G., Maracchini and F., Clementi. 2017, Building Engineering, Vol 10, pp. 166-182.

24. *A multi-layer shell element for shear walls based on OpenSEES.* Xie, Linlin, et al. 2015, Finite Elements in Analysis & Design, pp. 98: 14-25.

25. OpenSees documentation. [Online] https://opensees.github.io/OpenSeesDocumentation/user/manual/model/elements/ASDShellQ4.html.

26. OpenSees documentation. [Online] https://opensees.github.io/OpenSeesDocumentation/user/manual/model/elements/zeroLengthContactASDimplex.html.

27. *Numerical modeling of reinforced concrete columns strengthened with composite materials.* Barkhordari, M.A., et al. 2013, Asian Journal of civil engineering, Vol 15, pp. 557-576.

28. *Micro-scale continuous and discrete numerical models for nonlinear analysis of masonry shear walls.* Petracca, Massimo M, et al. 2017, Construction and Building Materials, vol 149, pp. 296-314.

29. *An implicit/explicit integration scheme to increase computability of non-linear material and contact/friction problems.* Olive, J., A.E. Huespe and Cante, J.C. 2008, Computer Methods in Applied Mechanics and Engineering, vol 197, pp. 1865-1889.

30. *fib Model Code for concrete structures 2010.* s.l. : John Wiley & Sons, 2013.

31. *Guidelines for Nonlinear Finite Element Analysis of Concrete Structures.* Water, et al. 2020, p. version 2.2.

32. Chopra, Anil K. *Dynamics of Structures Theory and Applications to Earthquake Engineering, IV edition.* University of California at Berkeley : Pearson, 2014.

33. Pinho, Rui, Bianchi, Federica and Nascimbene, Roberto. *Valutazione sismica e tecniche di intervento per edifici esistenti in c.a.* s.l. : Maggioli Editore, 2022.

34. Pandolfi. Analisi non lineari di strutture con il metodo degli Elementi Finiti. *Tesi di dottorato.* Politectino di Milano : s.n., 2003.

35. *Tracking multi-directional intersecting cracks in numerical modelling of masonry shear walls under cyclic loading.* Savvas, Saloustros, Miguel, Cervera and Luca, Pelà. 2017, Meccanica, vol 53, pp. 1757-1776.

36. *Seismic vulnerability of building aggregates through hybrid and indirect assessment techniques.* Maio, R., Vicente, R., Formisano, A. et al. 2015, Bull Earthquake Eng 13, pp. 2995–3014.

37. *Regularization of first order computational homogenization for multiscale analysis of masonry structures.* Petracca, M., Pelà, L. and R., Rossi. 2016, Comput Mesh, vol 57, pp. 257–276.

Acknowledgements

First, I would like to thank Professor Fabio di Trapani for giving me the opportunity to be part of a group of passionate researchers who are completely dedicated to their work. He not only provided me with the tools and all his knowledge, but also trusted my abilities beyond any exam results. His commitment and dedication were the main motivation to overcome the day-to-day difficulties.

Secondly, I would like to thank Professor Guido Camata and Massimo Petracca, PhD from ASDEA software, Pescara, for facilitating the use of the software employed. The quality of the models and results achieved would not have been possible without their continuous help.

A Marilisa di Benedetto, per il suo impegno e la sua dedizione nei miei confronti durante sette intensi mesi di lavoro. Spero che ce ne siano molti altri! Ad Antonio, per la sua inesauribile pazienza e disponibilità durante i corsi.

A Hernán San Martín, un excelente profesor, jefe y amigo, por inculcarme su amor por la enseñanza y su entusiasmo por la vida. Por su apoyo incondicional durante toda la carrera.

A mis amigos, viejos y nuevos, que me dieron todo su apoyo en los momentos más difíciles y me acompañaron en los momentos felices. A quienes conocí en Torino, gracias por haber hecho de mi experiencia la mejor. A Guga, gracias por acompañarme en esta aventura.

A mi familia, por su amor incondicional, por haberme inculcado el valor del estudio y el trabajo, e impulsarme a cumplir mis metas. A la distancia los abrazo.

A Berni, por creer en mi desde el primer momento.

Quisiera dedicarle esta tesis a Mamá, Papá y Jose, por enseñarme a no rendirme.